

Miniaturized Electrochemiluminescence (ECL) Platforms to Detect Various Bioanalytes: A Machine Learning Approach

THESIS

Submitted in partial fulfilment
of the requirements for the degree of

DOCTOR OF PHILOSOPHY

by

Manish Laxminarayan Bhaiyya

ID. No. 2020PHXF0026H

Under the Supervision of

Prof. Sanket Goel

&

Under the Co-supervision of

Prof. Prasant Kumar Pattnaik & Prof. Karthik Shankar



BITS Pilani
Pilani | Dubai | Goa | Hyderabad

BIRLA INSTITUTE OF TECHNOLOGY AND SCIENCE, PILANI

2023

BIRLA INSTITUTE OF TECHNOLOGY AND SCIENCE, PILANI
CERTIFICATE

This is to certify that the thesis titled **Miniaturized Electrochemiluminescence (ECL) Platforms to Detect Various Bioanalytes: A Machine Learning Approach** is submitted by **Manish L. Bhaiyya** bearing ID No. **2020PHXF0026H** for award of Ph.D. of the Institute embodies original work done by him under our supervision.

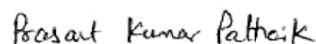


Signature of the Supervisor

Name in capital letters: Prof. Sanket Goel

Designation: Professor, Department of Electrical & Electronics Engineering, BITS Pilani, Hyderabad Campus

Date: 22 May 2023



Signature of the Co-Supervisor

Name in capital letters: Dr. Prasant Kumar Pattnaik

Designation: Professor, Department of Electrical & Electronics Engineering, BITS Pilani, Hyderabad Campus

Date: **22nd May 2023**



Signature of the Co-Supervisor

Name in capital letters: Prof. Karthik Shankar

Designation: Professor, Professor, Department of Electrical & Computer Engineering, University of Alberta

Date: 23rd May 2023

Acknowledgements

I always believed that teacher is the next most powerful human influencer after mother. In my opinion, if we want to live joyfully/successful life, everyone should have a good charioteer who guides us through life complexities and helps us make the proper decisions. The best charioteer in the world and the one who genuinely shapes your life is your teacher. I am eternally grateful to God for providing me the opportunities throughout my career to seek advice from such teachers. I would like to take this opportunity to thank my Supervisor Prof. Sanket Goel to guide me throughout my Ph.D. program. Without him, this journey would not have been possible. His extensive knowledge and experience have motivated me in both my academic work and daily activities. His commitment to his work and love for it are truly motivating. He has constantly provided me with excellent supervision throughout my Ph.D. I owe him a thank-you note for his unending support, kindness, and constant supervision as well as for his assistance in a number of other personal issues in addition to my research. I would like to thank my co-supervisor Prof. Prasant Kumar Pattnaik and Prof. Karthik Shankar for agreeing to be guide me and rendering all the support and advice during my Ph.D. I would like to thank Prof. Prasant Kumar Pattnaik for their continuous guidance and unconditional support during my Ph.D. His guidance really helped me a lot to stay focus, calm and target oriented. It's my privilege to have him as a co-supervisor. Although I never got the pleasure to meet Prof. Karthik Shankar in person, we frequently communicated via email, and I really admire his ability to write effective emails. I usually get the impression that he is chatting to me while I read his emails.

In addition to my supervisors, I would like to express my gratitude to my Doctoral Advisory Committee members, Dr. Satish Kumar Dubey and Dr. Subhradeep Pal for their insightful ideas during my research. I specially thanks Dr. Satish Kumar Dubey for providing valuable suggestions during weekly presentation. I also thank Dr. Arshad Javed for providing valuable suggestions during weekly presentation. I am grateful to all of them who took part in bringing this thesis into final form. I would also like to offer my sincere thanks to MEMS, Microfluidics and Nanoelectronics (MMNE) Lab, Department of EEE, to provide all facilities during PhD work. I would like to acknowledge the assistance provided by Department of EEE and Central Analytical laboratory, Clean Room: Micro/Nano fabrication facility without which my work could not be carried out smoothly. I also very thankful to Mr. Sreekanth T for his kindness and help throughout this duration. I learned lot of things from Sreekanth Sir. Special thanks to Mrs. Krishnaveni and Mr. Dashrath for their help while conducting labs.

There are very few people who will ping you without any work. There are very few with whom you would like to spend time. Having good friends is the most valuable asset in life. I would like to take this opportunity to thank all my childhood and my college friends. My special thanks to my friend Dr. Prakash. He is the one who actually motivates me to pursue Ph.D. His help during my Ph.D. can't be expressed in words. He taught me all the fabrication techniques, and without his support, I would not have been able to write my first research paper. His advice greatly aided me in conducting my research in the appropriate manner. The greatest accomplishment would be to have a friend like him.

My gratitude would not be complete without thanking my lab members who have supported me at all times during my Ph.D. work. I would like to thank my seniors, Dr. J Murali Mohan, Dr. Sangam T, Mr. Sohan Dudala, Dr. Jayapiriya Mahinder, Dr. Gauri Mahalle, Dr. Dipankar Nath, Mr. Abhishesh Pal, Dr. Madhusudan, Dr. Tata Rao, Mrs. Mrunali Wagh, Dr. Avinash, Dr. Amreen, and Dr. Prashanth Kumar for their help in lab and memorable events we had during our Ph.D. work. My special thanks to Mr. Sanjeet Srivastava for always motivation. He is the person who guided me while I was preparing for Machine Learning. It's my privilege to work with him. I would also thank to all my lab members for their help/support.

Finally, my spinal cord, my family members. I would like to dedicate this thesis to my parents, my brother, my wife and son. Without their support this journey could not be possible. Special thanks to my wife Komal for her sacrifice, understanding and support during my Ph.D.

Abstract

Electrochemiluminescence (ECL) consists of three words, Electro, Chem, and Luminescence, denoting electrical stimulation, chemical reaction, and emission of light, respectively. In this context, ECL is the property of a material to emit light over the surface of the electrode on the application of the external voltage. Miniaturized ECL systems are widely recognized as a high-detection, user-friendly, and turnkey strategy to develop point-of-care devices (PoC). The ECL sensing approach provides numerous advantages over other conventional sensing methodologies, such as photoluminescence, chemiluminescence, and electrochemical (EC). The key features of ECL based sensing approach is it does not require any external light source to initiate the ECL reaction, the intensity of ECL signal can be easily controlled with applied external potential, it provides higher selectivity, selectivity, and less electrode fouling. In addition, it also provides a wide linear range. Hence, ECL systems are widely used in a range of applications such as water and food analysis, bio-warfare agent detection, immunoassay, environmental detection, pharmaceutical analysis, to eventually realize PoC devices.

PoC diagnostic devices can potentially improve the healthcare facilities even in the remotest corner of the world through an early diagnosis, and therefore lead to timely intervention and remediation for multiple diseases and disorders. These low-cost and portable devices can potentially benefit a large population in developing countries that do not have direct access to conventional diagnostics. In addition to easy accessibility, the PoC devices offer options for continuous monitoring of a particular biomolecule or analyze that can be tracked through a smartphone-based application over an extended duration. Various bioanalytes have traditionally been used for diagnosing human health due to their direct correlation with multiple diseases and health conditions. The irregularities in the biomarkers can cause potential ailments in humans. Biosensors open a new window for researchers to develop miniaturized PoC devices to detect various diseases at the early stage, which helps cure patients and ultimately reduces the treatment cost. Compared to the traditional testing approaches, biosensors have provided numerous advantages such as fast response, less sample volume, inexpensive, and on-site or near patient diagnosis can be possible.

In this work, a variety of Bioanalytes, such as Glucose, Lactate, Choline, Dopamine, and Cholesterol, have been thoroughly studied and detected using the ECL approach. Glucose is a type of sugar that serves as the primary source of energy for the body cells. It is particularly important for the brain, which relies almost entirely on glucose for its energy needs.

Maintaining stable blood glucose levels is crucial for overall health and is particularly important for people with diabetes. Lactate is a byproduct of anaerobic metabolism that can accumulate in the body during exercise or other forms of strenuous activity. While high levels of lactate can cause muscle fatigue and discomfort, it also has important functions in the body, such as helping to regulate blood pH and serving as a source of energy for certain cells. Cholesterol is a type of fat that is found in all cells in the body. While high levels of cholesterol can increase the risk of heart disease, cholesterol also has important functions in the body, such as helping to produce hormones and aiding in the digestion of fats. Choline is a nutrient that is important for brain function, liver health, and cell membrane structure. Dopamine is a crucial neurotransmitter that plays a critical role in several essential functions of the brain and body, including reward and pleasure, motivation, movement, attention and learning, and mood regulation. Overall, these biomarkers play important roles in many biological processes and are crucial for maintaining good health. However, it is important to note that excessive or insufficient levels of these substances can have negative effects on the body, so it is important periodically check these biomarkers for better health. The conventional ECL systems are costly and difficult for on-site applications because they comprise photomultiplier tube or CCD cameras, an electrochemical setup, and a personal computer. Modern Android smartphones offer a wide range of features, storage, excellent cameras, and high processing capabilities, making them the ideal option for use in visual ECL analysis. Thus, a portable smartphone assisted by ML-based approach is in great demand in order to accelerate ECL detection, increase work efficiency, and make it a comprehensive ECL system. In addition, AI and ML are enriching MEMS by improving their design, performance, reliability, and maintenance, making them more effective in a wide range of applications such as sensors, actuators, microfluidics, and PoC.

In this context, the first phase broadly gives an idea about the designing, fabrication, optimization, and validation of the PoC systems and their use to detect numerous bioanalytes. Different low-cost microfabrication methodologies, including laser assisted methods and three-dimensional printing (3DP), were comprehensively discussed and used to fabricate miniaturized ECL devices. The last phase provides an in-depth understanding of how the prediction of different biomarkers can be made using the Machine Learning (ML) approach. Different ML regression models such as Huber, Random Sample Consensus (RANSAC), Theil-Sen, Support Vector Machine Regression (SVR), K-Nearest Neighbor (KNN), Decision

Tree, and Random Forest, Adaptive boosting, Gradient boosting, Extreme Gradient boosting were used to predict the concentration of various biomarkers.

Overall, in this work, taking into consideration the advantages of PoC devices, we have successfully developed a cost-effective, pocket-sized ECL system integrated with smartphones using 3D printing technology. The developed innovative system was assisted by ML and successfully tested for various bioanalytes which includes glucose, lactate, choline, dopamine, cholesterol, vitamin B₁₂ and C. The ML approach was not only used to improve the overall accuracy of the ECL sensors but also to provide fast diagnosis results. Following are the key features of the developed ECL platforms: 1) smartphone integrated, 2) no requirement of external power supply, 3) can performed testing in open environment, 4) have user friendly Graphical User Interface, 4) integrated with android application using that one can take real time ECL images, calculates intensity for region of interest, share/stores data, plot calibration plots, and also performs predictions using ML algorithms. We have successfully completed lab-based testing using developed ECL platform for various bioanalytes and achieved Technology Readiness Level (TRL) four.

Keywords: Electrochemiluminescence (ECL); Point-of-Care (PoC); Biomarkers; Sensors; Laser Assisted; Three-Dimensional Printing (3DP); Machine Learning

Contents

CERTIFICATE	i
Acknowledgements	ii
Abstract	iv
List of Tables	xi
List of Figures	xii
List of Abbreviations	xviii
Chapter 1. Introduction	1
1.1 Background and Need	1
1.2 Introduction to Electrochemiluminescence (ECL).....	1
1.3 ECL Reagents.....	2
1.4 ECL Systems	4
1.4.1 Bipolar electrode based ECL device.....	4
1.4.2 Single electrode based ECL device.....	5
1.5 ECL fabrication techniques and their applications in PoC	5
1.6 Benchmark research work reported on ECL devices	6
1.7 Gaps in existing research and possible solutions	8
1.8 Objectives of the Ph.D. thesis work	10
1.9 Organization of Ph.D. thesis	10
1.10 Summary.....	11
Chapter 2. Laser-Induced Graphene Based ECL Devices	12
2.1 Introduction to Laser-Induced Graphene	12
2.2 LIG-Based Open Bipolar Electrode ECL Device	12
2.2.1 Fabrication flow for LIG based Open BPE-based ECL device (LIG-BPE-ECL) ..	13
2.2.2 Materials and Reagents	14
2.2.3 Data acquisition and analysis.....	15
2.2.4 Assay optimization for LIG-BPE-ECL device	16
2.2.5 Sensing of H ₂ O ₂ and Glucose using LIG-BPE-ECL device.....	19
2.2.6 Real sample analysis of H ₂ O ₂ and Glucose using LIG-BPE-ECL device	20
2.3 LIG-Based closed bipolar electrode ECL device.....	21
2.3.1 Design, fabrication, and sensing principle of two and three-channel LIG-Closed-BPE-ECL device (LIG-C-BPE-ECL)	21
2.3.2 Characterization of LIG-C-BPE-ECL device	23
2.3.3 Analytical performance of two-channel LIG-C-BPE-ECL device.....	24
2.3.4 Analytical performance of two-channel LIG-C-BPE-ECL device.....	26

2.3.5 Real sample analysis of Vitamin B ₁₂ and Vitamin C using three-channel LIG-C-BPE-ECL	27
2.4 LIG-Based Single Electrode ECL Device (LIG-SE-ECL)	29
2.4.1 Design, fabrication, and sensing principle of Single Electrode LIG-ECL device (LIG-SE-ECL)	30
2.4.2 Sensing of xanthine and dopamine using LIG-SE-ECL device.....	31
The concentrations of Xanthine and Dopamine varied from 0.1 μM to 500 μM. Under optimized conditions, LIG-SE-ECL device was utilized to determined xanthine and dopamine, with linear range 0.1 to 100 μM and detection limit of 1.25 μM (R ² = 0.9556, n = 3) and 3.40 μM (R ² = 0.9734), respectively.	32
2.4.3 Stability and Interference study of LIG-based electrode	32
2.5 Summary of LIG-ECL devices	34
Chapter 3. Three Dimensional Printed (3DP) ECL Devices.....	35
3.1 Introduction to 3DP-ECL devices.....	35
3.2 3D printed closed bipolar ECL (3DP-C-BPE-ECL) device	35
3.2.1 Working principle and fabrication of 3DP-C-BPE-ECL.....	36
3.2.2 Materials and instrumentation used	37
3.2.3 Data capturing and analysis for 3DP-C-BPE-ECL.....	38
3.2.4 Characterization for 3DP electrodes	40
3.2.5 Assay optimization for 3DP-C-BPE-ECL	41
3.2.6 Sensing of Choline and Dopamine using 3DP-C-BPE-ECL	43
3.3 Multiplexed and Simultaneous Biosensing in a 3D-Printed Portable Six-Well ECL device	45
3.3.1 Working principle and fabrication of six-well 3DP-CBPE-ECL	45
3.3.2 Data acquisition and analysis.....	46
3.3.3 Analytical performance of six-well 3DP-CBPE-ECL	47
3.3.4 Real Sample analysis of glucose and choline	49
3.3.5 Interference study of glucose and choline with other biomolecules.....	50
3.4 Stereolithography 3d printed ECL platform with random grade graphite electrodes: detection of H ₂ O ₂ and cholesterol using a smartphone.....	51
3.4.1 Operating Principle and Fabrication of GP-SE-ECL Device	52
3.4.2 Chemicals and Material	53
3.4.3 Preparation of cholesterol and luminol	54
3.4.4 Optimization of applied voltage, luminol and channel length.....	54
3.4.5 Sensing of H ₂ O ₂ using different graded pencil-based GP-SE-ECL device	56
3.4.6 Sensing of cholesterol using HB graded pencil-based GP-SE-ECL device	58
3.4.7 Interference study using HB graded pencil-based GP-SE-ECL device.....	59

3.4.8 Real sample analysis of H ₂ O ₂ and cholesterol in milk and blood serum using GP-SE-ECL device.....	60
3.4.9 Stability and reproducibility analysis using HB graded pencil-based GP-SE-ECL device	60
3.5 Summary of 3DP-ECL devices.....	61
Chapter 4. Paper Based ECL Devices.....	63
4.1 Introduction to paper-based devices	63
4.2 Concept and fabrication flow for P-SE-ECL device.....	64
4.3 Data acquisition and analysis.....	65
4.4 Characterization of P-SE-ECL device	66
4.5 Parameters optimization for P-SE-ECL device	67
4.6 Analytical performance of P-SE-ECL device.....	67
4.7 Selectivity and storage stability analysis of P-SE-ECL device	68
4.8 Real sample analysis using P-SE-ECL device.....	70
4.9 Summary for P-SE-ECL device.....	70
Chapter 5. A Machine Learning Approach for ECL Based Point of Care Testing Device to Detect Multiple Biomarkers	72
5.1 Introduction to Machine Learning approach to detect various biomarkers	72
5.2 Fabrication and working concept of ECL biosensors	74
5.3 Chemicals and materials	75
5.4 Results and discussion	75
5.4.1 Parameter optimization	75
5.4.2 Analytical performance of ECL biosensors.....	77
5.4.3 Repeatability, reproducibility, and interference study using ECL biosensor	79
5.4.4 Real sample analysis and its validation using ML.....	80
5.5 ML Modeling to validate the analytical performance of ECL biosensors.....	81
5.5.1 Linear regression.....	81
5.5.2 Decision tree	83
5.5.3 Ensemble methods	83
5.5.4 Distance based methods.....	85
5.5.5 Comparative regression metrics for different ML models.....	85
5.6 Conclusion	86
Chapter 6. Conclusion and Future Scope.....	88
6.1 Conclusion	88
6.2 Limitations of The Presented Work.....	90
6.2.1 Smartphone Dependency	90

6.3 Future Scope	90
6.3.1 Droplet microfluidic based ECL systems	90
References.....	92
Research Output	102
Papers Published	102
International Conference.....	103
Patent File	104
Appendix.....	104
Biographies	108
Biography of the candidate: Manish Bhaiyya.....	108
Biography of the supervisor: Dr. Sanket Goel.....	108
Biography of the co- supervisor: Dr. Prashant Kumar Pattnaik	109
Biography of the co-supervisor : Dr. Karthik Shankar	109

List of Tables

Table 1. 1 Basic ECL Chemical Reactions Reagents.....	2
Table 1. 2 Benchmarking of the research work reported on Miniaturized ECL Devices	6
Table 2. 1 Real Sample Glucose Analysis in Human Serum	21
Table 2. 2 Analytical performance of two-channel LIG-C-BPE-ECL device	26
Table 2. 3 Parameters related to three-channel LIG-C-BPE-ECL for simultaneous sensing of vitamin B ₁₂ and vitamin C.	27
Table 2. 4 Real sample analysis of vitamin B ₁₂ and vitamin C using three-channel LIG C-BPE-ECL device.....	28
Table 2. 5 Research summary on Vitamin B ₁₂ and Vitamin C using different methods.	28
Table 2. 6 Interference study of dopamine and xanthine	33
Table 3. 1 Summary of the outcome from the real sample analysis	50
Table 3. 2 Real Sample Analysis of H ₂ O ₂ and Cholesterol	60
Table 4. 1 Real sample analysis for glucose and lactate using P-SE-ECL device.	70
Table 5. 1 Optimized Parameters	77
Table 5. 2 Real sample analysis using ECL biosensor	80
Table 5. 3 Comparative Regression Metrics for different ML Models	86
Table 6. 1 Overall summary for different ECL devices.....	89

List of Figures

Figure 1.1 Time taken by conventional lab-based testing and PoCT devices for diagnosis.	1
Figure 1.2 (a) and (b) The reaction mechanism of the pro-duction of ECL using Luminol/H ₂ O ₂ and Ru(bpy) ₃ ²⁺ /TPA.....	3
Figure 1.3 Different ECL systems. (a) Open bipolar electrode based ECL device. (b) Closed bipolar electrode based ECL device. (c) Single electrode based ECL device.	4
Figure 1.4 Proposed schematic of ECL system to overcome the challenges.....	9
Figure 2.1 Fabrication Process for LIG-BPE-ECL Device. (a) Polyimide (PI) sheet (250 μm thickness). (b) Laser induced graphene. (c) Formation of microfluidics channel over PI. (d) fabricated engraved microchannel with DE and BPE. (e) Pipetting microfluidic channel with required ECL reagents. (f) Detection of ECL signal using mobile phone.....	13
Figure 2.2 (a) 3D Printed black box with device holder. (b) LIG-BPE-ECL imaging sensing platform.....	16
Figure 2.3 (a) Luminol (mM) Vs ECL Intensity (RLU); Luminol = 1, 2, 3, 4, 5, 6 and 7 mM; H ₂ O ₂ : 1 mM; Applied Voltage = 7 V. (b) pH Vs ECL Intensity (RLU); pH = 7, 8, 9, 10, 11 and 12; H ₂ O ₂ = 1 mM; Luminol = 4 mM; Applied voltage = 7.0 V. (c) Applied Voltage (V) Vs ECL Intensity (RLU); Applied voltage = 3.0, 4.0, 5.0, 6.0, 7.0, 8.0, 9.0, 10 and 11 V; H ₂ O ₂ = 1 mM; Luminol = 4 mM; pH = 9. Error bar representing the standard deviations for three independent experiments.	18
Figure 2.4 (a) H ₂ O ₂ (μM) Vs ECL Intensity (RLU); H ₂ O ₂ : 5, 10, 30, 50, 100, 1000, 2000, 3000, 4000 and 5000 μM; Luminol = 4 mM; pH: 9; Applied Voltage = 7 V. (b) Glucose Vs ECL Intensity (RLU); Glucose: 1, 10, 20, 30, 40, 50, 60, 70 and 100 μM; Luminol = 4 mM; pH: 9; H ₂ O ₂ = 1 mM; Applied Voltage = 7 V. Error bar representing the standard deviations for three independent experiments.	20
Figure 2.5 Final fabricated two and three-channel LIG-C-BPE-ECL devices, (a) Working principle of two-channel LIG based C-BPE-ECL device. (b) Working principle of three-channel LIG based C-BPE-ECL device with supporting and reporting channel, driving (DE) and bipolar (BPE) electrodes.	22
Figure 2.6 (a) Polyimide sheet before inducing CO ₂ laser. (b) SEM image of polyimide sheet after inducing CO ₂ laser. (c) XPS analysis of LIG based electrodes. (d) RAMAN Spectroscopy for the LIG based ECL device.	24

Figure 2.7 (a) H₂O₂ Vs ECL intensity (RLU): H₂O₂ varied from 0.5 to 100 μM, Applied Voltage = 7 V, Luminol = 4 mM (9 pH), (b) Vitamin B₁₂ Vs ECL intensity (RLU): Vitamin B₁₂ varied 0.5 to 1000 nM, Applied Voltage = 7 V, Luminol = 4 mM, (c) Vitamin C Vs ECL intensity (RLU): Vitamin C varied from 1 to 1000 μM, Applied Voltage = 7 V, Luminol = 4 mM.....26

Figure 2.8 Simultaneous detection of Vitamin B₁₂ and Vitamin C. (a) 3 channel LIG-C-BPE-ECL system having Vitamin B₁₂ = 0.5 nM, Luminol = 4 mM, Vitamin C = 1 μM and PBS = 0.1 M, applied voltage = 7 V. (f) Bar graph for vitamin B₁₂ Vs ECL intensity (RLU). (g) Bar graph for vitamin C Vs ECL intensity (RLU), Error bar represents standard deviation for three experiments.....27

Figure 2.9 (a) 3D structure with microchannel depth (120 μm). (b) Schematic of Single Electrode laser Induced Graphene ECL (LIG-SE-ECL) system with device dimensions. (c) Working principle of LIG-SE-ECL device. (d) Fabricated LIG-SE-ECL device with driving electrode (8 mm x 6 mm) and fluidic channel (28 mm x 7 mm).....30

Figure 2.10 (a) Xanthine (μM) Vs ECL intensity (RLU). Xanthine = 0.1, 1, 10, 30, 50, 70, 100, 200, 300 and 500 μM; Applied voltage = V; Luminol = 5 mM (pH = 10). (b) Dopamine (μM) Vs ECL intensity (RLU). Dopamine = 0.1, 1, 10, 30, 50, 70, 100, 200, 300 and 500 μM; Applied voltage = 7 V; Luminol = 5 mM (pH = 10); Error bar represents standard deviation for three independent experiments (n=3).31

Figure 2.11 (a) Stability analysis of Laser Induced Graphene based electrodes. Applied voltage = 7 V; Luminol = 5 mM (pH = 10); H₂O₂ = 1 mM; Error bar represents standard deviation for three independent experiments. (b) Applied Voltage (V) Vs ECL Intensity (RLU); In panel, applied voltage = varied from 3 to 10 volts; luminol = 5 mM (pH = 10); in panel, Dopamine = 500 μM; applied voltage = varied from 3 to 12 volts, luminol = 5 mM (pH = 10); in panel, Xanthine = 500 μM; applied voltage: varied from 3 to 13 volts; luminol = 5 mM (pH = 10); Error bar represents standard deviation for three independent experiments (n=3).....32

Figure 3.1 (a) Working concept of 3DP-BPE-ECL device. (b) Image of the final fabricated 3DP-C-BPE-ECL device showing the supporting and reporting channels, bipolar and driving electrodes.36

Figure 3.2 PMT based approach for data acquisition and analysis; (a) Block diagram representation of Photomultiplier tube PMT module; (b) schematic representation of PMT based approach to detect ECL signal: IoT and bluetooth module with other electronics

component mounted on solo PCB; (c) Mobile embedded ThinkSpeak IoT platform; (d) real-time data logging using Smartphone.....38

Figure 3.3 Smartphone based approach for data acquisition and analysis. (a) 3D printed miniaturized ECL imaging system with black box, DC-DC converter and smartphone. (b) ImageJ software based calculation of ECL intensity.....40

Figure 3.4 SEM images for conductive graphene filament, (a) without DMF treatment. (b) after DMF treatment.....40

Figure 3.5 Optimization of various parameters. (a) TPrA (mM) Vs PMT Output (Volts); TPrA = 10, 20, 30, 40, 50 and 60 mM, applied voltage = 7 V, voltage gain = 0.6, Ru(bpy)₃²⁺ = 500 μM, PBS = 0.1 M (pH =7). (b) Applied voltage Vs PMT Output (Volts); applied voltage = 4, 5, 6, 7, 8, 10, 11 and 13, TPrA = 30 mM, Ru(bpy)₃²⁺ = 500 μM, voltage gain = 0.6, PBS = 0.1 M (pH = 7) (n = 3).41

Figure 3.6 Effect of DMF treatment on graphene filament; (a) Smartphone based approach to sense Ru(bpy)₃²⁺; Ru(bpy)₃²⁺ (μM) Vs ECL Intensity (RLU), Ru(bpy)₃²⁺ = 50 to 700 μM, applied voltage = 8V, TPrA = 30 mM, PBS = 0.1 M (pH =7).42

Figure 3.7 (a) Dopamine (μM) Vs PMT Output (Volts), Dopamine = 0.5, 1, 50, 70 and 100 μM, TPrA = 30 mM, PBS = 0.1 M (pH =7), voltage gain = 0.6, Ru(bpy)₃²⁺ = 100 μM, applied voltage = 8V. (b) Dopamine (μM) Vs ECL Intensity (RLU); Dopamine = 0.5, 1, 50, 70 and 100 μM, TPrA = 30 mM, PBS = 0.1 M (pH =7), Ru(bpy)₃²⁺ = 100 μM, applied voltage = 8V. (c) Choline (μM) Vs PMT Output (Volts), choline = 30, 100, 300, 500 and 700 μM, Luminol = 4 mM, voltage gain = 0.6, choline oxidase = 10 mg/mL, applied voltage = 7V, PBS = 0.1 M (pH =7), (d) Choline (μM) Vs ECL Intensity (RLU), choline = 30, 100, 300, 500 and 700 μM, choline oxidase = 10 mg/mL, Luminol = 4 mM, applied voltage = 7V, PBS = 0.1 M (pH =7). (N=3).....44

Figure 3.8 (a) Working principle of six-well 3DP-CBPE-ECL device with anodic, cathodic and enzymatic reactions. (b) and (c) top and side view for 3DP-CBPE-ECL device with dimensions. (d) final fabricated 3DP-CBPE-ECL device.....45

Figure 3.9 Data acquisition and analysis, (a) 3D printed black box assembly integrated with smartphone and converter, (b) Display for android ECL Intensity app, (c) captured real time image, (d) selected region of interest and calculated ECL intensity.....47

Figure 3.10 (a) Schematic representation of glucose with different concentration, (b) ECL intensity Vs Glucose, Glucose = 0.1, 1, 3, 5, 7 and 10 mM, Luminol = 4 mM, GOx = 10 mg/mL, Applied voltage = 7V, (c) Schematic representation of choline with different concentration, (d) ECL intensity Vs Choline, Choline = 0.1, 0.5, 0.7, 1, 3 and 5 mM, Luminol = 4 mM, COx =

10 mg/mL, Applied voltage = 7V, (e) simultaneous detection of glucose and choline using six channel CBPE-ECL device, (f) real time ECL signal image corresponding to various concentration of glucose and choline. [N = 3]48

Figure 3.11 Interference study. (a) interference study of glucose with choline, creatine, uric acid, ascorbic acid: glucose = 5 mM, choline = 1 mM, creatine = 0.5 mM, uric acid = 0.5 mM, ascorbic acid = 0.1 mM, Luminol = 4 mM, GOx = 10 mg/mL and applied voltage = 7 V. (b) interference study of choline with glucose, creatine, uric acid, ascorbic acid: choline = 2 mM, glucose = 1 mM, creatine = 0.5 mM, uric acid = 0.5 mM, ascorbic acid = 0.1 mM, Luminol = 4 mM, COx = 10 mg/mL and applied voltage = 7 V, n=3.51

Figure 3.12 (a) Schematic representation for working concept of P-SE-ECL device with redox process: Fabrication flow for P-SE-ECL device. (b) design of 3D CAD model with dedicated slots. (c) 3D CAD model with graphite-based driving electrodes. (d) final fabricated GP-SE-ECL device. Three different diameter inlets (2.2 mm for HB and F, 2.4 mm for 3B and 3 mm for 6B & 8B) were used to insert the electrodes.53

Figure 3.13 Optimization of different parameters. (a) optimization of applied voltage, luminol = 5mM, H₂O₂ = 1 mM and applied voltage varied from 1 to 6 V. (b) optimization of applied luminol, applied voltage = 4V, H₂O₂ = 1 mM and luminol varied from 1 to 5 mM. (c) optimization of channel length, luminol = 3 mM, applied voltage = 4V, H₂O₂ = 0.1 mM. (d) time optimization for cholesterol sensing, CHOx = 50 mg/mL, cholesterol = 1 mM, luminol = 3 mM, applied voltage = 4 V. (e) luminol = 3 mM, applied voltage = 4V, CHOx = 10, 30, 50, 70 and 100 UN/mL, cholesterol = 1 mM, n=3.55

Figure 3.14 Sensing of H₂O₂ using different grade pencils. (a) sensing of H₂O₂ using H grade pencil. (b) sensing of H₂O₂ using F grade pencil. (c) sensing of H₂O₂ using 3B grade pencil. (d) sensing of H₂O₂ using 6B grade pencil. (e) sensing of H₂O₂ using 8B grade pencil. (f) sensing of H₂O₂ using HB grade pencil. Parameter used for experiments: luminol = 3 mM, applied voltage = 4V, H₂O₂ = 1 to 100 μM. The error bar denotes the standard deviation for three experiments (n=3).57

Figure 3.15 (a) time optimization for cholesterol to react with cholesterol oxidase. (b) Luminol/H₂O₂ chemistry-based cholesterol detection: luminol = 3 mM (100 μL), applied voltage = 4 V, CHOx = 50 mg/mL (2.5μL), cholesterol = 50, 100, 200, 300, 400, 500, 700, 1000, 2000, 3000 μM, time to produced H₂O₂ = 3 minutes, n = 3.58

Figure 3.16 Interference study of cholesterol with other interfering compounds: luminol = 3 mM (100 μL), applied voltage = 4 V, CHOx = 50 mg/mL (2.5μL), cholesterol = 1000 μM,

glucose = 1000 μ M, lactate = 1000 μ M, xanthine = 1000 μ M, uric acid = 1000 μ M, creatinine = 1000 μ M, choline = 1000 μ M, n = 3.59

Figure 3.17 (a) Stability analysis of GP-SE-ECL device: (a) Cholesterol-based stability analysis, luminol = 3 mM (100 μ L), cholesterol = 1000 μ M (100 μ L), CHOx = 50 mg/mL (2.5 μ L), applied voltage = 4V. (b) reproducibility analysis using, cholesterol = 500 μ M, (100 μ L), CHOx = 50 mg/mL (2.5 μ L), applied voltage = 4 V, n = 3.61

Figure 4. 1 (a) Schematic representation of P-SE-ECL device with anodic and cathodic reactions. (b) Fabrication flow for paper based single electrode ECL device.65

Figure 4. 3 Data acquisition using mobile application: (a) real image of 3D printed black box with in house smartphone and buck boost converter to capture ECL signal. (b) mobile based ECL intensity calculator. (c) capture real time image or pick image from gallery option present in mobile app. (d) selected high intensity area of ECL image. (e) calculation of intensity using ECL intensity calculator. (f) ECL signal intensity calculation using ImageJ software.66

Figure 4. 4 characterization of P-SE-ECL device: (a) SEM analysis. (b) RAMAN analysis. (c) XPS analysis. (d) TEM analysis.67

Figure 4. 5 Analytical performance of P-SE-ECL device; (a) Glucose (μ M) Vs ECL Intensity (RLU), Glucose = 50, 100, 300, 500, 700 and 1000 μ M, , Luminol = 5 mM, Applied Voltage = 7 V; Glucose oxidase = 10 mg/mL; (b) Lactate (μ M) Vs ECL Intensity (RLU), Lactate = 100, 500, 1000, 2000, 3000 and 5000 μ M, lactate oxidase = 25 units/mL, n = 3.68

Figure 4. 6 Selectivity analysis using P-SE-ECL device. (a) selectivity analysis for glucose with lactate, glucose = 1000 μ M, glucose oxidase = 10 mg/mL, applied voltage =7V, lactate = 1000 μ M, Ascorbic acid = 1000 μ M, Xylose = 1000 μ M, Galactose = 1000 μ M. (b) selectivity analysis for lactate with glucose, lactate = 1000 μ M, lactate oxidase = 25 units/mL, glucose = 1000 μ M, Ascorbic acid = 1000 μ M, Xylose = 1000 μ M, Galactose = 1000 μ M , applied voltage = 7 V. (c) Stability analysis for rGO based single electrode device. H₂O₂ = 1 mM, Luminol = 5 mM, applied voltage = 7V, n = 3.69

Figure 5.1 (a) Schematic of the fabricated ECL biosensor with oxidation and reduction, (b) sketch drawing for one-well 3DP-IDE-CBPE-ECL biosensor.74

Figure 5.2 Parameters optimization; (a) IDEs optimization, luminol = 5 mM, voltage = 6 V, H₂O₂ = 1 mM, PBS = 0.1 mM. (b) effect of DMF, luminol = 5 mM, glucose = 5 mM, GOx = 10 mg/mL, voltage = 6 V, PBS = 0.1 mM. (c) voltage optimization, luminol = 5 mM, H₂O₂ =

1 mM, voltage = varied from 3 V to 8 V, PBS = 0.1 mM. (d) luminol optimization, voltage = 6 V, H₂O₂ = 1 mM, luminol = varied from 3 mM to 6 mM, PBS = 0.1 mM. (e) pH optimization, voltage = 6 V, H₂O₂ = 1 mM, luminol = 3 mM, pH = varied from 7 to 11, PBS = 0.1 mM. (f) The ECL imaging and analysis system; n = 3.76

Figure 5. 3 Sensing of glucose and lactate; (a) time optimization for glucose sensing, luminol = 5mM, glucose = 5mM, GOx = 10 mg/mL, applied voltage = 6V, PBS = 0.1 mM. (b) glucose sensing, luminol = 5mM, glucose = varied from 0.05 to 7mM, GOx = 10 mg/mL, applied voltage = 6V, PBS = 0.1mM. (c) time optimization for lactate sensing, luminol = 5mM, lactate = 4 mM, LOx = 50 UN/mL, applied voltage = 6V, PBS = 0.1 mM. (d) lactate sensing, luminol = 5mM, lactate = varied from 0.1 to 10mM, LOx = 50 UN/mL, applied voltage = 6V. (e) time optimization for choline sensing, luminol = 5 mM, COx = 10 mg/mL, applied voltage = 6V, PBS = 0.1 mM. (f) choline sensing, luminol = 5 mM, choline = varied from 0.0007 to 4mM, COx = 10 mg/mL, applied voltage = 6V, PBS = 0.1 mM: n = 3.78

Figure 5.4 Repeatability, reproducibility and interference study; (A) repeatability analysis, luminol = 5mM, lactate = 3mM, LOx = 50 UN/mL, applied voltage = 6V, PBS = 0.1mM; (B) reproducibility analysis, luminol = 5mM, lactate = 3mM, LOx = 50 UN/mL, applied voltage = 6V, PBS = 0.1mM; (C) interference study, glucose = 3mM, GOx = 10 mg/mL, cholesterol = xanthine = uric acid = lactate = choline = creatinine = 1mM, PBS = 0.1mM, n = 3.79

Figure 5.5 Mapping of Linear Regressors - Huber Regression, RANSAC Regression, and Theil-Sen Regression for (A) glucose, (B) lactate, and (C) choline.82

Figure 5.6 Ensemble techniques: Decision Tree (a) Glucose, (b) Lactate, and (c) Choline. Random Forest techniques for (d) Glucose, (e) Lactate, and (f) Choline. Gradient Boosting techniques for (g) Glucose, (h) Lactate, and (i) Choline.84

Figure 5.7 KNN models for (a) glucose, (b) lactate and (c) choline85

Figure 6.1 (a) Overall ECL devices fabricated with different microfabrication technique. (b) Portable pocket size ML assisted ECL system to detect various biomarkers.89

Figure 6.2 Schematic for Droplet/Continuous microfluidic based ECL systems.90

List of Abbreviations

PoC: Point-of-Care
ECL: Electrochemiluminescence
LIG: Laser-Induced Graphene
3DP: Three-Dimensional Printing
ML: Machine Learning
BPE: Bipolar Electrode
SE: Single Electrode
GOx: Glucose Oxidase
LOx: Lactate Oxidase
CHx: Choline Oxidase
CHOX: Cholesterol Oxidase
CCD: Charge Coupled Devices
PMT: Photo Multiplier Tube
RLU: Relative Light Unit
PI: Polyimide
DE: driving Voltage
LoD: Limit of Detection
CH: Channel
SC, RC: Supporting and Reporting Channel
PBS: Phosphate Buffer Solution
TPrA: Tripropylamine
H₂O₂: Hydrogen Peroxide
DMF: Dimethylformamide
SLA: Stereolithography
GP: Graphite Pencil
rGO: reduce Graphene Oxide
SVM: Support Vector Machines
kNN: K-Nearest Neighbor
DT: Decision Tree

LR: Linear Regression,

IDE: Inter-Digited Electrodes

MAE: Mean Absolute Error

MSE: Mean Squared Error

RMSE: Root Mean Squared Error

XGB: Xtreme Gradient Boost

RF: Random Forest

GB: Gradient Boost

CoD: Coefficient of Determination

Chapter 1. Introduction

1.1 Background and Need

Point-of-Care (PoC) diagnostic devices can potentially improve the healthcare facilities in the remotest corner of the world through an early diagnosis, and therefore enable timely intervention and remediation for multiple diseases and disorders. These low-cost and portable devices can potentially benefit a large population in developing countries that do not have direct access to conventional diagnostics [1][2]. In addition to easy accessibility, the PoC devices offer options for continuous monitoring of a particular biomarker or analysis that can be tracked through a smartphone-based application over an extended duration. Biomarkers have traditionally been used for diagnosing human health due to their direct correlation with multiple diseases and health conditions [3][4]. Biosensors open a new window for researchers to develop miniaturized PoC devices to detect various diseases at the early stage, which helps cure patients and ultimately reduces the treatment cost [5][6]. Compared to the traditional testing approaches, biosensors provide numerous advantages, such as fast response, less sample volume, inexpensive, and possibility of on-site or near-patient diagnosis [7][8]. The relative comparison between conventional lab-based testing and PoCT devices is shown in Fig. 1

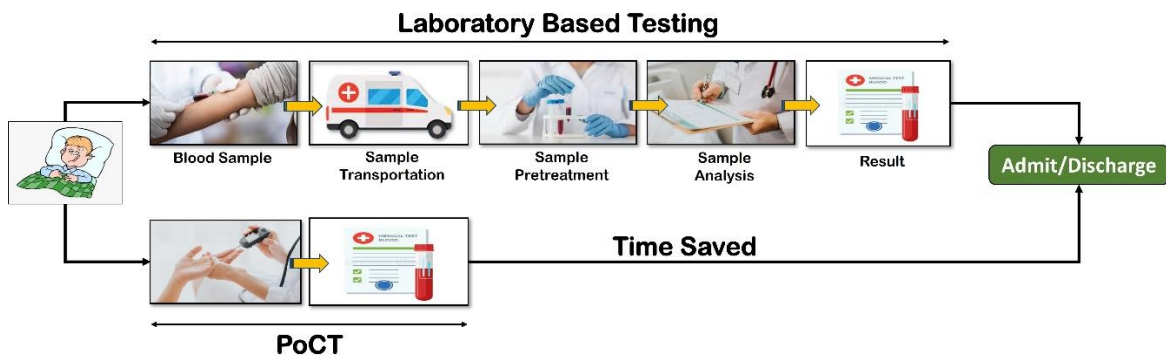


Figure 1.1 Time taken by conventional lab-based testing and PoCT devices for diagnosis.

1.2 Introduction to Electrochemiluminescence (ECL)

Recent research work indicates that biosensors can be easily integrated with electrochemical [9], electrochemiluminescence (ECL) [10][11], and colorimetric sensing methods [12][13]. In recent times, ECL-based biosensors have gained immense popularity because of their high sensitivity and selectivity [14][15], extensive operating range, minimum set-up requirement, low or minimum background signal, and reasonable control over the generated ECL signal

[16]. In addition, ECL biosensors are being explored as faster, inexpensive, and more efficient alternative to traditional solutions based on conventional detectors, such as the photomultiplier tube and charge-coupled devices, for biomarker detection. In brief, electrochemiluminescence is also called electrogenerated chemiluminescence due to the fact that on the application of an external potential, the light gets generated on the electrode surface because of chemical reactions [17][18].

1.3 ECL Reagents

Two major ECL reactions, luminol and ruthenium $[Ru(bpy)_3^{2+}]$ have been widely considered for biosensors application based on enzymes and DNA sensing, respectively [19]. When Ruthenium gets reacted with its co-reagents Tripropylamine (TPA), ECL signal get generated having a wavelength in between 600 nm to 700 nm. Similarly, when Luminol gets reacted with its co-reagents hydrogen peroxide (H_2O_2), ECL signal get generated having a wavelength in between 355 nm to 540 nm. Table 1. Represents the most reported ECL reagents with their co-reactant and respective wavelength [20]–[22].

Table 1. 1 Basic ECL Chemical Reactions Reagents

ECL Reagents	Ruthenium $Ru(bpy)_3^{2+}$ based	Luminol based
Wavelength	600 nm – 700 nm	355 nm – 540 nm
Co-reactant	Tripropylamine (TPA)	H_2O_2

Luminol (Fluorescence) and $Ru(bpy)_3^{2+}$ (Phosphorescence) are both chemical compounds that exhibit luminescence, which means they emit light when excited. However, they differ in the type of luminescence they display. Fluorescence and phosphorescence are both types of photoluminescence, which means they involve the emission of light by a substance that has been excited by absorbing light of a certain wavelength. However, they differ in several important ways: 1) Lifetime of the excited state: The excited state in fluorescence typically lasts for a very short time (on the order of nanoseconds), while the excited state in phosphorescence lasts much longer (milliseconds to seconds). This is due to the different pathways by which the excited state returns to its ground state: in fluorescence, the energy is typically lost through the emission of a photon almost immediately, while in phosphorescence, the energy is often transferred to another molecule or undergoes other energy-dissipating

processes before a photon is emitted. Both luminol and $\text{Ru}(\text{bpy})_3^{2+}$ are highly efficient emitters of light, making them valuable tools for a variety of applications. Their photophysical properties, including their absorption and emission spectra, as well as their quantum yields and lifetimes, are critical factors that influence their performance in various assays. In summary, while both luminol and $\text{Ru}(\text{bpy})_3^{2+}$ emit light when excited, they do so in different ways. Luminol is fluorescent and emits light quickly, while $\text{Ru}(\text{bpy})_3^{2+}$ is phosphorescent and emits light more slowly. The reaction mechanism of the production of ECL using Luminol/ H_2O_2 and $\text{Ru}(\text{bpy})_3^{2+}$ /TPA is shown in following Figure 1.1.

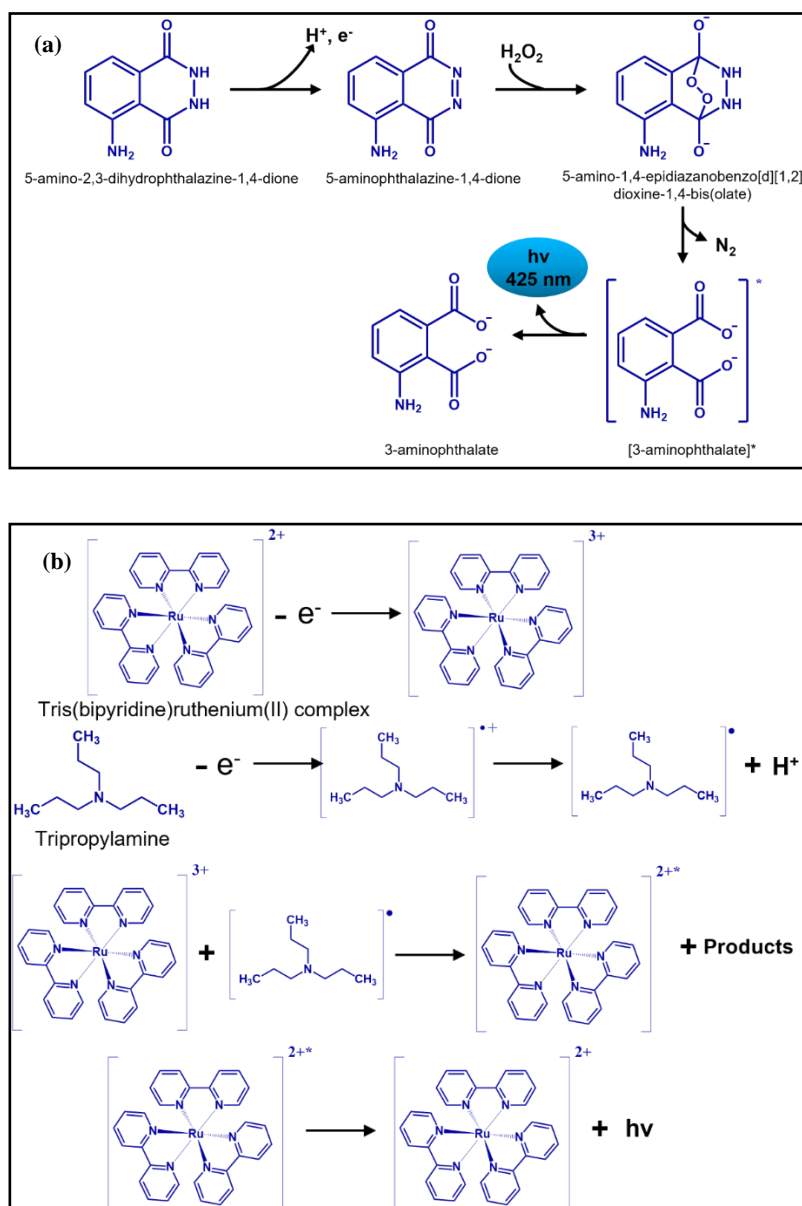


Figure 1.2 (a) and (b) The reaction mechanism of the production of ECL using Luminol/ H_2O_2 and $\text{Ru}(\text{bpy})_3^{2+}$ /TPA.

1.4 ECL Systems

The reported ECL systems can be roughly classified in two categories: bipolar electrodes (BPE-ECL) and single electrode (SE-ECL)[23]. The bipolar and single electrode based ECL system schematic is shown in Figure 1.1.

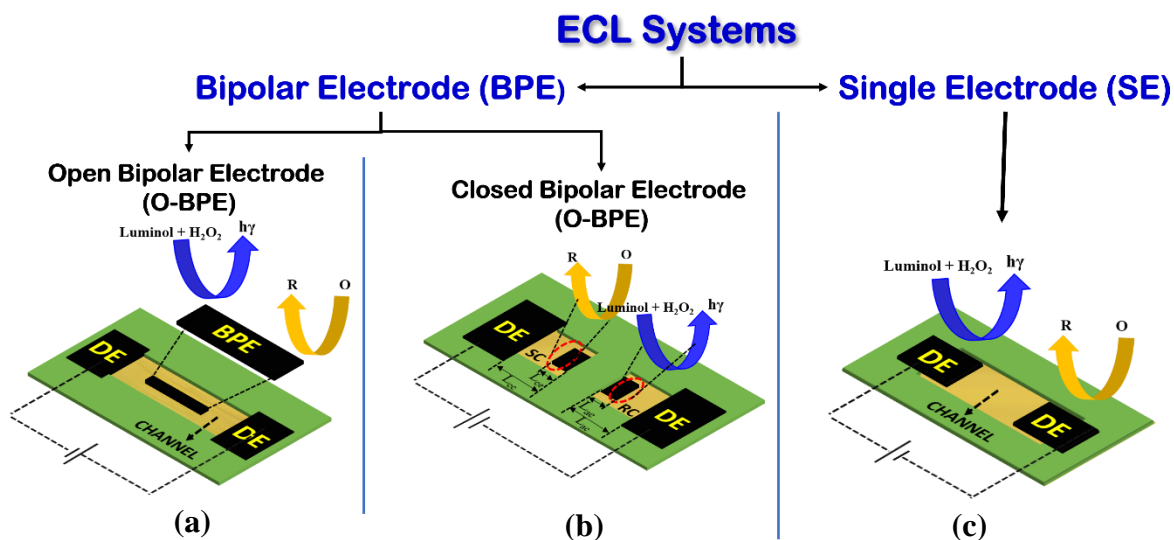


Figure 1.3 Different ECL systems. (a) Open bipolar electrode based ECL device. (b) Closed bipolar electrode based ECL device. (c) Single electrode based ECL device.

1.4.1 Bipolar electrode based ECL device

Recently, BPE-based ECL systems have sparked the interest of researchers because they offer several key advantages over conventional three-electrode systems, including low cost, ease of operation, miniaturization and portability, and amenability to high throughput, making them ideal for PoC applications [24]. As shown in Figure 1.1 (a) and (b), such BPE-ECL systems can be further classified into open BPE (O-BPE- ECL) based and closed BPE (C-BPE-ECL) based ECL systems. The BPE-based ECL device utilizes only one electrode, which acts as both the anode and cathode without a direct electrical connection to applied external potential as compared with the conventional three-electrode systems [25]. In the case of O-BPE-ECL, the BPE is completely immersed into the channel, and two driving electrodes (DEs) are connected at the end of the channel. A channel is defined as a place where ECL reagents (usually luminol or ruthenium) can be dropped in conjunction with the analytes to be sensed. One of the unique facets of BPE-ECL devices is that the orientation of poles of the BPE has opposite polarity to the DEs. After applying a sufficient voltage to DEs, an electric field gets generated across the channel, leading to a redox reaction (reduction and oxidation) at the

opposite poles of the BPE (working electrode). At the anode and cathode of the BPE, simultaneous oxidation and reduction occur, and an ECL signal is generated at the anode. The intensity of the generated ECL signal is highly reliant on the electric field. For the O-BPE-ECL device, Equation (1) manifests the relation between change in the electric field and applied potential [26][27].

$$\Delta E_{ELEC} = E_{tot} \left(\frac{L_{BPE}}{L_{channel}} \right) \dots \dots \dots (1)$$

where, ΔE_{ELEC} is a change in the electric field across BPE, E_{tot} is the total applied voltage across DEs, L_{BPE} and $L_{channel}$ are the length of BPE and channel, respectively. The working principle of the O-BPE-ECL device is illustrated in Figure 1.1 (a).

In the case of C-BPE-ECL, the poles of the BPE electrodes are physically separated by the supporting (SC) and reporting channels (RC). The anode and cathode of BPE can be found in RC and SC, as shown in Figure 1. 1 (b) [25]. Equation 2 shows the relation between change in electric field and applied potential [28].

$$\Delta E_{ELEC} = E_{tot} \left[\frac{L_{ce} + L_{ae}}{L_{cc} + L_{ac}} \right] \dots \dots \dots (2)$$

1.4.2 Single electrode based ECL device

Wenyue Gao et al. [29] reported the SE-ECL systems for the first time and successfully demonstrated their applications. In contract to the BPE systems, SE devices consist of only one electrode to perform the ECL reaction. The working principle of the SE-ECL device with two rectangular driving electrodes (DEs) and the channel is illustrated in Figure 1.1 (c). In the SE-ECL, an external voltage is applied to two DEs, resulting in a potential difference between the two DEs, which produces an electric field across the channel, initiating the redox processes at the surfaces of the anode and cathode of the DEs. The potential difference between (DEs) two DEs in an SE-ECL device is given by Equation (3), where V_{TOT} denotes total applied external potential and L_c and L_e are the channel and DE lengths, respectively [30].

$$\Delta E_c = \frac{V_{TOT} * L_c}{L_e} \dots \dots \dots (3)$$

1.5 ECL fabrication techniques and their applications in PoC

For the PoC, there is a growing concern in developing low-cost portable and miniaturized ECL platforms for a variety of applications such as water testing, disease diagnostics, environmental

monitoring, and food safety [31]. Since then, the most commonly used methods for the fabrication of ECL devices have been screen printing, photolithography, 3D-printing, and laser writing. All those fabrication methods with in-detail explanation are describe in the subsequent chapters.

1.6 Benchmark research work reported on ECL devices

Based on the diversified work accomplished to develop miniaturized ECL devices by leveraging different fabrication methods, Table 1. 2 covers the summary of research work on miniaturized ECL devices. Accordingly, several research gaps have been identified and possible solutions, which are summarized in the next section.

Table 1. 2 Benchmarking of the research work reported on Miniaturized ECL Devices

Material used for device fabrication	Type of Electrode	Chemical used	Enzymes Used	Fabrication technique	Application	LOD in μM	Detection Methodology	References
Filter paper	O-BPE	$\text{Ru}(\text{bpy})_3^{2+}/\text{TPrA}$	-	Screen-printing	Dopamine	0.5	Smartphone	[32]
Filter paper	O-BPE	Luminol/ H_2O_2 and $\text{Ru}(\text{bpy})_3^{2+}/\text{TPrA}$	-	Screen-printing	TPrA and	8.7	CCD	[23]
					H_2O_2	46.6		
Cloth	C-BPE	Luminol/ H_2O_2 and $\text{Ru}(\text{bpy})_3^{2+}/\text{TPrA}$	GOD	Screen-printing	TPrA	85	CCD	[33]
					H_2O_2	24		
					Glucose	195		
Filter paper	O-BPE	Luminol/ H_2O_2	GOD	Screen-printing	H_2O_2	1.75	Smartphone	[34]
					Glucose	17		
Cloth	O-U-BPE	Luminol/ H_2O_2	GOD	Screen-printing	H_2O_2	24	CCD	[35]
					Glucose	23		
Filter paper	O-U-BPE	Luminol/ H_2O_2	COx, LOx and ChOx	Screen-printing	H_2O_2	0.424	CCD	[36]
					Choline	0.573		
					Lactate	3.132		
					Cholesterol	7.418		

ITO glass	C-BPE	Ru(bpy) ₃ ²⁺ /TPrA	-	Screen-printing	HL-60 cancer cells	80 cells/mL	CCD	[37]
Paper	O-BPE	Ru(phen) ₂ dpz] ²⁺ /TPrA	-	Screen-printing	DNA of Listeria monocytogenes	10 copies/μL	PMT	[38]
Cloth	O-BPE	Luminol/H ₂ O ₂ and Ru(bpy) ₃ ²⁺ /TPrA	GOD	Screen-printing	TPrA	1.265	CCD	[21]
					H ₂ O ₂	27		
					Glucose	32		
Paper	-	Ru(bpy) ₃ ²⁺ /TPrA	-	Screen-printing	2-(dibutylamino)-ethanol (DBAE)	0.9	Smartphone	[39]
					Nicotinamide adenine dinucleotide	72		
Paper	-	Luminol/H ₂ O ₂	LOx	Screen-printing	Lactate	5	PMT	[40]
ITO glass	-	Luminol/H ₂ O ₂	GOD, COX and LOX	Photolithography	Glucose	14	CCD	[41]
					Choline	97		
					Lactate	40		
PI	O-BPE	Luminol/H ₂ O ₂	GOD	LIG	H ₂ O ₂	5.87	Smartphone	[42]
					Glucose	0.138		
PI	SE	Luminol/H ₂ O ₂	No enzymes used	LIG	H ₂ O ₂	1.71	Smartphone	[43]
					Glucose	3.76		
					Xanthine	1.25		
					Dopamine	3.40		
PI	O-U-BPE	Luminol/H ₂ O ₂	No enzymes used	LIG	H ₂ O ₂	4.36	Smartphone	[10]
					Glucose	2.51		
					Choline	4.01		
					Lactate	5.32		
PI	O-U-BPE and SE	Luminol/H ₂ O ₂	No enzymes used	LIG	Vitamin B ₁₂	0.107 nM and 0.094 nM	Smartphone	[44]
ITO glass	SE	Luminol/H ₂ O ₂	-	Other	H ₂ O ₂	0.27	Smartphone	[45]

ITO glass	SE	Luminol/H ₂ O ₂	-	Other	H ₂ O ₂	0.26	PMT	[30]
3DP	O-BPE	Luminol/H ₂ O ₂ and Luminol/O ₂	GOD	Other	H ₂ O ₂	0.069	Smartphone	[46]
					O ₂	0.15(mg/L)		
					CO ₂	0.45(mg/L)		
					Glucose	0.31		
<p>O-BPE = Open bipolar electrode, C-BPE = Closed bipolar electrode, ITO = Indium tin oxide, SE = Single electrode, O-U-BPE = Open U-shaped bipolar electrode, PI = Polyimide, LIG = Laser-induced graphene, GOD = Glucose oxidase, CO_x = Choline oxidase, LO_x = Lactate oxidase, ChO_x = Cholesterol oxidase. CCD = Charge-coupled device, PMT = Photomultiplier tube</p>								

1.7 Gaps in existing research and possible solutions

Various researchers have made significant efforts in recent years to develop a miniaturized ECL framework suitable for diversified real-world applications. Even though a lot of work has been reported to realize miniaturized ECL devices, still, there is a significant gap to make such devices commercially viable:

- Screen-printing technique has been widely used to fabricate paper and cloth-based ECL devices. As the screen-printing method necessitates a number of fabrication steps, one-step fabrication of ECL devices using screen-printing methodology is not possible, resulting in a complex and time-consuming process.
- In most cases, the PMT and CCD have been employed to capture the ECL signal. As the cost of such a detector is very high, the overall cost of the ECL imaging system increases.
- Several studies have reported that an external power supply is required to power the ECL device as well as to the ECL image capturing systems (PMT or CCD), which makes the overall ECL system bulky and prevents such systems from being used as a portable system.
- To the best of our knowledge, no one has reported sensing of more than one analyte using a single ECL platform.
- For the most part, people have used ImageJ or MATLAB-based coding to analyses of ECL signals (to calculate the ECL signal intensity). This is a time-consuming process that necessarily involves the use of professionals to measure the ECL signal intensity.

To address the aforementioned challenges, the following possible solutions are proposed:

- Laser written and 3D-printed ECL platforms would be the best solution because they offer several advantages over traditional fabrication methods, including fast prototyping and one-step fabrication with high repeatability and reproducibility.
- Low-cost, quick-response multichannel ECL platforms based on smartphones imaging systems would be the best solution for simultaneous sensing of multiple analytes.
- Hence, 3D-printed or Laser written miniaturized, portable, and low-cost platform embedded with a smartphone to perform a variety of functions should be developed. The smartphone can power the ECL device, capture the ECL signal, and calculate the ECL signal intensity value by using a customized application which can transfer data wirelessly/IoT to a medical practitioner.
- Addition of Machine learning approach would be the revolutionary to predict the concentration of biomarkers based on intensity values. Fig. 2 is the proposed schematic of the ECL system to overcome the aforementioned challenges.

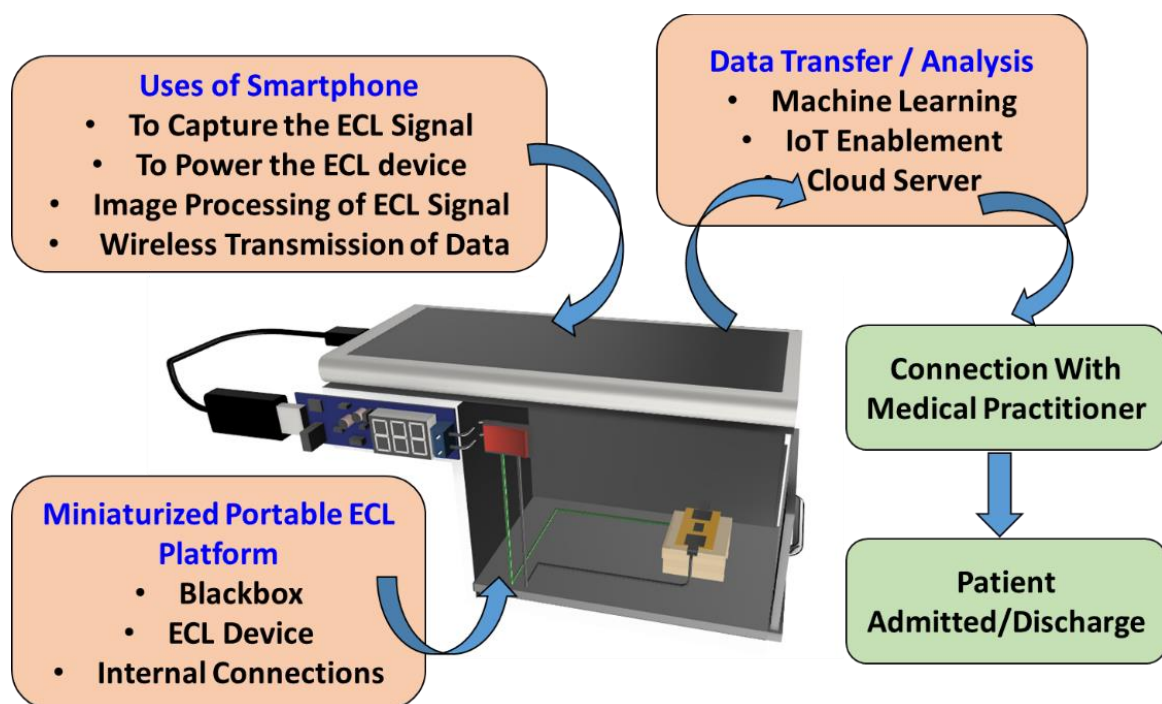


Figure 1.4 Proposed schematic of ECL system to overcome the challenges.

1.8 Objectives of the Ph.D. thesis work

This study intended to develop a cost-efficient, miniaturized, portable smartphone based ECL system to detect various biomarkers such as glucose, cholesterol, dopamine, choline, lactate, and vitamins (C and B₁₂.) The overall objectives of this work are as mentioned below:

- i. Fabrication of microfluidic ECL device for biosensing applications.
- ii. Characterization and optimization of microfluidic ECL devices for various biosensing applications.
- iii. Use of Machine Learning approach to reliably predict the unknown concentrations of various biomarkers.
- iv. Prototype development and sensing of various biomarkers using a portable and PoC ECL system.

1.9 Organization of Ph.D. thesis

In this Ph.D. thesis, aligned with the objectives, the methodology, results and discussions are provided here and arranged as chapters. The contents of the thesis have been organized into 6 chapters as described:

Chapter 1: The thesis begins with establishing the background and need for the work. The chapter further describes various fundamentals pertaining to the detailed work. Fundamental of ECL, different ECL systems are explained in this chapter. Existing research gaps and probable solutions followed with objective of the Ph.D. work are thoroughly explained in this chapter.

Chapter 2: In this chapter, comprehensive discussion is carried out on Laser-Induced Graphene based ECL Devices. In depth explanation regarding material selection, fabrication, characterization, and validation is provided in this chapter. Open bipolar, closed bipolar and single electrode LIG-based ECL devices and their applications are thoroughly explained in this chapter. How the fabricated LIG based ECL devices were used to detect H₂O₂, and Glucose are explained in-depth.

Chapter 3: Here, thorough discussion is carried out on three-dimensional printing based ECL devices. In depth explanation regarding material selection, fabrication, characterization, and validation is provided in this chapter. Closed bipolar and single electrode 3DP ECL devices and their applications are explicitly explained in this chapter.

Chapter 4: In this chapter, in-depth discussion is carried out on paper based ECL devices. Detailed explanation regarding material selection, fabrication, characterization, and validation is provided in this chapter. Paper based single electrode ECL devices, and their applications are explicitly explained in this chapter.

Chapter 5: This chapter describes the fabrication of 3DP ECL devices, and their application in the field of biomarkers detection. Regression based machine learning (ML) algorithms were effectively used to predict the different biomarkers and compared the performance of different ML algorithms based on different regression metrics. Finally, the device performance was validated by doing the real sample analysis.

Chapter 6: In this chapter, important findings are summarized, and inferences are described. The limitations of present work along with the future scope have also been discussed in the concluding chapter.

1.10 Summary

This chapter lays foundation for the thesis. The chapter begins with the background and need of the work carried out as a part of this thesis. The fundamentals of ECL and its salient features have been discussed thoroughly. Followed by fundamentals of ECL various ECL system, such as bipolar and single electrode-based systems, have been explained in detailed. Later different fabrication methods were introduced followed by benchmark research work reported on ECL devices. At the end of the chapter, the objectives, work plan and organization of the thesis work have also been discussed. With this chapter dealing with introductory discussion, the following chapter covers fabrication of ECL systems using by exploring various fabrication methods to detect various biomarkers.

Chapter 2. Laser-Induced Graphene Based ECL Devices

In this chapter, comprehensive discussion is carried out on Laser-Induced Graphene Based ECL Devices. Detailed explanation regarding material selection, fabrication, characterization, and validation is provided in this chapter. Open bipolar, closed bipolar and single electrode LIG-based ECL devices and their applications are also thoroughly explained here.

2.1 Introduction to Laser-Induced Graphene

Laser assistant processing techniques have proven to be a powerful tool in different applications from surgical pathology to manufacturing materials. Laser-based devices have increased the attention of the researchers because of their high performance and high capacity of patterning [47][48]. At an ambient temperature and optimized parameters (speed and power), Laser-Induced Graphene (LIG) material is produced by ablating CO₂ laser directly over a relevant material [49]. LIG provides several benefits like high thermal steadiness, huge surface area and very high conductivity. Taking advantage of those properties provided by LIG, now such devices are used in wide applications, such as sensing, energy harvesting and electrocatalysis even in miniaturized or microfluidic scale [50][51].

Recently, polyimide (PI) has gained huge acceptance for CO₂ laser ablation as it provides graphene in a single step with remarkable morphological, electrical, chemical and physicochemical properties [50]–[52]. By carbonization, CO₂ laser transforms the nonconducting surface of PI into conducting zone. Accordingly, LIG is produced when sp³ carbon atoms get converted into sp² carbon atoms due to the ablation of CO₂ laser over PI surface. The CO₂ laser directed polyimide material is used in several applications such as electromechanical systems, energy harvesting and biomedical. Furthermore, the fabrication of devices using CO₂ laser directed PI offers many advantages such as low-cost fabrication, more relativity, greater stability, easy reproducibility and rapid prototyping [53][51].

2.2 LIG-Based Open Bipolar Electrode ECL Device

Bipolar electrode (BPE) based ECL sensing devices have become popular and received much attention because of the absence of background signal, high specificity, good selectivity, simplified instrumentation and good controllability. In addition, BPE-ECL based devices have added advantages like fast processing, ease-of-use and multiplexing [19][23]. The open BPE-based ECL device have only one electrode, which acts as both the anode and cathode without a direct electrical connection to applied external potential as compared with the conventional

three-electrode systems [25]. In the case of O-BPE-ECL, the BPE is completely immersed into the channel, and two driving electrodes (DEs) are connected at the end of the channel. One of the unique facets of BPE-ECL devices is that the orientation of poles of the BPE has opposite polarity to the DEs. After applying a sufficient voltage to DEs, an electric field gets generated across the channel, leading to a redox reaction (reduction and oxidation) at the opposite poles of the BPE (working electrode). At the anode and cathode of the BPE, simultaneous oxidation and reduction occur, and an ECL signal is generated at the anode.

2.2.1 Fabrication flow for LIG based Open BPE-based ECL device (LIG-BPE-ECL)

Fabrication process of the device is displayed in Figure 2.1. First, the required design was drawn in CorelDraw X7. By choosing an appropriate power and speed of CO₂ laser, LIG has been produced over PI material. The formation of LIG over PI surface is highly depends on the speed and power of CO₂ laser and it varies application to application. In various applications such as energy harvesting [50], [53] and biomedical sensing [54] different speed (4.5 %) and power (6.5 %) of CO₂ laser have been used. When CO₂ laser was induced over polyimide sheet, with carbonization process, the non-conductive surface turns to be conductive surface.

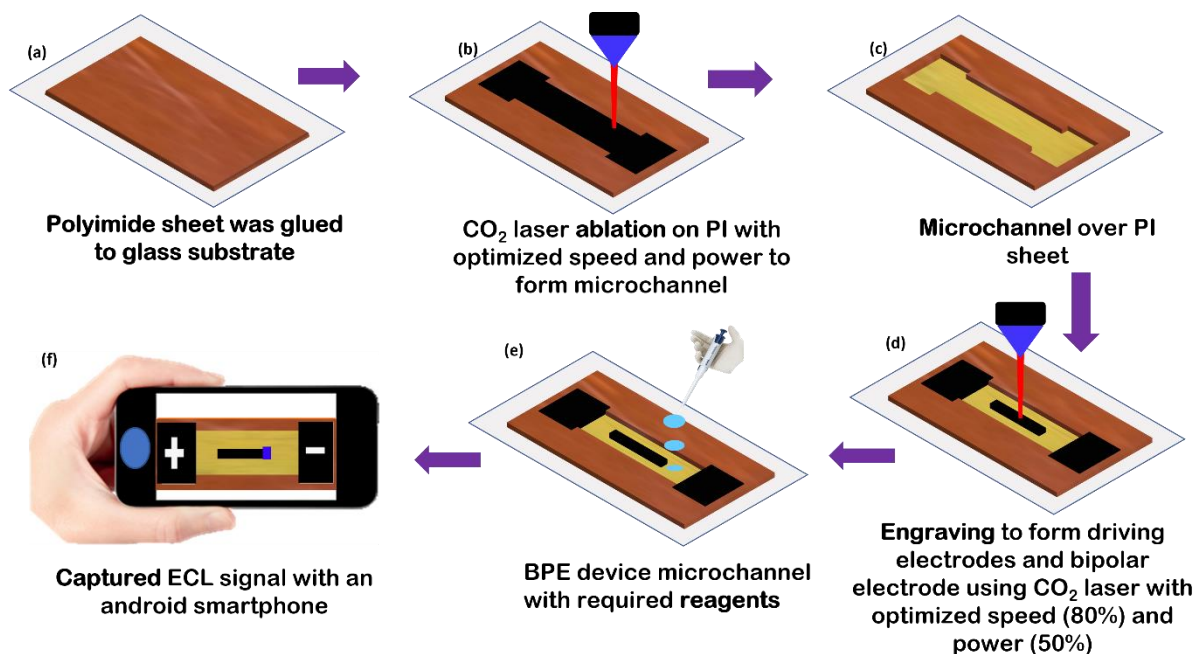


Figure 2.1 Fabrication Process for LIG-BPE-ECL Device. (a) Polyimide (PI) sheet (250 μm thickness). (b) Laser induced graphene. (c) Formation of microfluidics channel over PI. (d) fabricated engraved microchannel with DE and BPE. (e) Pipetting microfluidic channel with required ECL reagents. (f) Detection of ECL signal using mobile phone.

Subsequently, after numerous trials, for fabricating a microchannel, the CO₂ laser was again induced over PI surface with optimized power (50%) and speed (10%) as revealed in Figure 2.1 (b). Then, PI surface was cleaned using acetone and DI water, and kept for drying at room temperature for 5 min. Therefore, with the optimized parameters of CO₂ laser, a microchannel has been crated over PI surface as shown in Figure 2.1 (c). In the proposed work, after numerous trials the optimized speed (80 %) and power (50 %) was used to form LIG over the surface of PI. With optimized power and speed of CO₂ laser, engraving process has been accomplished to form the DEs and BPE over microchannel shown in Figure 2.1 (d). Once the channel is filled with required reagents and on application of optimized voltage, ECL signal gets generated over the surface of BPE electrode, shown in Figure 2.1 (e) and (f).

2.2.2 Materials and Reagents

Commercially available Polyimide sheet (250 μm thickness) was procured from Dali Electronics India. A CO₂ laser (VLS 3.60 from Universal Laser System, AZ, USA) was used to fabricate LIG BPE-ECL device. eHUB DC-DC 5V to 1.2-24 V USB step-up step-down adjustable power supply module boost buck converter was used to provide external voltage to LIG BPE-ECL. An android smartphone was used to capture ECL signal as well as to drive the adjustable power supply using an OTG cable adapter.

Luminol 97%, Hydrogen Peroxide (H₂O₂) 35%, D- Glucose, and Glucose Oxidase (GO_x), from *Aspergillus Niger* were procured from Sigma Aldrich, India. The additional analytical grade reagents such as Sodium hydroxide (NaOH), Phosphoric Acid, acetone, isopropyl alcohol and were purchased from SRL Chemicals, India. All the chemical preparations were accomplished in DI water. 10 mM solution of luminol stock solution was prepared in 50 ml DI water. As luminol is not soluble in water, but it is soluble in base, 0.1 M base solution was prepared with the help of Sodium hydroxide (NaOH). Then, 47 mL DI water, 3 mL base solution and luminol were mixed to form 10 mM luminol concentration. As ECL signal is highly dependent over luminol concentration, so for optimization, different molar concentration luminol were prepared using stock solution. ECL signal intensity is also highly dependent on pH concentration, hence luminol solutions with different pH values have been prepared by using base (NaOH) and acid (Phosphoric Acid). For the detection of glucose, GO_x (Glucose oxidase) has been immobilized over bipolar electrode [28]. Here, 5 μL GO_x solution has been drop casted on the surface of BPE anode and kept for 5 min at room temperature for immobilization. Enzymes are important biological reagents that are widely used in various applications,

including diagnostic assays, therapeutic treatments, and research studies. The cost, stability, and shelf-life of these reagents are critical factors that can impact their suitability and effectiveness for different applications. The cost of enzymes can vary widely depending on the source, quality, and quantity required. Stability and shelf-life are also important considerations for enzymes. Enzymes can be susceptible to denaturation and degradation over time, especially if they are exposed to unfavourable conditions such as high temperature. Antibodies can also be subject to degradation, as well as to changes in conformation or binding affinity over time. It is important to store enzymes and antibodies under appropriate conditions, such as at the appropriate temperature and pH, to ensure their stability and prolong their shelf-life.

For the real sample analysis, the random blood samples were taken with a blood sugar of 109 mg/ml (5.9 mM) calculated using GOD-POD (glucose oxidase-phenol-4-aminophenazone peroxidase) method. In the GOD-POD method, a sample of glucose is combined with a solution of phenol-4-aminophenazone and GOx (Glucose Oxidase). The reaction between glucose and GOx produces H_2O_2 , which, in the presence of peroxidase, interacts with phenol-4-aminophenazone to produce a colourful product. A spectrophotometer may be used to detect the intensity of the colour produced, which is directly proportional to the concentration of glucose in the sample. This test and sample collection was carried out at the Medical Center of BITS Pilani Hyderabad campus, India. This was performed using semi-automatic analyser (ERBA CHEM -7 Biochemistry Analyzer for Hospital Use) and centrifuged for at least 15 minutes at 2200 RPM for serum separation. Prior to experimentation, it was further diluted in PBS (0.1 M, pH = 7).

2.2.3 Data acquisition and analysis

In this work, no external power supply was used to drive LIG BPE-ECL device. Commercially available eHUB DC-DC 5V to 1.2-24V USB step-up step-down adjustable power supply module boost buck converter was used to provide external voltage to LIG BPE-ECL. An android smartphone was used to drive the DC-to-DC buck boost converter. The smartphone was connected to DC-to-DC buck boost converter through USB data cable. The output of DC-to-DC buck boost converter was fed to LIG BPE-ECL device. The different values of voltages were obtained by using DC to DC buck boost converter and ECL signal intensity was calculated.

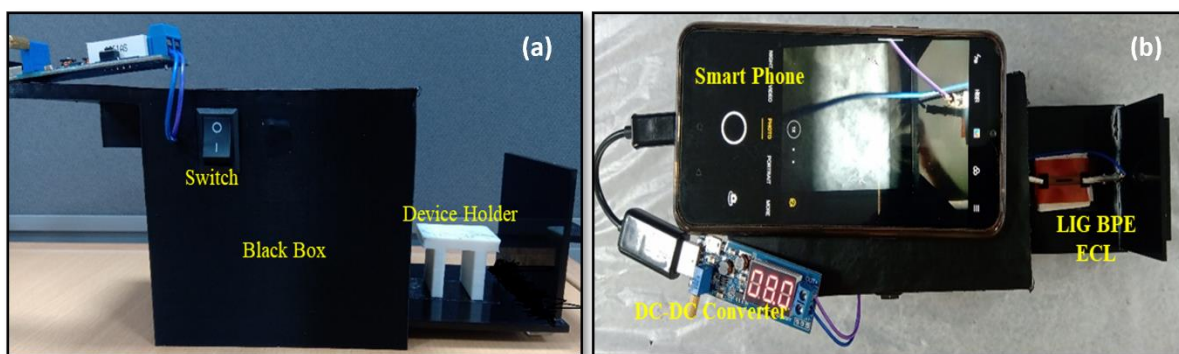


Figure 2.2 (a) 3D Printed black box with device holder. (b) LIG-BPE-ECL imaging sensing platform.

For data acquisition and analysis, the same Android smartphone and ImageJ Software (open ware free imaging software) were used. To capture image, the smartphone was perfectly aligned over anode of the bipolar electrode. For better analytical performance it is very essential to optimize the distance between BPEs and smartphone. Initially, it was observed that if the distance between BPE anode and smartphone was less than 10 cm, blur images were captured. On the other hand, if the distance between smartphone camera and BPE was more than 10 cm, low intensity ECL signal was captured. Hence, for reported work minimum distance between BPE anode and smartphone was kept at 10 cm. After capturing the ECL signal by the smartphone, the captured JPG images were analysed using ImageJ Software. Then to calculate the ECL intensity, each desirable image was cut into single picture and 2000 pixels high intensity area was considered for analysis and the mean gray value was obtained. The ECL imaging system is depicted in Figure 2.2.

2.2.4 Assay optimization for LIG-BPE-ECL device

Luminol/ H_2O_2 based electrochemical reactions were carried to validate the performance of ECL device. Following device fabrication, chemical preparation few important parameters were optimized on which ECL intensity is highly dependent. Width and length of BPE electrode, channel length, applied voltage, luminol concentration and pH were thoroughly studied. First, it was observed that increasing the width and length of microchannel, consumption of reagent and applied voltage will increase. Hence, it affects the stability of electric field. This aspect should be kept in consideration, accordingly herein, the total channel length (including length of driving electrode and BPE containing channel) was optimized to 32 mm.

The ECL signal intensity is highly dependent on luminol concentration, hence optimization of luminol has been carried out by varying it from 1 mM to 7 mM as shown in Figure 2.3 (a). As can be seen, the ECL signal intensity increased linearly in the luminol concentration window of 1 to 4 mM, which may be because the rate of luminol endoperoxide formation has increased with the increased concentration of luminol. In the absence of luminol, the obtained ECL signal was equivalent to the background signal. Here, the highest ECL signal intensity was obtained at 4 mM luminol concentration. As the concentration of luminol increased above 4 mM, it was found that ECL signal intensity reduced, this was because of assertion of self-quenching phenomenon due to higher concentration of the luminol [55]. The ECL signal intensity was measured in the relative light unit (RLU). RLU refers to the amount of light that is available at a specific area or region, compared to the amount of light that would be present in the standardized conditions. In scientific terms, relative light intensity is often measured in lux or foot candles and is a way of quantifying the amount of light that is available for various applications. Moreover, RLU intensity is an important factor in the field of ECL, which is a technique used to detect and quantify targeted analytes based on their luminescent properties. In ECL, a luminophore is attached to an electrode surface, and when an electrical potential is applied to the electrode, the luminophore undergoes an electrochemical reaction that results in the emission of light. The intensity of the light emitted by the luminophore is proportional to the amount of the target analyte present in the sample being tested. The RLU in ECL is important because it directly affects the sensitivity and detection limit of the technique. The presence of higher RLU promotes to quantify the even the trace amounts of the target analyte with greater accuracies, and vice versa.

The concentration of luminol was taken as 4 mM during the subsequent experiments. For the optimization of luminol, H_2O_2 was kept constant at 1 mM, applied voltage was taken 7 volts and luminol value was varied from 1 to 7 mM. Figure 2.3 (b). illustrates the graph between pH and ECL signal intensity where pH values varied from 7 to 12. It was observed that at pH value of 7, the obtained ECL signal was nearly equivalent to the background signal. As the pH value increases from 7 to 9, the ECL signal intensity also increased linearly which happened because of luminol based ECL reaction being more efficient in alkaline media. As the value of pH concentration increased above 9 it was found that ECL signal intensity has been reduced which was due to strong alkaline conditions leading to a decrease in the luminous quantum yield of the phthalate ion [56]. Hence, throughout the experimentation, pH value was kept as constant.

For the optimization of pH value, luminol concentration was kept to 4 mM, H₂O₂ as 1 mM and applied voltage was chosen to be 7 volts.

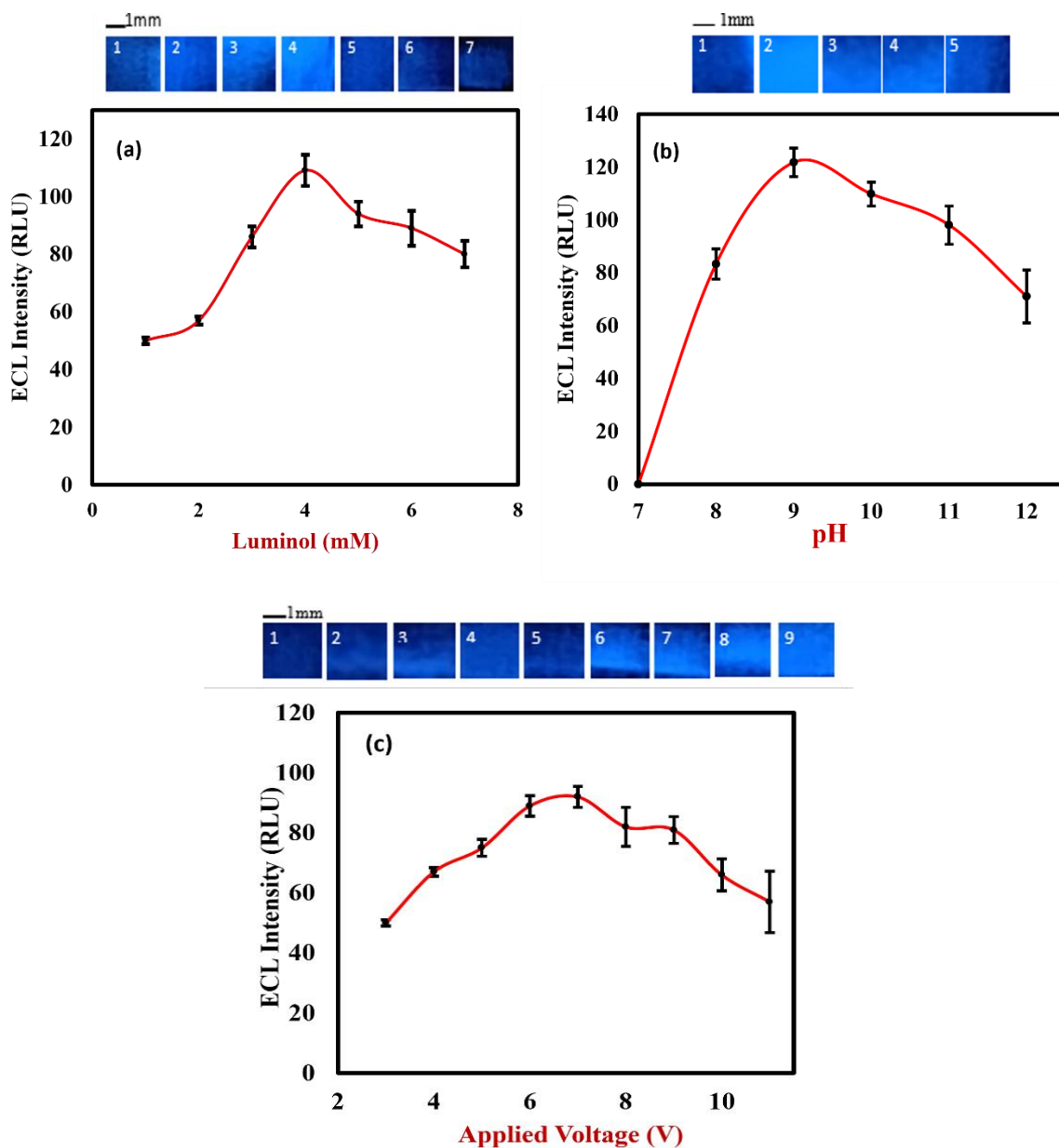


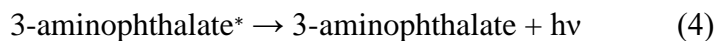
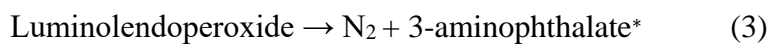
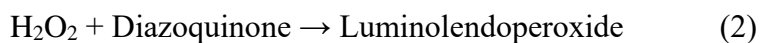
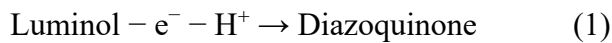
Figure 2.3 (a) Luminol (mM) Vs ECL Intensity (RLU); Luminol = 1, 2, 3, 4, 5, 6 and 7 mM; H₂O₂: 1 mM; Applied Voltage = 7 V. (b) pH Vs ECL Intensity (RLU); pH = 7, 8, 9, 10, 11 and 12; H₂O₂ = 1 mM; Luminol = 4 mM; Applied voltage = 7.0 V. (c) Applied Voltage (V) Vs ECL Intensity (RLU); Applied voltage = 3.0, 4.0, 5.0, 6.0, 7.0, 8.0, 9.0, 10 and 11 V; H₂O₂ = 1 mM; Luminol = 4 mM; pH = 9. Error bar representing the standard deviations for three independent experiments.

The driving voltage is one of the principle factors influencing the ECL signal for the given sensing network. Figure 2.3 (c). illustrates the relation between the applied voltage and the

ECL signal intensity. It was found that no chemical reaction took place between luminol and H₂O₂ when applied voltage was less than 3 V, and therefore no ECL signal was detected. When the applied voltage varied from 3 V to 7 V, the ECL signal intensity increased linearly. This happens because of an increase in the EC oxidation rate of luminol to form 3-aminophthalate. When the voltage was increased above 7 volts it was found that ECL signal intensity began to reduce [25][56][57]. This was because of the initiation of the background reaction, such as oxidation of water, due to application of high applied voltage. Oxidation of water forms oxygen that interferes ECL emission, both chemically and physically. For the optimization of applied voltage, luminol concentration was kept to 4 mM (pH= 9), H₂O₂ as 1 mM and applied voltage was varied from 3 V to 11 V.

2.2.5 Sensing of H₂O₂ and Glucose using LIG-BPE-ECL device

Figure 2.4 (a) replicates the relationship between H₂O₂ and ECL signals. H₂O₂ is widely used in cosmetics such as hair shining products, mouth fresheners, hand sanitizer, etc. But the excess concentration of H₂O₂ can affect the health of the human being. Here, both glucose and H₂O₂ detection are possibly due to intuitive nature of the ECL reaction mechanism. For the determination of H₂O₂ or Glucose, the luminescent reaction is widely applied which is based on Luminol/ H₂O₂. The reactions of luminol and H₂O₂ are given below.



Different concentrations of H₂O₂ (5 μM to 5000 μM) were taken and with respect every concentration ECL signal intensity has been calculated. ECL signal intensity increased linearly for the range of 5 μM to 100 μM as illustrated in Figure 2.4 (a). As a result, the limit of detection (LOD), was obtained to be 4.8729 μM (R² = 0.9658, n=3). This value of LOD is much less than the other materials i.e., Paper and cloth used for ECL sensing with the limit of detection 24 μM, 41 μM and 7.57 μM respectively [19][58][59]. For H₂O₂ sensing, luminol concentration was kept to 4 mM (pH=9), H₂O₂ was varied from 1 μM to 5000 μM, applied voltage kept constant to 7 volts. H₂O₂ sensing is the basics to determine glucose during ECL reaction.

The presented device has been successfully used to detect D-Glucose. Figure 2.4 (b) replicates the relationship between ECL signal and D-Glucose. To determine glucose, anode of BPE was modified with 3 μL GO_x (1 mg/mL) and the device was kept at room temperature for 5 minutes. Then, equal amounts of glucose and luminol were dropped into channel. The ECL signal intensity was linearly proportional to the concentration of glucose. The concentration of glucose was varied from 1 μM to 100 μM by keeping luminol (4 mM, pH=9), H_2O_2 (1 mM) and applied voltage (7 V) constant. The limit of detection (LOD) for the available data was calculated using prevailing techniques and for the developed device the LOD to detect glucose was found to be 0.138 μM ($R^2 = 0.9875$, $n=3$).

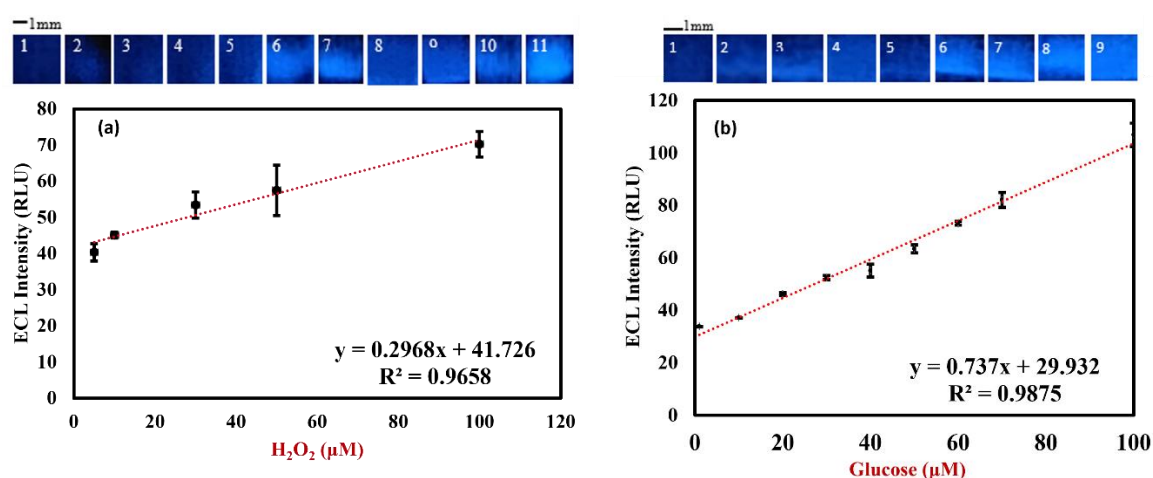


Figure 2.4 (a) H_2O_2 (μM) Vs ECL Intensity (RLU); H_2O_2 : 5, 10, 30, 50, 100, 1000, 2000, 3000, 4000 and 5000 μM ; Luminol = 4 mM; pH: 9; Applied Voltage = 7 V. (b) Glucose Vs ECL Intensity (RLU); Glucose: 1, 10, 20, 30, 40, 50, 60, 70 and 100 μM ; Luminol = 4 mM; pH: 9; H_2O_2 = 1 mM; Applied Voltage = 7 V. Error bar representing the standard deviations for three independent experiments.

2.2.6 Real sample analysis of H_2O_2 and Glucose using LIG-BPE-ECL device

Finally, real sample analysis has been performed using LIG-BPE-ECL system. The random blood sample was taken, and blood glucose was measured which was found to be 106 mg/dl (5.9 mM). Then obtained blood sugar was diluted to 20 μM and ECL intensity was calculated. Furthermore, different concentrations of glucose were spike into real samples and with respect to every spike, ECL intensity was calculated which is tabulated in following table. Applicability of LIG-BPE-ECL device was shown by the recovery values.

Table 2. 1 Real Sample Glucose Analysis in Human Serum

Clinical method (μM) (diluted)	This method (μM)	Added (μM)	Found (μM)	Recovery (%)
20	19.22	5	24.58	101.48
		10	29.48	100.88
		20	39.69	101.19

2.3 LIG-Based closed bipolar electrode ECL device

Though open BPE-ECL systems possess several key benefits, but it lacks the current efficiency and provide huge driving voltage background signal. Which ultimately leads to degradation of the overall performance of the open BPE-ECL systems. Xiaowei Zhang et. al. demonstrated the significance of current efficiency in O-BPE-ECL and C-BPE-ECL systems. The current efficiency (η_c) can be defined as it is the ratio of current flowing through the BPE (I_{BPE}) to the current flowing through the channel (I_{channel}) [26].

$$\eta_c = \left(\frac{I_{\text{BPE}}}{I_{\text{channel}}} \right) \dots \dots (1)$$

The channel current is a combination of two possible currents, ionic current (I_s) and faradaic current (I_{BPE}) flowing through the electrolyte and BPE respectively. In the case of open BPE-ECL, the majority of the channel current passes through the electrolytes, reducing current efficiency significantly. In the case of closed BPE-ECL, however, BPE connects two channels, namely reporting channel and supporting channel, so maximum current flows through only BPE, leading to provide up to 100 % current efficiency in ideal scenario [60]. Moreover, the generated background signal by the anode of DEs in open BPE is eliminated by closed BPE [58].

2.3.1 Design, fabrication, and sensing principle of two and three-channel LIG-Closed-BPE-ECL device (LIG-C-BPE-ECL)

To fabricate two and three channel closed BPE-ECL devices, the same fabrication steps were followed as depicted in Figure 2.1. Luminol/ H_2O_2 based chemical reactions were carried out to understand the working principle of the two-channel LIG-C-BPE-ECL system. The working principle of fabricated two and three-channel LIG-based C-BPE-ECL device with bipolar and driving electrodes is shown in Figure 2. 5 (a) and (b).

In the case of a two-channel LIG-C-BPE-ECL device, the anode and cathode of the BPE electrode are separately located in reporting channel and supporting channel respectively. To initiate the Luminol/H₂O₂ based chemical reactions, an external power supply was supplied to the positive and negative terminals of DEs which are placed in the supporting channel and reporting channel respectively. When the external potential was applied to the DEs, the potential difference (ΔE_{elec}) across the bipolar electrode can be determined using the following equation.

$$\Delta E_{ELEC} = E_{tot} \left[\frac{L_{ce} + L_{ae}}{L_{cc} + L_{ac}} \right] \dots \dots (2)$$

where, E_{TOT} = represents the applied external potential, L_{ce} (2 mm) and L_{ae} (2 mm) represents the total length of the BPE electrode excluding the length of BPE over which no solution was present, $L_{cc} + L_{ac}$ = represents the total distance between two DEs (10 mm). When ΔE_{elec} is sufficient across the BPE, the redox process (oxidation at anode and reduction at the cathode) at both the poles of BPE is triggered. For example, in the case of a two-channel LIG-C-BPE-ECL device, for Luminol/H₂O₂ based chemical reactions, the supporting channel was filled with PBS and reporting channel was filled with Luminol/H₂O₂. When an applied external potential is sufficient, Luminol/H₂O₂ is oxidized in the reporting channel and simultaneous reduction of O₂ takes place in the supporting channel leading to generate ECL signal at the anode of BPE which is shown in Figure 2.5 (a).

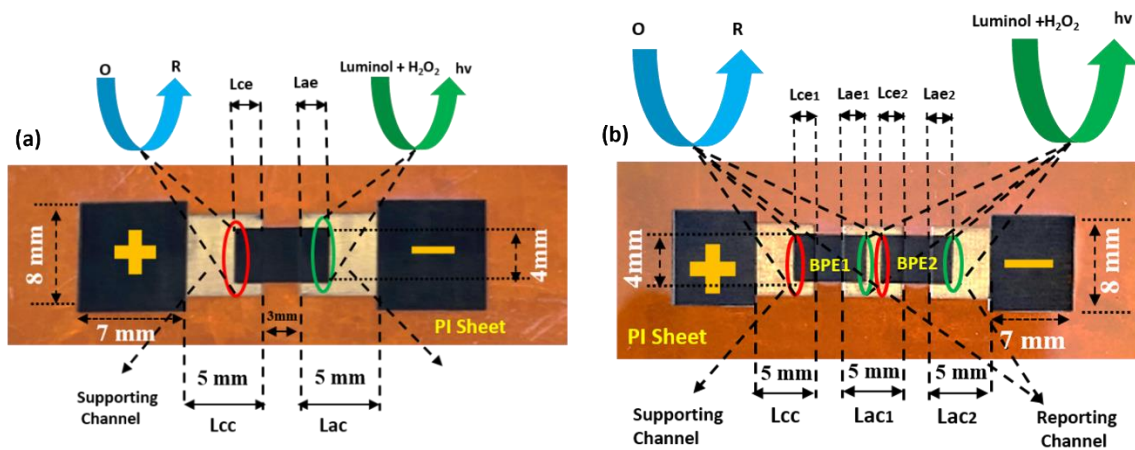


Figure 2.5 Final fabricated two and three-channel LIG-C-BPE-ECL devices, (a) Working principle of two-channel LIG based C-BPE-ECL device. (b) Working principle of three-channel LIG based C-BPE-ECL device with supporting and reporting channel, driving (DE) and bipolar (BPE) electrodes.

Similarly, in the case of a three-channel LIG-C-BPE-ECL device, two reporting and one supporting channel are present as illustrated in Figure 2.5 (b). When the applied external potential was adequate, concurrent oxidation and reduction took place at the opposite poles of BPE1 and BPE2 (oxidation at the anode and reduction at the cathode of BPE1 and BPE2) leading to generate ECL signal at the anode of BPE1 and BPE2. The potential difference (ΔE_{elec}) across the bipolar electrode (BPE1 and BPE2) can be determined using the following equation.

$$\Delta E_{ELEC} = E_{tot} \left[\frac{L_{ce1} + L_{ce2} + L_{ae1} + L_{ae2}}{L_{cc} + L_{ac1} + L_{ac2}} \right] \dots \dots (3)$$

where, L_{ce1} , L_{ce2} , L_{ae1} and L_{ae2} (2 mm each) represents the total length of BPE electrode excluding the length of BPE over which no solution was present, $L_{cc} + L_{ac1} + L_{ac2} =$ represents the total distance between two DEs (15 mm).

2.3.2 Characterization of LIG-C-BPE-ECL device

The surface morphological analysis of PI sheet before and after CO₂ laser ablation was carried out using SEM, as shown in Figure 2.6 (a) and (b), respectively. It was observed that no LIG was present over the bare PI sheet. When CO₂ laser was directed over PI sheet with optimized speed and power, showing honeycomb structure of graphene material, confirming the LIG material over PI sheet as illustrated in Figure 2.6 (b).

Then, as depicted in Figure. 2.6 (c), elemental characterization of LIG was performed using XPS showing carbon and oxygen contents of 97.61% and 2.39% respectively. Finally, to confirm the presence of graphene material, RAMAN Spectroscopy analysis was carried out which showed principal RAMAN peaks (D, G and 2D) as shown in Figure 4 (d). The I_D/I_G ratio measures the defects present in the LIG structure whereby the higher ratio (towards 1) shows more defects while the lower ratio (towards 0) shows less structural defects. Here, the ratio I_D/I_G was calculated to 0.53 confirming reasonably less structural defects in the formed LIG zones. Further, I_{2D}/I_G ratio was calculated to 0.58 confirming few layers (~ 10 to 15) of graphene material in the formed LIG zones [50][61]. Furthermore, the conductivity of the ECL device was measured using a standard four-point probe device. The conductivity analysis was carried out by increasing the input voltage to 2 V in 0.1 V increments for a total of 25 repetitions. The conductivity of the LIG sample was calculated to be 64.16 S/m for optimized CO₂ parameters (speed = 80% and power = 50%).

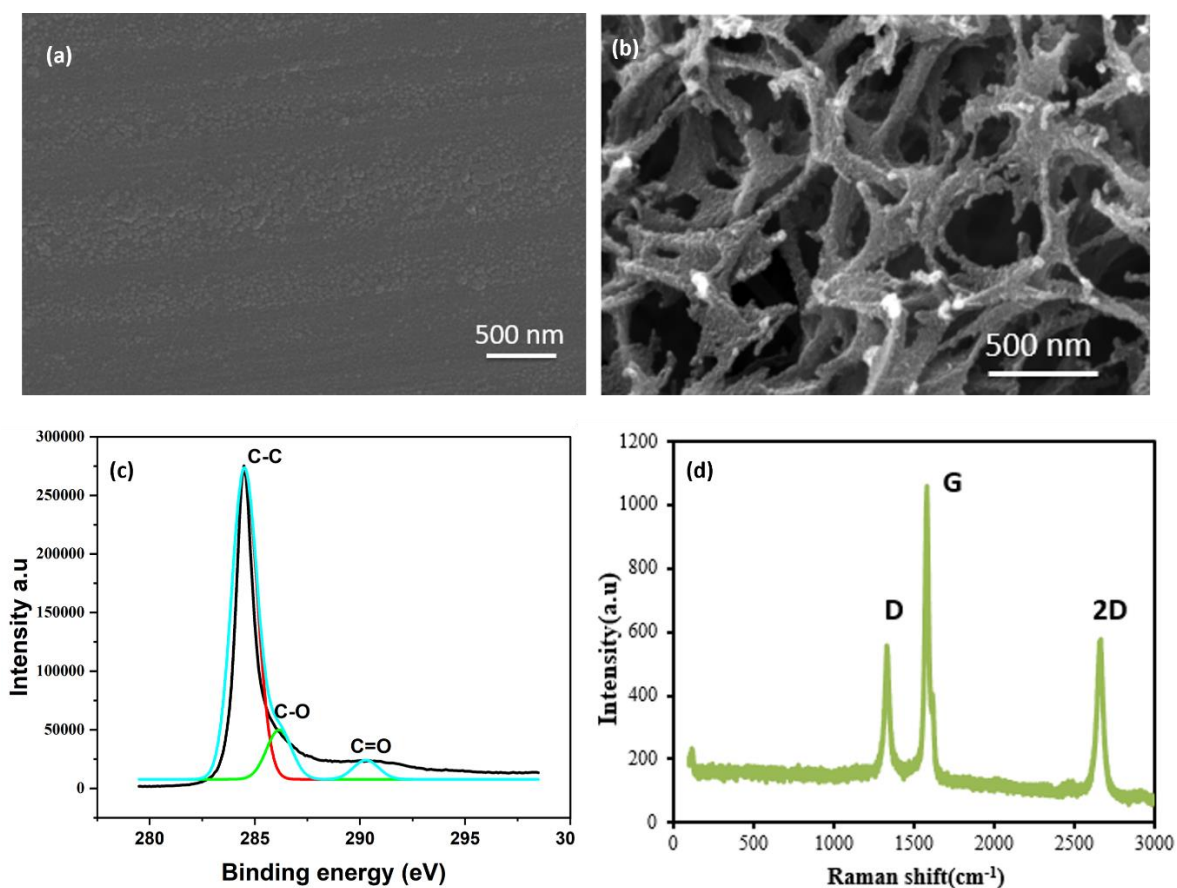


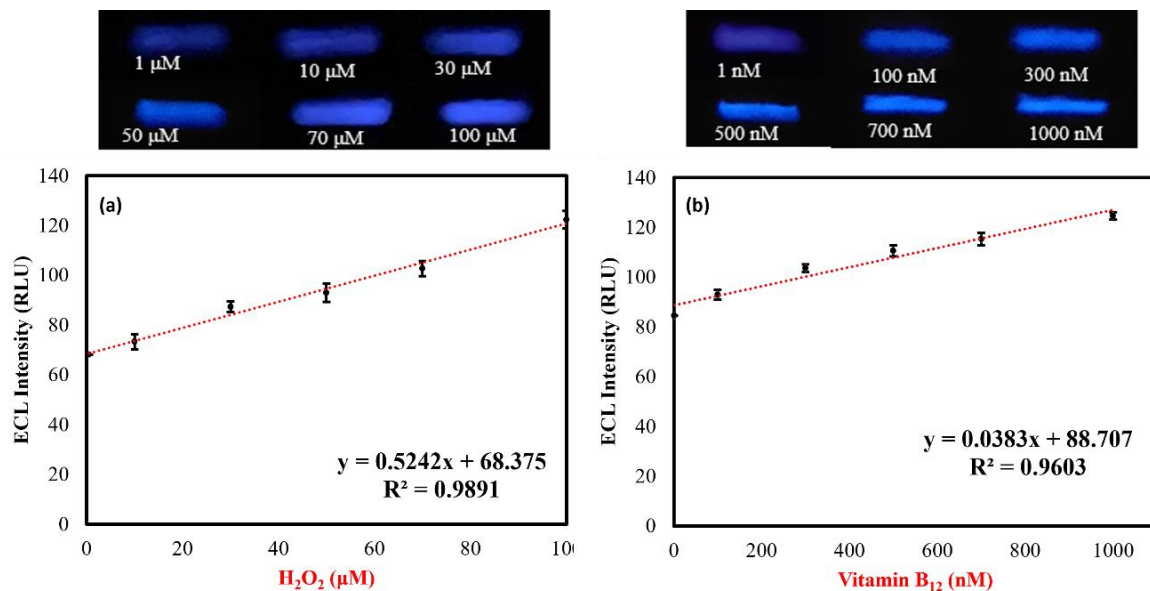
Figure 2.6 (a) Polyimide sheet before inducing CO₂ laser. (b) SEM image of polyimide sheet after inducing CO₂ laser. (c) XPS analysis of LIG based electrodes. (d) RAMAN Spectroscopy for the LIG based ECL device.

2.3.3 Analytical performance of two-channel LIG-C-BPE-ECL device

Herein, a fabricated LIG-C-BPE-ECL device was effectively demonstrated for the detection of hydrogen peroxide (H₂O₂), vitamin B₁₂ and vitamin C. Vitamins play a crucial role in the human metabolism system and are involved in various activities such as the immune system, metabolism of some compounds and in biosynthesis. For human metabolism, vitamin B₁₂ is very essential and its deficiency can lead to anemia and large red blood cells [62][63]. Vitamin B₁₂ natural values in the human body differ from 160 to 950 picograms per milliliter (pg/ml) or 0.118 to 0.7 nM [64]. Further, vitamin C (ascorbic acid) is an essential micronutrient and plays a vital role in the psychological system, whole deficiency may cause various diseases including scurvy. The normal range from vitamin C varies from 33.3 μM to 111 μM [65]. Evidently, H₂O₂ is the first step for the detection of glucose and is widely used in cosmetic products. Its excessive use may cause health related issues such as hair fall, skin burn and blisters [36]. Hence, herein, a compact, accurate and reliable laser-induced graphene-based

ECL system was developed for the sensing and monitoring of various analytes such as vitamin B₁₂, vitamin C, and H₂O₂. All the optimized parameters were used to detect H₂O₂ and Vitamins. ECL signal based on Luminol/ H₂O₂ chemical reactions is highly dependent on parameters such as the concentration of luminol, pH and applied external potential [66]. For Luminol/ H₂O₂ based chemical reactions, optimized values for luminol (4 mM), pH (9) and applied external potential (7 V) was taken from the section 2.2.4 [42].

To validate the adaptability of the fabricated two-channel LIG-C-BPE-ECL device, individual sensing of H₂O₂, Vitamin B₁₂ and Vitamin C have been carried out. The sensing of H₂O₂ was carried out in the linear range 0.5 to 100 μM with limit of detection (LOD) of 0.303 μM (R²= 0.98, n=3). The LOD was calculated by using the formula $LOD = \frac{3 * \delta}{m}$ where, m = slope and δ is standard deviation [67][68]. The relation between H₂O₂ and ECL intensity is shown in Figure 2.7 (a). The sensing of vitamin B₁₂ and vitamin C was performed by achieving linear range 0.5 to 1000 nM and 1 to 1000 μM with LoD 0.109 nM (R²=0.96, n=3) and 0.96 μM (R²=0.98, n=3) respectively illustrated in Figure 2.7 (b) and (c) respectively. The analytical performance of two-channel LIG-C-BPE-ECL device is tabulated in Table 2.2. These linear values of H₂O₂, vitamin B₁₂ and vitamin C were taken for the subsequent analysis using three-channel LIG-C-BPE-ECL system.



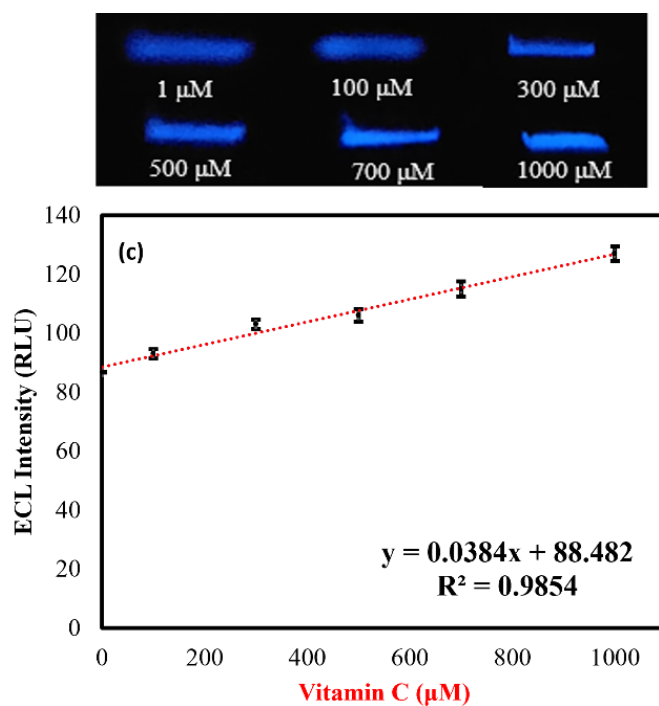


Figure 2.7 (a) H_2O_2 Vs ECL intensity (RLU): H_2O_2 varied from 0.5 to 100 μM , Applied Voltage = 7 V, Luminol = 4 mM (9 pH), (b) Vitamin B_{12} Vs ECL intensity (RLU): Vitamin B_{12} varied 0.5 to 1000 nM, Applied Voltage = 7 V, Luminol = 4 mM, (c) Vitamin C Vs ECL intensity (RLU): Vitamin C varied from 1 to 1000 μM , Applied Voltage = 7 V, Luminol = 4 mM.

Table 2. 2 Analytical performance of two-channel LIG-C-BPE-ECL device

Analytes	Linear range	Limit of detection (LOD)
H_2O_2	0.5 to 100 μM	0.303 μM
Vitamin B_{12}	0.5 to 1000 nM	0.109 nM
Vitamin C	1 to 1000 μM	0.96 μM

2.3.4 Analytical performance of two-channel LIG-C-BPE-ECL device

A Three-channel LIG-C-BPE-ECL device was fabricated for simultaneous enzyme less sensing of vitamin B_{12} and vitamin C. In the case of vitamin B_{12} and vitamin C, CH 1 was filled with luminol/vitamin B_{12} , CH 2 was filled with luminol/vitamin C and CH 3 was filled with PBS. The detailed information related to parameters used for the simultaneous detection of vitamin B_{12} and vitamin C using a three-channel LIG-C-BPE-ECL system is tabulated in Table 2.3.

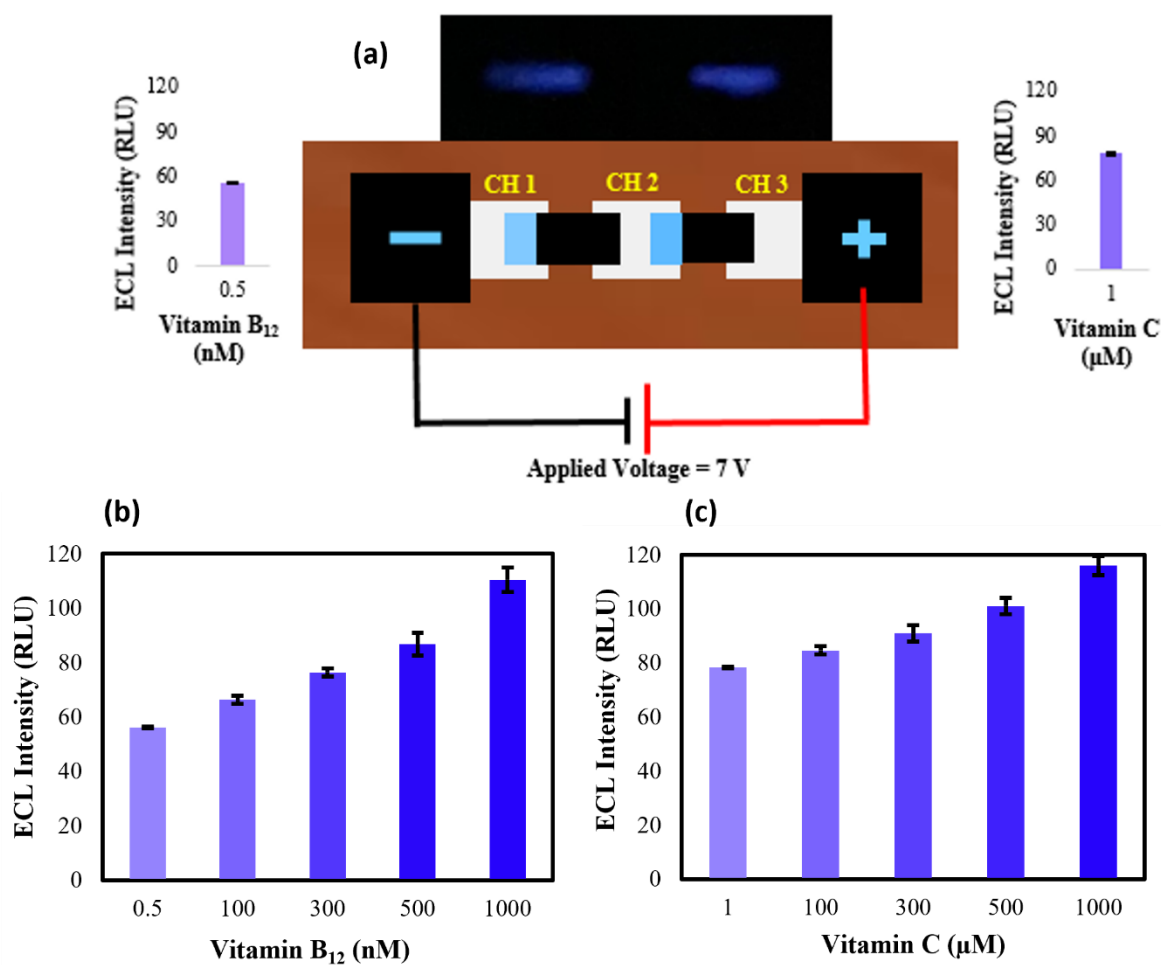


Figure 2.8 Simultaneous detection of Vitamin B₁₂ and Vitamin C. (a) 3 channel LIG-C-BPE-ECL system having Vitamin B₁₂ = 0.5 nM, Luminol = 4 mM, Vitamin C = 1 μM and PBS = 0.1 M, applied voltage = 7 V. (f) Bar graph for vitamin B₁₂ Vs ECL intensity (RLU). (g) Bar graph for vitamin C Vs ECL intensity (RLU), Error bar represents standard deviation for three experiments.

Table 2. 3 Parameters related to three-channel LIG-C-BPE-ECL for simultaneous sensing of vitamin B₁₂ and vitamin C.

Channel	Solution	Concentration
1	Luminol and Vitamin B ₁₂	Luminol (4 mM) and Vitamin B ₁₂ (0.5-1000 nM)
2	Luminol and Vitamin C	Luminol (4 mM) and Vitamin C (1-1000 μM)
3	PBS	PBS (pH = 7, 0.1 M)

For the production of H₂O₂ from graphene oxide and oxygen, optimized external voltage (7 V) was applied for the optimized time period (30 sec) followed by steering operation to initiate chemical reaction [69]–[71]. To obtain the ECL signal, the power supply was turned on and

successive generated ECL signals were captured by a smartphone. The concentration of vitamin B₁₂ and vitamin C varied from 0.5 to 1000 nM and 1 to 1000 μM respectively. As the concentration of vitamin B₁₂ and vitamin C increased from 0.5 to 1000 nM and 1 to 1000 μM, respectively, the ECL intensity was also augmented linearly. With each concentration of vitamin B₁₂ and vitamin C, ECL signal intensity was calculated, and resultant bar graphs were plotted as depicted in Figure 2.8 (b) and (c). Hence, successful simultaneous detection of vitamin B₁₂ and vitamin C has been accomplished with the help of three-channel LIG-C-BPE-ECL system.

2.3.5 Real sample analysis of Vitamin B₁₂ and Vitamin C using three-channel LIG-C-BPE-ECL

To strengthen the workability of three-channel LIG-C-BPE-ECL, real sample analysis for Vitamin B₁₂ and Vitamin C has been performed using the standard addition method and a good recovery rate was obtained. The following procedure was accomplished for real sample analysis using three-channel LIG-C-BPE-ECL.

Table 2. 4 Real sample analysis of vitamin B₁₂ and vitamin C using three-channel LIG C-BPE-ECL device.

Analytes	Added	Found	RSD (%)	Recovery (%)
Vitamin B ₁₂	100 nM	98.58 nM	2.29	98.58
	300 nM	306.3 nM	3.18	102.1
Vitamin C	50 μM	52.8 μM	3.78	105.6
	100 μM	104.23 μM	4.35	104.2

First, an unknown blood sample was diluted 10 times to prevent interference and to fit into the linear range. In addition, various concentration of vitamin B₁₂ and vitamin C were added into the real sample and ECL intensity was calculated with each added concentration. The recovery rate for different added concentration of vitamin B₁₂ and vitamin C are summarized in Table 2.4. Based on the obtained recovery values, the fabricated three-channel LIG-C-BPE-ECL device was found to be capable of being used in various biomedical applications in point-of-care testing (PoC). Table 2.5 shows the research summary on Vitamin B₁₂ and Vitamin C using different methods.

Table 2. 5 Research summary on Vitamin B₁₂ and Vitamin C using different methods.

Method	Electrodes	Linear range	LOD	Application	Data Acquisition	Ref.
EC	Three-electrode system	2.5 nM to 0.5 μ M	0.91 nM	Vitamin B ₁₂	Voltammetry	[63]
ECL	LIG based BPE and SE electrode	0.5 to 700 nM for BPE and 0.5 to 1000 nM for SE	107 And 94 pM	Vitamin B ₁₂	Smartphone	[44]
EC	Three-electrode system	240 to 1500 μ M	51 μ M	Vitamin C	Voltammetry	[72]
EC	Three-electrode system	0.1 to 1000 μ M	0.06 μ M	Vitamin C	Voltammetry	[73]
Fluorescent	Carbon Dots	0 to 60 μ M	100 μ M	Vitamin B ₁₂	Microscopy	[74]
EC	Three-electrode system	0 to 1500 pM	71.48 pM	Vitamin B ₁₂	Voltammetry	[75]
ECL	LIG based Closed BPE electrode	0.5 to 1000 nM for Vitamin B ₁₂ and 1 to 1000 μ M for Vitamin C	109 pM for Vitamin B ₁₂ and 0.96 μ M for Vitamin C	Vitamin B ₁₂ and Vitamin C	Smartphone	[2]

EC = Electrochemical, LIG = Laser-Induced Graphene, BPE = Bipolar Electrode, SE = Single Electrode.

2.4 LIG-Based Single Electrode ECL Device (LIG-SE-ECL)

For multiple analysis, the traditional electrochemical system and the bipolar electrochemical system harness multiple arrays of electrodes. Hence, it is very complex, time-consuming, and requires several fabrication steps to fabricate multiple electrode systems for diverse analysis [16][29]. In addition, SE based ECL signals eliminate the background signal generated by driving electrodes in BPE ECL system leads to improve the performance of ECL systems [16]. Hence, in this study, the LIG based SE-ECL device was fabricated and validated by sensing various analytes.

In this study non-enzymatic detection of xanthine and dopamine was performed using LIG-SE-ECL device. In human metabolism, a biological compound like xanthine, and dopamine play an important role. In the human body, during purine metabolic degradation, xanthine gets

produced, which is then oxidized to uric acid. Abnormalities in the concentration of metabolites lead to serious medical issues such as xanthinuria, toxemia during pregnancy, hyperuricemia, etc. [76][77]. Dopamine acts as a neurotransmitter, whereby it affects behavioural and physical activities performed by the human body such as kidney, heart, etc. Hence, monitoring dopamine helps to understand the functioning of the neurological system [76].

2.4.1 Design, fabrication, and sensing principle of Single Electrode LIG-ECL device (LIG-SE-ECL)

As shown in Figure 2.9 (a), LIG-SE-ECL system uses only one electrode pair rather than three electrodes (bipolar Electrode). Herein, two rectangular shape driving electrodes (DE) were connected at the end of the microfluidic channel. The optimized distance between the two driving electrodes was kept as 12 mm. The external voltage (V_{TOT}) was applied to the driving electrodes shown in Figure 2.9 (b). As the applied voltage was sufficient, it generated a potential difference between two driving electrodes, leading to the redox process (i.e. oxidation and reduction) [30]. Because of the applied external voltage, an electric field was developed across the microchannel. Very high intensity electric field was present at anode and the magnitude of electric field decreased linearly while moving towards cathode.

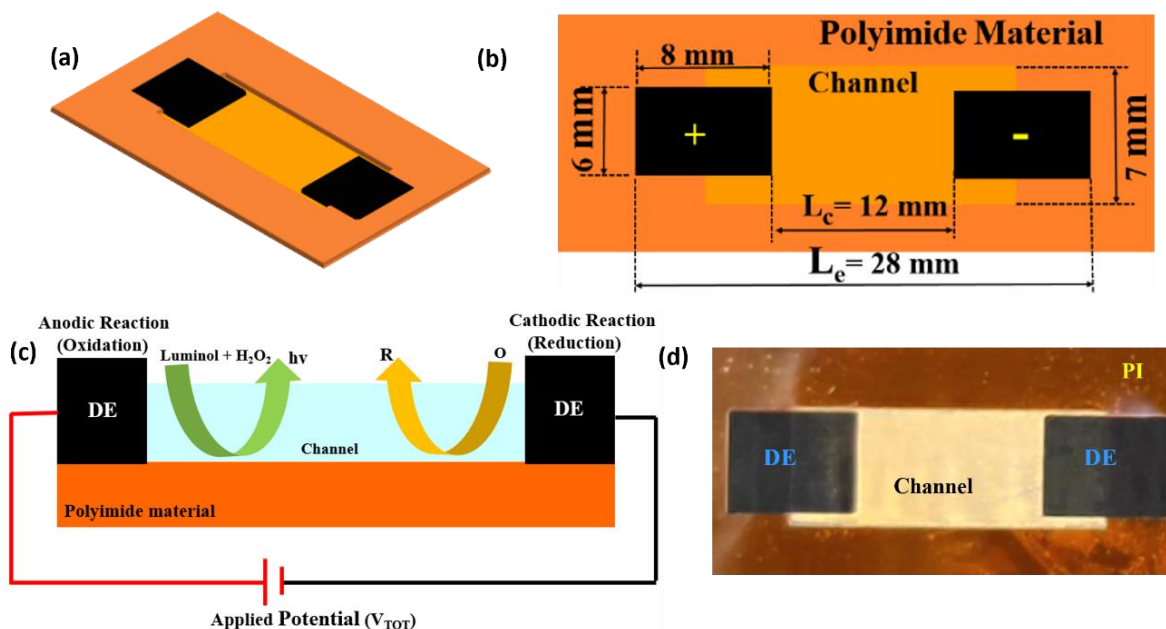


Figure 2.9 (a) 3D structure with microchannel depth (120 μm). (b) Schematic of Single Electrode laser Induced Graphene ECL (LIG-SE-ECL) system with device dimensions. (c) Working principle of LIG-SE-ECL device. (d) Fabricated LIG-SE-ECL device with driving electrode (8 mm x 6 mm) and fluidic channel (28 mm x 7 mm).

If the potential difference between two electrode (ΔE_C) is sufficient enough, then on the electrode surface oxidation and reduction is carried out simultaneously [45]. As depicted in Figure 2.9 (c) oxidation takes place because of the presence of luminol and hydrogen peroxide at the edge of anode, and reduction takes place because of the dissolved oxygen and hydrogen peroxide at the edge of cathode. Such phenomenon led to the generation of ECL signal at the edge of anode. Following procedure was followed to produce H_2O_2 using LIG-SE-ECL device. First, the solution was pipetted into microchannel ensuring contact with electrodes. Power supply was turned on to initiate H_2O_2 generation followed by steering the solution to initiate the chemical reaction [69]. The optimized time (60 sec) and voltage (7 V) conditions were used to produce H_2O_2 from oxygen and voltage reduced graphene oxide [70][71][78]. To observe the ECL signal, the power supply was again turned on and successive measurements were taken using a smartphone. Figure 2.9 (d) shows the final fabricated LIG-SE-ECL device on polyimide (PI) sheet with driving electrodes (DE) connected at the end of microfluidic channel.

2.4.2 Sensing of xanthine and dopamine using LIG-SE-ECL device

For the LIG-SE-ECL device, luminol/ H_2O_2 based electrochemistry were applied to quantify Xanthine and Dopamine. In the similar manner, LIG-SE-ECL device was efficiently used to determine xanthine and dopamine shown in Figure 2.10 (a) and (b) respectively.

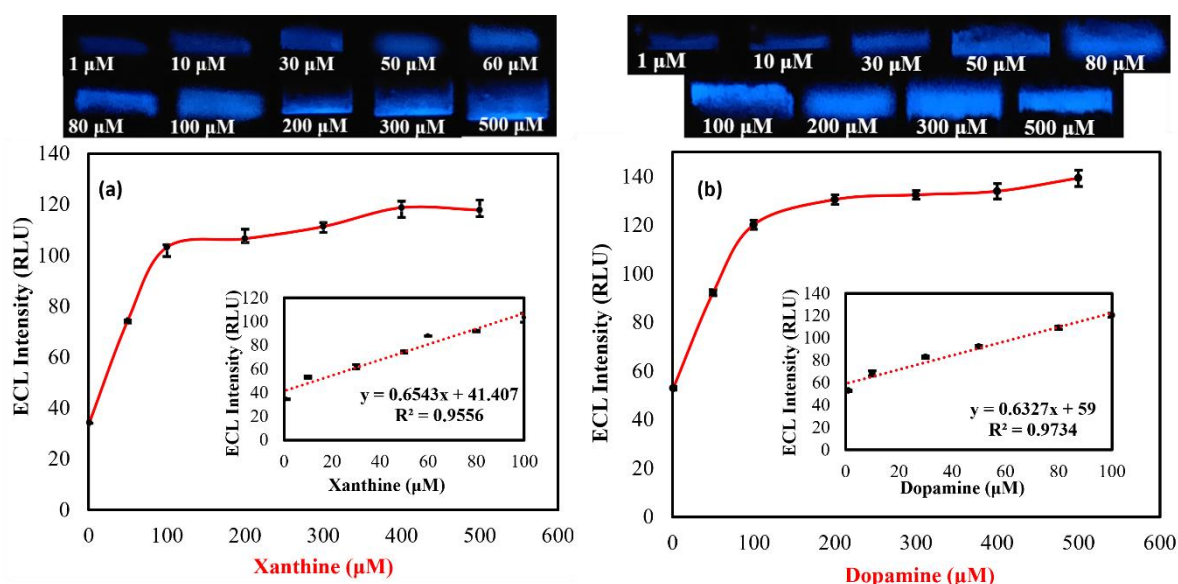


Figure 2.10 (a) Xanthine (μM) Vs ECL intensity (RLU). Xanthine = 0.1, 1, 10, 30, 50, 70, 100, 200, 300 and 500 μM ; Applied voltage = 7 V; Luminol = 5 mM (pH = 10). (b) Dopamine (μM) Vs ECL intensity (RLU). Dopamine = 0.1, 1, 10, 30, 50, 70, 100, 200, 300 and 500 μM ; Applied voltage = 7 V; Luminol = 5 mM (pH = 10); Error bar represents standard deviation for three independent experiments (n=3).

The concentrations of Xanthine and Dopamine varied from 0.1 μM to 500 μM . Under optimized conditions, LIG-SE-ECL device was utilized to determined xanthine and dopamine, with linear range 0.1 to 100 μM and detection limit of 1.25 μM ($R^2 = 0.9556$, $n = 3$) and 3.40 μM ($R^2 = 0.9734$), respectively.

2.4.3 Stability and Interference study of LIG-based electrode

Stability of electrodes plays an important role in their development and applications. Hence, to check the stability of LIG based electrode, several experiments has been performed for continuous 7 days and stability of LIG-based electrodes has been validated.

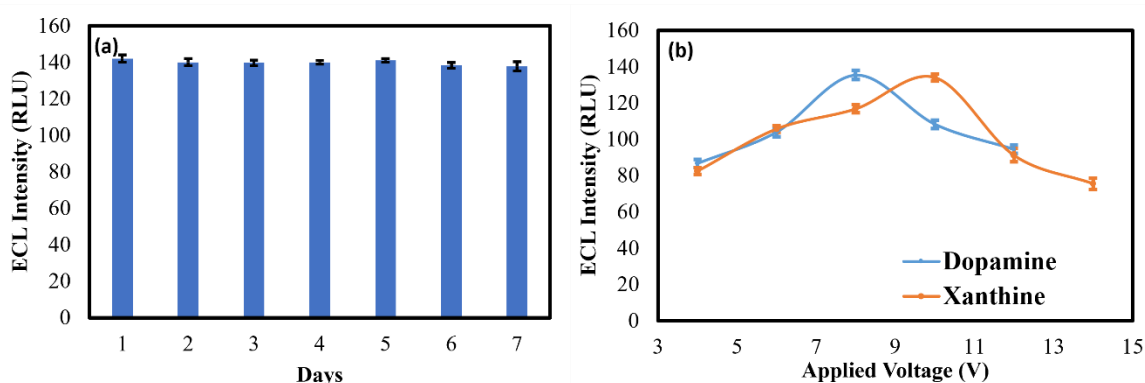


Figure 2.11 (a) Stability analysis of Laser Induced Graphene based electrodes. Applied voltage = 7 V; Luminol = 5 mM (pH = 10); H_2O_2 = 1 mM; Error bar represents standard deviation for three independent experiments. (b) Applied Voltage (V) Vs ECL Intensity (RLU); In panel, applied voltage = varied from 3 to 10 volts; luminol = 5 mM (pH = 10); in panel, Dopamine = 500 μM ; applied voltage = varied from 3 to 12 volts, luminol = 5 mM (pH = 10); in panel, Xanthine = 500 μM ; applied voltage: varied from 3 to 13 volts; luminol = 5 mM (pH = 10); Error bar represents standard deviation for three independent experiments ($n=3$).

Luminol/ H_2O_2 based ECL reactions were carried out to check the stability of proposed LIG based electrodes. As a result, it was observed that less than 5% change in ECL signal was observed. Hence, it was clearly evident that the LIG-SE-ECL device provides excellent stability for long duration and might be suitable for long transport in remote areas. Graphical representation of the stability analysis is provided in Figure 2.11 (a).

It is very essential to analyze the possible interference of these three biochemical with each other, as they co-exist in the physiological system. With no interference, when analytes are present together, they must give different values of ECL intensities, achieving good specificity of the ECL platform. Herein, rigorous interference study has been carried out by adopting the following procedure. First, Individual analytes were taken and dependency of each analytes

were determined with respect applied voltage. Herein, first experiment was conducted in which 20 μL of 5 mM of luminol and 20 μL of 500 μM dopamine were pipetted into the microchannel. Next, applied voltage was varied in the range of 3 to 12 volts. Then, with respect to every individual value of applied voltage, ECL intensity was calculated, and resultant graph was plotted which is shown in Figure 2. 11 (b). It was observed that in case of dopamine, at 8 V maximum ECL intensity signal was obtained. Similar approach was followed to perform interference study for xanthine, and it was observed that at 10 V maximum ECL intensity signal were obtained for xanthine. Finally, with those optimised voltage values, interference study was performed for the dopamine and xanthine.

Table 2. 6 Interference study of dopamine and xanthine

#	Xanthine		Dopamine		Luminol		% change
	C μM	V μL	C μM	V μL	C mM	V μL	
1	100	10	100	10	5	20	3.7
2	500	5	500	5	5	20	1.7
3	500	10	500	10	5	20	3.2
4	1000	10	1000	10	5	20	1.4
5	500	10	500	10	5	20	4.4
# = Experiments, C = Concentration, V = Volume							

As shown in Figure 2. 10 (b), the maximum ECL intensity was obtained for dopamine and xanthine at 8V and 10 V, respectively. Following procedure was followed for interference study of dopamine with other analytes for five different combinations summarized in Table 2. For instance, for combination 3, first, 500 μM dopamine (10 μL) and 5 mM luminol (20 μL) was pipetted into microchannel. Next, optimised value of applied voltage (8 V) was applied to the device and ECL intensity was calculated. Then, interference study was carried out by pipetting dopamine with other interfering compounds [xanthine = 500 μM (10 μL), glucose = 500 μM (10 μL)] in the microchannel. Here, during interference study, H_2O_2 was not considered because H_2O_2 acts as a coreactant for luminol and it was observed that if H_2O_2 would be added with other interfering components, then obtained ECL signal would be only because of H_2O_2 .

2.5 Summary of LIG-ECL devices

The development of LIG based ECL sensors and their applications to detect various analytes have been thoroughly discussed in this chapter. This work delves upon the development of the novel LIG-ECL device using a simple, inexpensive and rapid method by ablating a CO₂ laser on polyimide material. First, the LIG-BPE-ECL device was fabricated, and enzymatic detection of glucose was carried out using Luminol/H₂O₂ electrochemistry. With the optimized parameters, the imaging system was successfully used for the determination of Hydrogen Peroxide (H₂O₂) and D-Glucose, with detection of limit (LOD) 5.8729 μM and 0.138 μM, respectively. Second, LIG based two and three-channel closed bipolar systems (LIG-C-BPE-ECL) were developed for the sensing of vitamin c and B₁₂. Two-channel LIG-C-BPE-ECL device with Luminol/ H₂O₂ based chemical reaction was effectively utilized for the sensing of H₂O₂, Vitamin B₁₂ and Vitamin C for the linear range 0.5 to 100 μM, 0.5 to 1000 nM and 1 to 1000 μM with limit of detection (LOD) 0.303 μM, 0.109 nM, 0.96 μM, respectively. Simultaneous detection of Vitamin B₁₂ and Vitamin C was accomplished with the help of a three-channel LIG-C-BPE-ECL device. Finally, the LIG-SE-ECL device was fabricated, and its analytical performance was validated by sensing dopamine and xanthine. Under optimized conditions, LIG-SE-ECL device was utilized to determined xanthine and dopamine, with linear range 0.1 to 100 μM and detection limit of 1.25 μM ($R^2 = 0.9556$, $n = 3$) and 3.40 μM ($R^2 = 0.9734$) respectively. The smartphone not only captured the ECL signal but also powered the ECL device through DC-to-DC buck-boost converter. In the following chapter, it is shown how miniature ECL devices can be fabricated using a three-dimensional printing technique and how they could be utilized to detect different biomarkers.

Chapter 3. Three Dimensional Printed (3DP) ECL Devices

In this chapter, systematic discussion is carried out on three-dimensional printing based ECL devices. In depth explanation regarding material selection, fabrication, characterization, and validation is provided in this chapter. Closed bipolar and single electrode 3DP ECL devices and their applications are also explicitly explained here.

3.1 Introduction to 3DP-ECL devices

Three-dimensional printing (3DP) is a layer-by-layer fast prototyping or additive manufacturing technique that has piqued the interest of researchers and is widely used in diverse applications including automotive, defense industries [79][80], point-of-care testing, biochemical applications, Lab-on-chip, organ printing, industrial design, and healthcare [81][82]. When compared to traditional fabrication methods, such as photolithography, 3DP fabrication methodology provides various many crucial benefits such as low cost, fast prototyping [83], reduced manufacturing time, and complicated designs that may be easily created [84][85]. Further, numerous biochemical sensing techniques, such as chemiluminescence, electrochemical, electrochemiluminescence, are compatible with the 3DP technique [44][86]. However, selecting an optimal and adaptive detection methodology to incorporate 3DP devices for biochemical sensing is critical for such sensing techniques. Amongst them, ECL, whereby electrical energy is converted to the radiative one [17][87][88], is the most promising approach since it provides major advantages such as being very selective and sensitive, having a wide operating range, having minimal background noise, and many more [34][89].

3.2 3D printed closed bipolar ECL (3DP-C-BPE-ECL) device

Keeping the advantages of the C-BPE-ECL system in mind, 3D printed closed bipolar ECL (3DP-C-BPE) devices are developed for sensing choline and dopamine utilizing Luminol and Ruthenium-based chemistry respectively.

Evidently, nutrients, such as choline and dopamine, are essential for the correct functioning of the human body. Choline plays a significantly important role in the human body which regulates several essential body activities such as cell membrane development and neuron transmission. Choline deficiency can lead to dementia, genetic abnormalities in infants, muscle and liver disorders, and cardiovascular disease [41]. Bananas, peanut butter, peanuts, cauliflower, coffee, meat and eggs are the primary sources of choline [90]. Dopamine is an important neurotransmitter that transfers information among neurons [76] whose deficiency

may result in mood swings, motivation, cognition, mobility, kidney, cardiovascular functioning, and renal blood flow [43][91]. Hence, monitoring choline and dopamine levels is essential for humans to function correctly.

Understanding the importance of continuous monitoring of dopamine and choline, various research groups have developed different kinds of miniaturized ECL devices. Hyun J. Kwon and the group developed a three-electrode paper-based device integrated with mobile phone to sense the dopamine levels. They have used screen printing methods to fabricate electrodes [25]. Furthermore, Ruoyuan Zhang and his group developed a cloth based closed bipolar ECL device to sense DNA. $\text{Ru}(\text{bpy})_3^{2+}$ /TPPrA based electrochemistry was used for sensing purpose [30].

The objective of the present work is to study the performance of novel 3DP-C-BPE-ECL device by sensing choline and dopamine using smartphone and PMT based approach for comparative analysis. The 3DP-C-BPE-ECL devices were fabricated using conductive graphene filament with dual-extruder 3D printer.

3.2.1 Working principle and fabrication of 3DP-C-BPE-ECL

Figure 3.1 (a) depicts a representation of working of the 3DP-C-BPE-ECL device, which is based on chemical interactions involving $\text{Ru}(\text{bpy})_3^{2+}$ /TPPrA or Luminol/ H_2O_2 . Herein, electrodes (BPE and DEs) were fabricated using conductive graphene filament. The BPE anode and cathode were placed independently in the reporting and supporting channels.

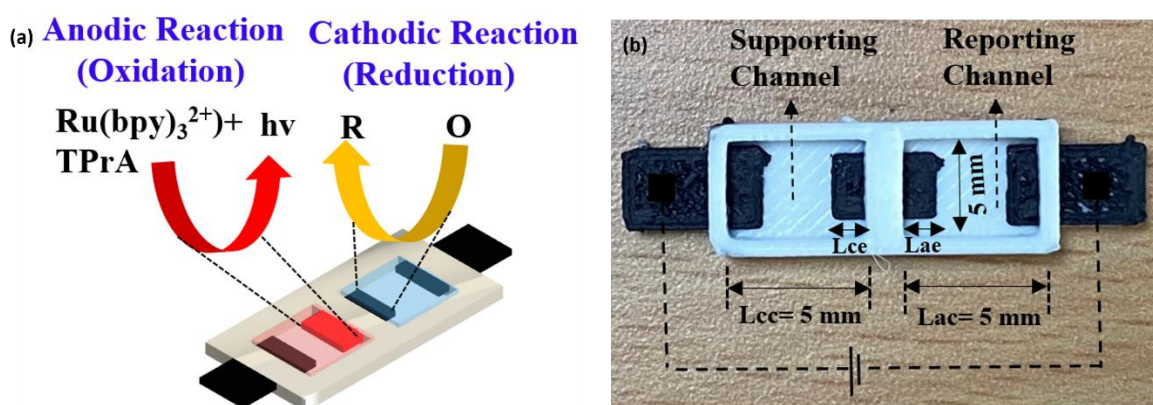


Figure 3.1 (a) Working concept of 3DP-BPE-ECL device. (b) Image of the final fabricated 3DP-C-BPE-ECL device showing the supporting and reporting channels, bipolar and driving electrodes.

The external “positive” and “negative” power supply connections were applied to the DEs that were positioned in the reporting and supporting channels to initiate the chemical reactions, as

shown in Figure 3.1 (b). To obtain the ECL signal, reporting channel was occupied with $\text{Ru}(\text{bpy})_3^{2+}/\text{TPrA}$ or Luminol/ H_2O_2 while supporting channel was filled with PBS solution. When external voltage (E_{TOT}) is adequate, strong electric field is produced across the channel, resulting initiations of faradic reaction at both the poles of BPE. Taking the case of $\text{Ru}(\text{bpy})_3^{2+}/\text{TPrA}$, when sufficient E_{TOT} is present, $\text{Ru}(\text{bpy})_3^{2+}/\text{TPrA}$ is oxidize and reduce simultaneously in reporting and supporting channel.

3.2.2 Materials and instrumentation used

Luminol ($\geq 98\%$ purity), Tris (2,2'-bipyridyl) dichloro-ruthenium (II) hexahydrate ($\geq 99.95\%$ purity) ($\text{Ru}(\text{bpy})_3^{2+}$), Tripropylamine ($\geq 98\%$ purity) (TPrA), Choline chloride ($\geq 98\%$ purity) and Dopamine were procured from Sigma Aldrich, India. Isopropanol (IPA) (2-propanol, 99 % purity) and N-Dimethylformamide (DMF) (99.5 % purity) were purchased from SRL, India. IPA (diluted to 60%) was used to clean the DMF-treated 3D printed C-BPE-ECL devices. Luminol was not directly soluble in water, therefore Sodium hydroxide (NaOH) was used to formulate the stock solution of Luminol. Sodium hydroxide (NaOH) was bought from SRL, India. Sodium phosphate monobasic dehydrate ($\text{NaH}_2\text{PO}_4 \cdot 2\text{H}_2\text{O}$) and Sodium phosphate dibasic dehydrate ($\text{Na}_2\text{HPO}_4 \cdot 2\text{H}_2\text{O}$) were purchased from Sigma Aldrich, India for the preparation of phosphate buffer solution (PBS). To confirm the analytical performance of 3DP-C-BPE-ECL devices all the chemicals were prepared in deionized water (DI). To fabricate BPE and DEs of 3DP-C-BPE-ECL devices, conductive graphene filament was used and purchased from Black Magic 3D, USA. White PLA filament was procured from Amazon, India. All these filaments have a diameter of 1.75 mm.

The 3DP-C-BPE-ECL devices were fabricated using a Fused deposition modeling (FDM) based 3D printer (Creator PRO from Flashforge, China). In this study, a photomultiplier tube (PMT)-based, and 3D printed miniaturized smartphone embedded-based ECL systems were used to detect ECL signals. In case of PMT based sensing approach, PMT H10722 series photosensor module was procured from Hamamatsu Photonics, Shizuoka, Japan. Isolated Module DC-DC Converter with Output ± 5 V, 200 mA and Input 4.5 V - 5.5 V (SPU01L-05) was purchased from Mean Well USA Inc. Bluetooth (HC-05) and IoT (ESP8266-01) module were procured from Amazon, India. On the other hand, in smartphone-based sensing approach, DC to DC (5 V input, 1.2 V to 24 V output) step up-step down converter and Samsung Galaxy M11 (12 MP camera) smartphone were purchased from Amazon, India.

3.2.3 Data capturing and analysis for 3DP-C-BPE-ECL

Following the fabrication of 3DP-C-BPE-ECL devices, chemical reactions based on $\text{Ru}(\text{bpy})_3^{2+}/\text{TPrA}$ or Luminol/ H_2O_2 were carried out to sense dopamine and choline. For the comparative study, two independent approaches were used to detect ECL signals: a PMT module embedded with IoT and a 3D printed miniaturized black box embedded with a smartphone.

3.2.3.1 PMT based data acquisition and analysis

Figure 3.2 (a) shows the block diagram representation of Photomultiplier tube (PMT). It comprises of DC-DC converter module produces a stable output voltage of ± 5 V required by the PMT module.

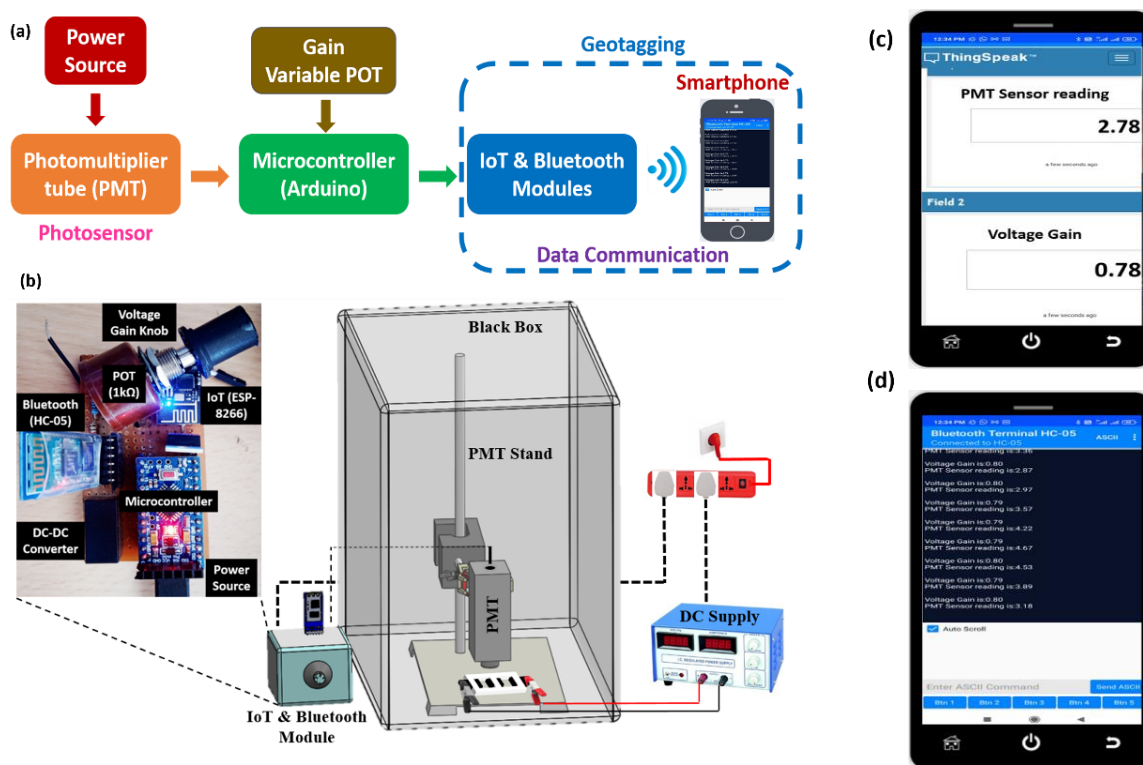


Figure 3.2 PMT based approach for data acquisition and analysis; (a) Block diagram representation of Photomultiplier tube PMT module; (b) schematic representation of PMT based approach to detect ECL signal: IoT and bluetooth module with other electronics component mounted on solo PCB; (c) Mobile embedded ThinkSpeak IoT platform; (d) real-time data logging using Smartphone

The Arduino based microcontroller was responsible for monitoring, controlling, and processing the photosensor. Voltage Gain variable Potentiometer (POT) was mainly used to adjust the sensitivity of the PMT. Bluetooth (HC-05) and IoT (ESP8266-01) modules were used for real-

time data acquisition through geotagging that was connected to the smartphone for an easy data logging facility. The schematic representation of PMT based module with complete electronic components mounted and integrated on a solo PCB platform is depicted in Figure 3. 2 (b). Herein, the PMT (H10722) module was used to sense ECL signals. The output of the PMT was in the form of current, which was fed to an amplifier, which converted it to voltage so that the signal could be processed easily. The microcontroller coordinates and processes the information to the data communication unit. The open-source software, arduino integrated development environment (IDE), was used to carry out the instructions (www.arduino.cc). The sensitivity adjustment was achieved by varying the voltage gain in the range of + 0.5 V to + 1.1 V using the potentiometer. The sensitivity adjustment circuit was designed and modified following initial simulations with NI Multisim software to test and improve the fine-tuning ability the voltage gain. Figure 3. 2 (d) shows the real-time data logging using Bluetooth (HC-05) and IoT (ESP-8266-01) modules accessible directly onto the smartphone making it easy for data acquisition. IoT module was utilized to retrieve PMT data in real time via the cloud, which could be accessed via a smartphone. The obtained data has been stored on the ThingSpeak platform. ThingSpeak is an IoT application to store, access, and return information from things/subjects using HTTP and MQTT protocol over the internet. Figure 3. 2 (c) shows Mobile embdded ThinkSpeak IoT platform to show real time data acquisition.

3.2.3.2 Smartphone based data acquisition and analysis

Figure. 3. 3 (a) depicts a smartphone-based approach for sensing ECL signals. To effectively capture the ECL signal, a 3D printed miniaturized black box, integrated with a smartphone and a DC-to-DC buck-boost converter, was used. A methodology, similar to the one discussed in our earlier published work, was used in this work [44]. The intensity of ECL signals was calculated using ImageJ software. As shown in Figure 3.3 (b), to determine the mean value of the ECL signal in relative light units (RLU), a high intensity area of roughly 3000 pixels was chosen.

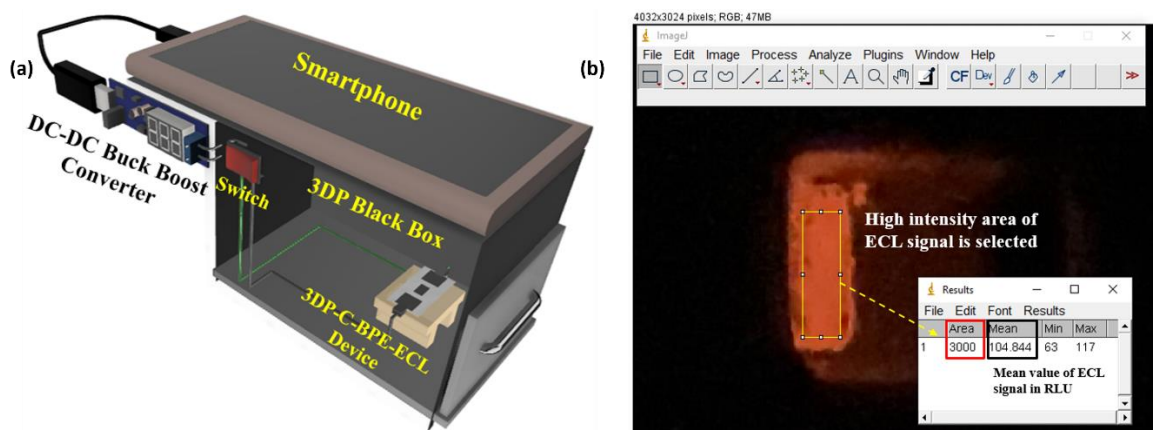


Figure 3.3 Smartphone based approach for data acquisition and analysis. (a) 3D printed miniaturized ECL imaging system with black box, DC-DC converter and smartphone. (b) ImageJ software based calculation of ECL intensity.

3.2.4 Characterization for 3DP electrodes

Scanning Electron Microscope (SEM) analysis was accomplished to examine the morphological modifications on the surface of electrodes for the fabricated 3DP-C-BPE-ECL device before and after N-dimethylformamide (DMF) treatment. The SEM images for conductive graphene filament without and with DMF treatment are shown in Figure 3.4 (a) and (b) respectively. As can be seen clearly in Figure 3.4 (b), after DMF treatment, the surface of the conductive graphene filament became more porous, resulting in an increase in ECL signal intensity and detection limit, as detailed in the following section.

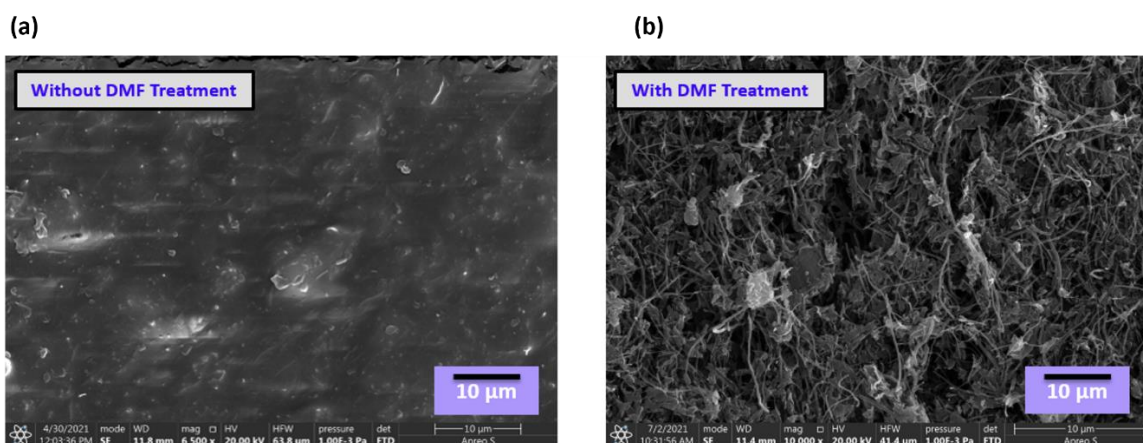


Figure 3.4 SEM images for conductive graphene filament, (a) without DMF treatment. (b) after DMF treatment.

3.2.5 Assay optimization for 3DP-C-BPE-ECL

Following the fabrication of the proposed device, the next step was to optimize the parameters on which the intensity of the ECL signal was highly dependent. The intensity of the ECL signal in $\text{Ru}(\text{bpy})_3^{2+}/\text{TPrA}$ based chemistry was significantly dependent on the concentration of TPrA and the applied voltage. Similarly, in Luminol/ H_2O_2 based chemistry, the intensity of ECL signal was dependent on luminol concentration and externally applied voltage.

3.2.5.1 Optimization of TPrA and external applied voltage for $\text{Ru}(\text{bpy})_3^{2+}/\text{TPrA}$

The concentration of TPrA was varied from 10 mM to 60 mM and the change in ECL intensity was observed with each concentration of TPrA. It was observed that as the concentration of TPrA varied from 10 mM to 30 mM, the intensity of ECL signal increased linearly, as shown in Figure 3.5 (a). An increase in TPrA concentration above 30 mM would not affect the intensity of the ECL signal. This could be due to reduced mass transfer towards electrodes. For the subsequent experiments, a concentration of 30 mM TPrA was selected.

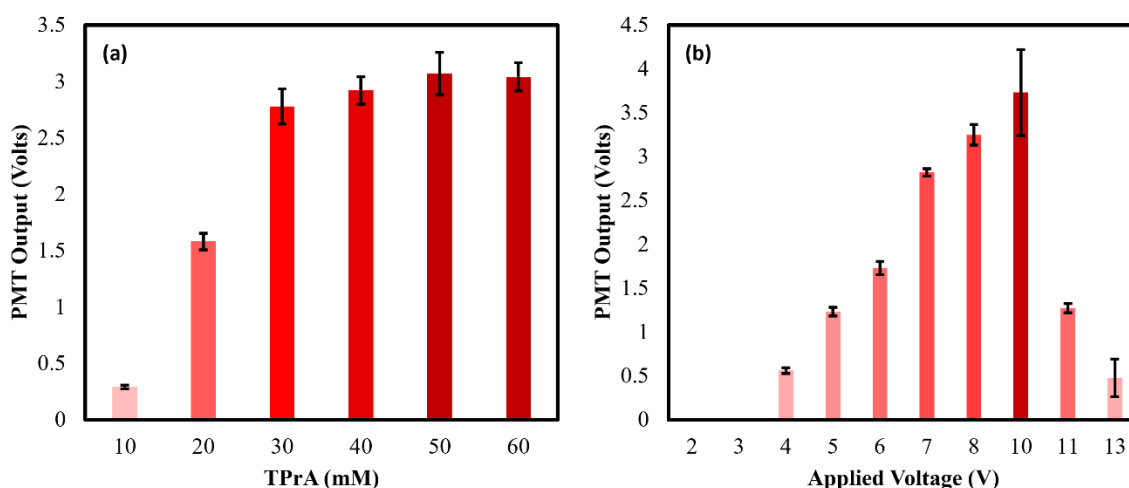


Figure 3.5 Optimization of various parameters. (a) TPrA (mM) Vs PMT Output (Volts); TPrA = 10, 20, 30, 40, 50 and 60 mM, applied voltage = 7 V, voltage gain = 0.6, $\text{Ru}(\text{bpy})_3^{2+}$ = 500 μM , PBS = 0.1 M (pH = 7). (b) Applied voltage Vs PMT Output (Volts); applied voltage = 4, 5, 6, 7, 8, 10, 11 and 13, TPrA = 30 mM, $\text{Ru}(\text{bpy})_3^{2+}$ = 500 μM , voltage gain = 0.6, PBS = 0.1 M (pH = 7) ($n = 3$).

Applied voltage is the second important parameter over which ECL intensity depends. The applied voltage was optimized by varying the voltage value from 3 V to 13 V. The intensity of the ECL signal was augmented linearly from 3 V to 8 V. For voltages less than 4 V, no ECL signal was recorded. However, strong but unstable ECL intensity signal was observed at 10 V,

shown in Fig. 5 (b). It was detected that when the applied voltage value increased, the intensity of the ECL decreased. This could be because, at higher voltages, a small amount of water being electrolyzed at the anode surface of BPE electrode, preventing the formation of the ECL signal [23]. For the subsequent experiments, 8 V as optimized value of applied voltage was used. Similarly, in the case of Luminol/H₂O₂ based chemistry, the ECL signal intensity depends on luminol concentration and external applied voltage. Herein, the optimized value for luminol (4 mM) and applied voltage (7 V) were taken from previously published work by our group [2].

3.2.5.2 Optimization of TPrA and external applied voltage for Ru(bpy)₃²⁺/TPrA

Lorena Manzanares Palenzuela et. al. reported 3D printed conductive graphene filament based electrodes for electrochemical sensing of ascorbic and picric acid [92]. They have developed an activation process for 3D printed graphene electrodes by performing DMF treatment. DMF treatment was studied for various time intervals (1, 10, 20, and 60 minutes), and it was found that 10 minutes was the optimal period necessary for activation desired effect for graphene-based electrodes.

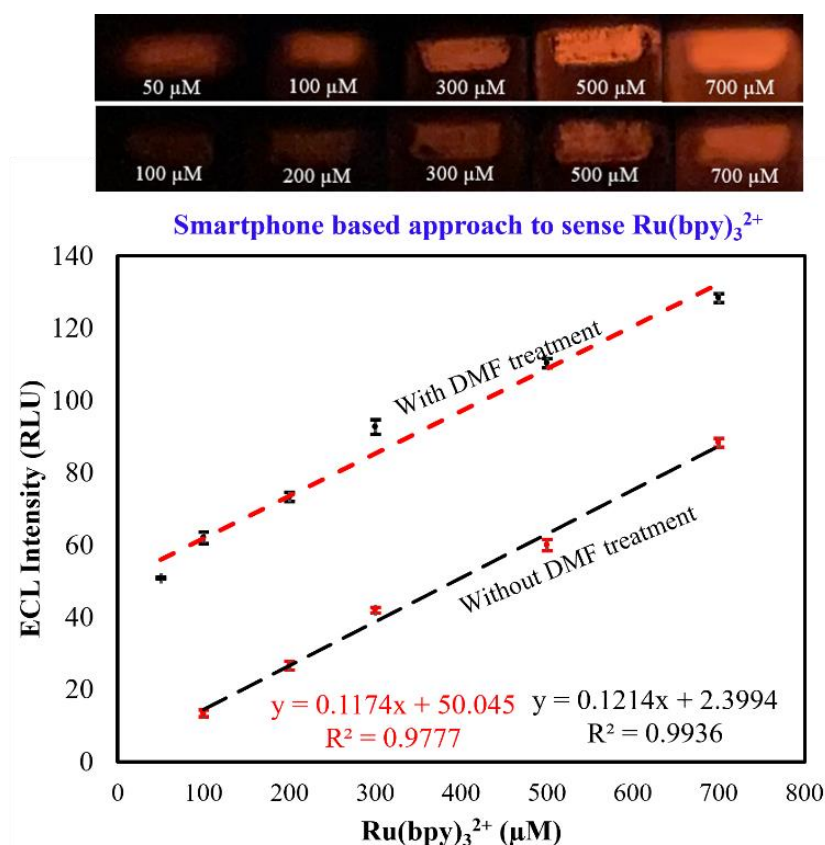
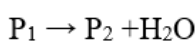
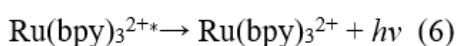
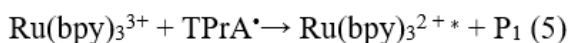
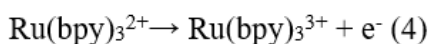


Figure 3.6 Effect of DMF treatment on graphene filament; (a) Smartphone based approach to sense Ru(bpy)₃²⁺; Ru(bpy)₃²⁺ (μM) Vs ECL Intensity (RLU), Ru(bpy)₃²⁺ = 50 to 700 μM, applied voltage = 8V, TPrA = 30 mM, PBS = 0.1 M (pH = 7).

In the present work, an optimal time period of 10 minutes was chosen for the DMF treatment. Both the supporting and reporting channels were filled with DMF for 10 minutes before being washed with IPA (60% diluted) and dried at room temperature for 6 to 7 hours. To determine the effect of DMF treatment, sensing of $\text{Ru}(\text{bpy})_3^{2+}$ was carried out using smartphone-based approach. The concentration of $\text{Ru}(\text{bpy})_3^{2+}$ was varied from 10 to 1000 μM and a linear range of 100 to 700 μM and 50 to 700 μM was achieved, with limit of detection (LOD) values of 22.21 μM and 5.25 μM for 3DP-C-BPE-ECL devices without and with DMF treatment, respectively. The relation between $\text{Ru}(\text{bpy})_3^{2+}$ Vs ECL Intensity (RLU) for with and without DMF treatment is illustrated in Figure 3.6. Based on the DMF treatment, a significant observation of improved linear range with lower limit of detection value was observed. Also, the percentage increase in ECL intensity was observed to be around 31.25 μM . Based on the observations, for subsequent analysis of dopamine and choline DMF treated 3DP-C-BPE-ECL devices were used.

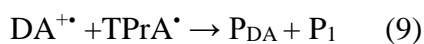
3.2.6 Sensing of Choline and Dopamine using 3DP-C-BPE-ECL

Following parameters optimizations to validate the diagnostic efficacy of 3DP-C-BPE-ECL was accomplished by sensing dopamine and choline using $\text{Ru}(\text{bpy})_3^{2+}/\text{TPrA}$ and Luminol/ H_2O_2 based chemistry respectively. Following are the chemical reactions involved while sensing dopamine using ruthenium-based electrochemistry.



Equation 1 to 4 refers to the generation of $\text{Ru}(\text{bpy})_3^{3+}$ and highly reductive TPrA^* over the surface of graphene electrode. Equation 5 and 6 shows the reaction between $\text{Ru}(\text{bpy})_3^{3+}/\text{TPrA}$, which relax electron to the ground state and emits lights. The ECL signal intensity is getting quenched in the presence of dopamine (DA). The quenching of ECL could be attributed to the generation of dopamine oxidation product, which was assumed to take place as follows:





where P_{DA} represent the reduced product of $\text{DA}^{+\bullet}$ and P_1 represent the oxidation product of TPrA^{\bullet} .

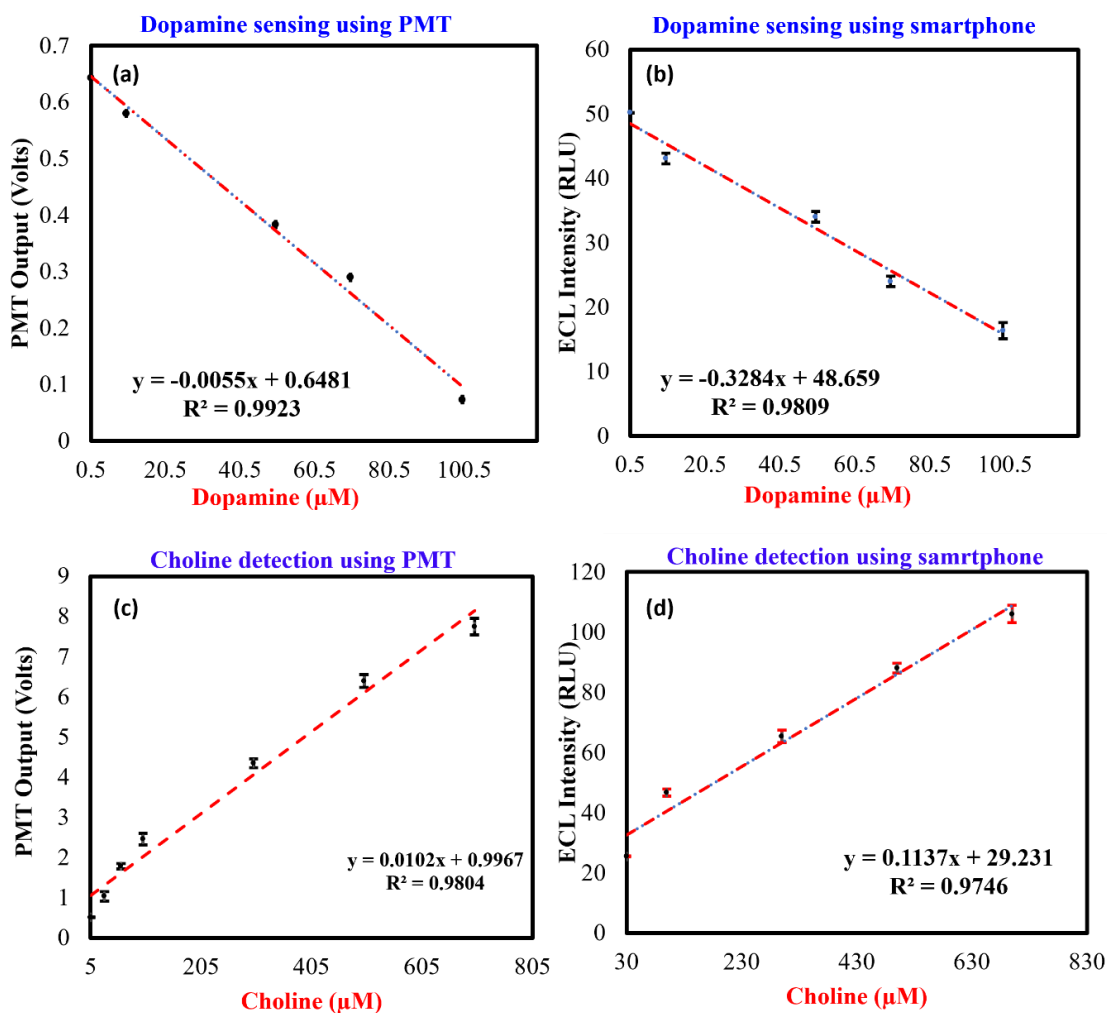


Figure 3.7 (a) Dopamine (μM) Vs PMT Output (Volts), Dopamine = 0.5, 1, 50, 70 and 100 μM , TPrA = 30 mM, PBS = 0.1 M (pH =7), voltage gain = 0.6, $\text{Ru}(\text{bpy})_3^{2+}$ = 100 μM , applied voltage = 8V. (b) Dopamine (μM) Vs ECL Intensity (RLU); Dopamine = 0.5, 1, 50, 70 and 100 μM , TPrA = 30 mM, PBS = 0.1 M (pH =7), $\text{Ru}(\text{bpy})_3^{2+}$ = 100 μM , applied voltage = 8V. (c) Choline (μM) Vs PMT Output (Volts), choline = 30, 100, 300, 500 and 700 μM , Luminol = 4 mM, voltage gain = 0.6, choline oxidase = 10 mg/mL, applied voltage = 7V, PBS = 0.1 M (pH =7), (d) Choline (μM) Vs ECL Intensity (RLU), choline = 30, 100, 300, 500 and 700 μM , choline oxidase = 10 mg/mL, Luminol = 4 mM, applied voltage = 7V, PBS = 0.1 M (pH =7). (N=3)

The sensing of dopamine was accomplished in the linear range 0.5 μM to 100 μM with LOD = 2 μM ($R^2 = 0.99$, N=3) using PMT based sensing approach, as shown in Figure 3.7 (a). Further, smartphone-based approach was used for the sensing of dopamine by achieving linear

range 0.5 μM to 100 μM with LOD = 0.33 μM ($R^2= 0.98$, $N=3$) as shown in Figure 3.7 (b). Last, sensing of choline was carried out using PMT and smartphone-based sensing approach by accomplishing linear range 5 μM to 700 μM and 30 μM to 700 μM with LOD values of 1.25 μM ($R^2= 0.98$, $N=3$) and 3.27 μM ($R^2= 0.97$, $N=3$) as shown in Figure 3.7 (c) and (d) respectively.

3.3 Multiplexed and Simultaneous Biosensing in a 3D-Printed Portable Six-Well ECL device

In this study, for the first time, a six-well 3D printed closed bipolar Electrochemiluminescence (3DP-CBPE-ECL) device has been successfully fabricated and validated by performing single-step detection of various biochemical such as glucose and choline. Luminol/ H_2O_2 based enzymatic reactions were performed with optimized parameters for selective sensing of glucose and choline. A smartphone was leveraged to execute multiple activities such as powering the ECL device, capturing ECL images and calculating the ECL intensity of the obtained ECL signal. The feasibility of a six-well 3DP-CBPE-ECL device was tested by sensing glucose and choline simultaneously in a single device at three different concentrations.

3.3.1 Working principle and fabrication of six-well 3DP-CBPE-ECL

Enzymatic reactions based on Luminol/ H_2O_2 have been carried out to better comprehend the working principle of the fabricated ECL device. The anode and cathode of BPE electrodes were placed in different channels.

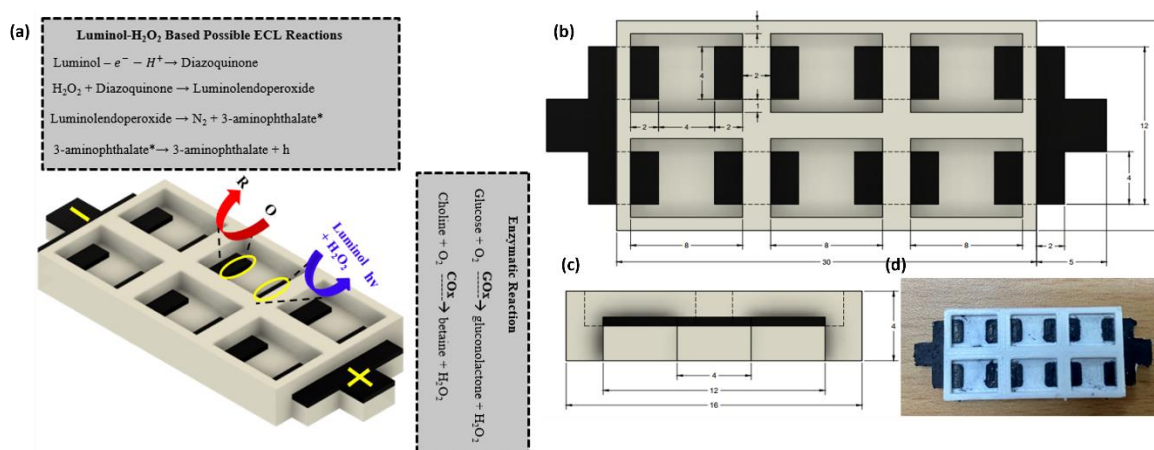


Figure 3.8 (a) Working principle of six-well 3DP-CBPE-ECL device with anodic, cathodic and enzymatic reactions. (b) and (c) top and side view for 3DP-CBPE-ECL device with dimensions. (d) final fabricated 3DP-CBPE-ECL device.

When a sufficient external voltage was provided to the ECL device, a strong electric field was formed across the closed bipolar electrode (CBPE), triggering ECL processes such as oxidation and reduction on the anode and cathode of the CBPE respectively, resulting in the emission of an ECL signal at the anode of the CBPE. The working principle of the six-well 3DP-CBPE-ECL device with anodic, cathodic and enzymatic reactions is depicted in Figure 3.8 (a). A dual-extruder FDM 3D printer was efficiently used to fabricate a six-well 3DP-CBPE-ECL. Prior to the fabrication, the ECL device design was created using Computer-Aided Design (CAD) software-fusion 360 and later design was saved in '.stl' format.

Following that, graphene and white PLA filament were used to create electrodes and channels by adjusting the temperature (220⁰C). The electrodes and device dimension are shown in Figure 3.8 (b) and (c). The generated file was then stored in the '.x3g' format, which is compatible with 3D printers. Finally, the completed design was sent to a Dual-Extruder FDM 3D printer through a graphical user interface (GUI). Image of final fabricated six-well 3DP-CBPE-ECL device with electrodes and channels is shown in Figure 3.8 (d).

After the device fabrication, the six-well 3DP-CBPE-ECL devices were DMF treated to enhance device performance on several fronts, such as the surface of the electrode being more porous, to achieve better detection limit [93]. All six wells of the device were filled with DMF for a ten-minute optimum time [92]. The device was then cleaned with 60% diluted IPA. Finally, DMF-treated devices were allowed to dry for 6 to 7 hours at room temperature.

3.3.2 Data acquisition and analysis

Herein, for the first-time smartphone was efficiently leveraged to carry out the following functions: 1) to power the ECL device through buck-boost converter which successfully makes the system portable and eliminates the usage of external bulky power supply, 2) to capture the ECL signals, and 3) to calculate the ECL intensity of captured signals which eliminates to use third-party software such as ImageJ and Matlab.

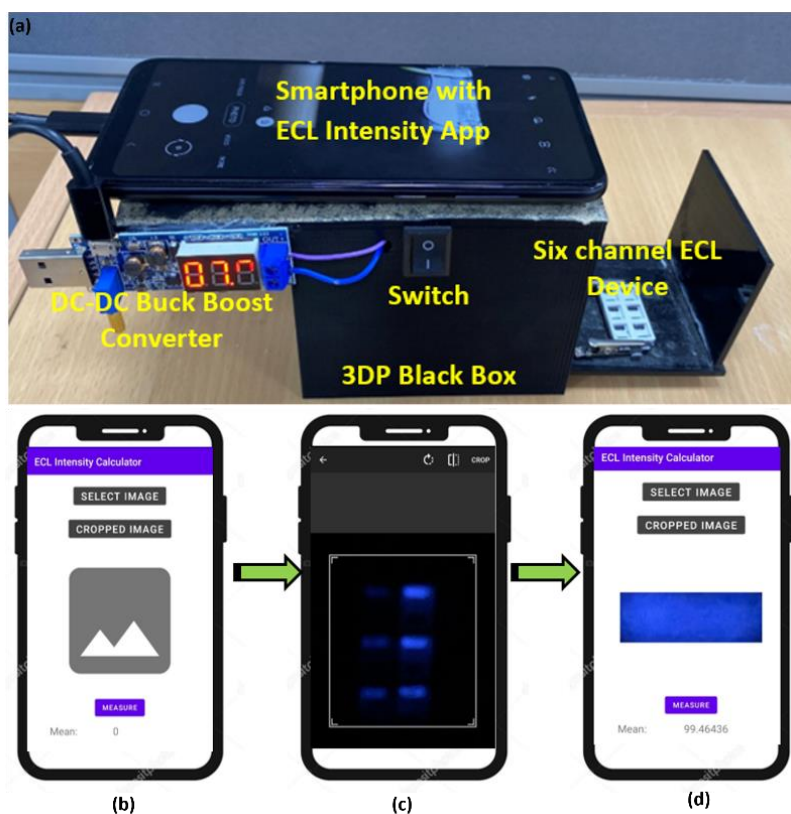


Figure 3.9 Data acquisition and analysis, (a) 3D printed black box assembly integrated with smartphone and converter, (b) Display for android ECL Intensity app, (c) captured real time image, (d) selected region of interest and calculated ECL intensity.

A mobile app, “ECL intensity calculator” was developed in java built-in android studio with read-write storage as shown in Figure 3.9 (b). The android app was designed in such way that it can calculate the intensity of real time captured images or saved images in a gallery. The captured ECL image using an android app is shown in Figure 3. 9 (c). After capturing the ECL signal, a high intensity portion of an image was clipped and ECL intensity was calculated by pressing the “MEASURE” button shown on the display displayed in Figure 3. 9 (d).

3.3.3 Analytical performance of six-well 3DP-CBPE-ECL

Before validating the analytical performance of the ECL device, it was mandatory to optimized several parameters over which ECL signal intensity was highly dependent. Primarily, in Luminol/H₂O₂ based chemistry, ECL signal strength is dependent on parameters such as concentration of pH, luminol and voltage.

All of the optimized values in this study were obtained directly from a prior article published by our group. For validation of the six-well 3DP-CBPE-ECL, the optimal values for luminol

(4 mM), pH (9) and voltage (7V) were used. The six-well 3DP-CBPE-ECL device was validated by detecting glucose and choline in a single step. First, before the sensing of glucose and choline, the response of blank was calculated. For this, all the six wells were filled with 4 mM luminol concentration and ECL intensity was calculated. It was observed that when only luminol concentration was used, no ECL signal was obtained. Next, the glucose was detected by keeping six different concentrations in six distinct channels, as illustrated in Figure 3.10 (a). To sense the glucose, glucose oxidase (10 mg/mL) was used and an enzymatic approach as described below was used. Experimentally, it was observed that minimum time of 3 minutes was required to react glucose with glucose oxidase to produce H₂O₂.

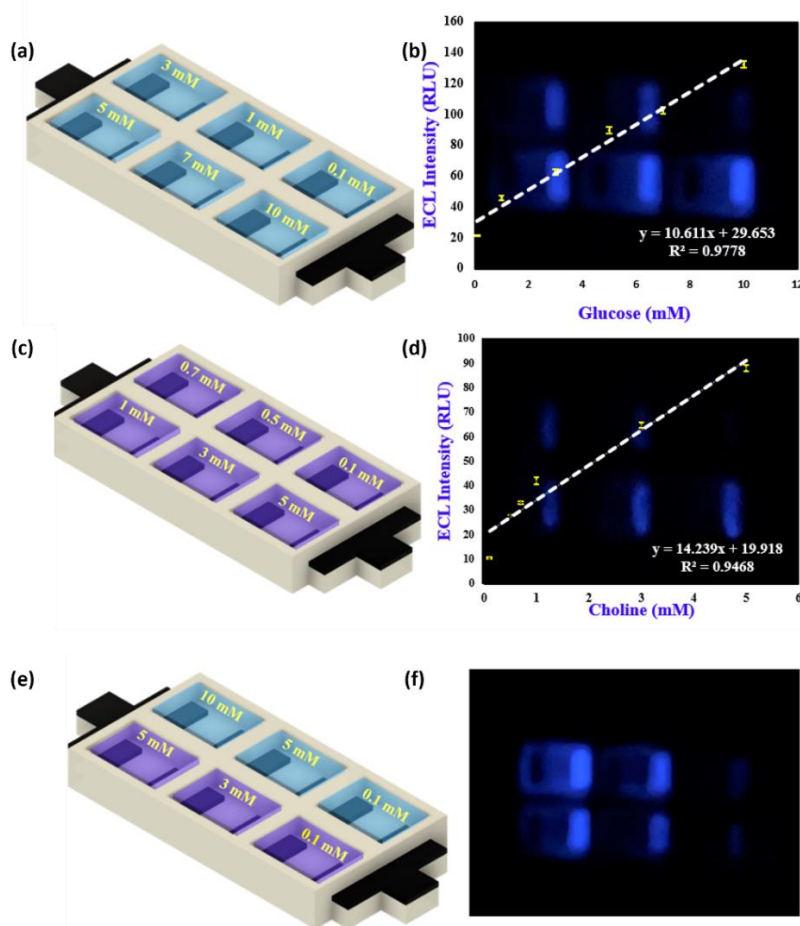


Figure 3.10 (a) Schematic representation of glucose with different concentration, (b) ECL intensity Vs Glucose, Glucose = 0.1, 1, 3, 5, 7 and 10 mM, Luminol = 4 mM, GOx = 10 mg/mL, Applied voltage = 7V, (c) Schematic representation of choline with different concentration, (d) ECL intensity Vs Choline, Choline = 0.1, 0.5, 0.7, 1, 3 and 5 mM, Luminol = 4 mM, COx = 10 mg/mL, Applied voltage = 7V, (e) simultaneous detection of glucose and choline using six channel CBPE-ECL device, (f) real time ECL signal image corresponding to various concentration of glucose and choline. [N = 3]

Hence, Luminol, glucose and glucose oxidase were pipetted into the channel for an optimized time period of three minutes. The ECL signal was then achieved by applying an optimized value of external voltage (7 V) to the anode and cathode of the ECL device, and the corresponding ECL signal was successfully captured with android smartphone. ECL signal intensity for different six concentrations is shown in Figure 3.10 (b). The single step detection of glucose was accomplished for the linear range 0.1 mM to 10 mM with a limit of detection (LOD) 24 μ M. Similarly, choline was detected by pipetting six different concentrations of choline with luminol and choline oxidase into the six distinct channels shown in Figure 3.10 (c). Choline, Luminol, and Choline oxidase were pipetted into the channel for ten minutes before applying an external voltage to the ECL device. Choline detection was carried out by obtaining linear range 0.1 mM to 5 mM with LOD 10 μ M. For each different concentration of choline, ECL signal intensity was calculated, and a related linear fit graph was plotted which is shown in Figure 3. 10 (d). To test the workability of the six-well CBPE-ECL device, simultaneous detection of varied concentrations of glucose and choline was performed, and it was found that the fabricated ECL device effectively sensed both analytes at the same time. The simultaneous detection of glucose and choline was accomplished by pipetting three different concentrations of each (glucose = 0.1, 5 and 10 mM and choline = 0.1, 3 and 3 mM) into separate channels and calculated ECL intensity as indicated in Figure 3.10 (e) and (f).

3.3.4 Real Sample analysis of glucose and choline

Finally, a real sample analysis was performed to assess the practicability of the fabricated ECL device. The original glucose concentration was estimated by intersecting the extrapolation of the fitting line with the concentration axis [59]. The original values of glucose before the sample being spiked was found to be 3.9 mM. The standard spiking (addition) method was adopted for the real sample analysis of glucose and choline. The following method was adopted to do the real sample analysis of glucose.

An unknown blood sample was collected from the medical center (BITS Pilani Hyderabad Campus, Hyderabad, India) and diluted to ten times to avoid interference. In our case, ten times dilution was performed by adding 100 μ L of real sample into 900 μ L of DI water. Real sample analysis was performed using the standard spiking method for different concentrations of glucose and choline and yielded a satisfactory recovery rate.

The following method was adopted to do the real sample analysis. The real sample was diluted to 10 times i.e. In present study, 100 μ L of real sample was added to 900 μ L DI water. Then,

known concentration of glucose (1000 μM) and diluted real sample having equal volume (30 μL each) added into well along with glucose oxidase (10 mg/mL having 20 μL volume) and ECL intensity was calculated. Recovery rate was calculated using following formula [94].

$$R = \frac{\text{Practical Concentration (found)}}{\text{Theoretical Concentration (added)}} * 100$$

Table 3. 1 Summary of the outcome from the real sample analysis

Analytes	Clinical Method (mM)	Using 3DP-CBPE-ECL device (mM)	Added (mM)	Obtained (mM)	% Recovery
Glucose	4.2	3.9	1000	4980	95.7
			2000	5988	96.6
			3000	7050	97.9
Choline	-	-	100	96.5	96.5
			500	477	95.5
			3000	2890	96.3

In a similar way, real sample analysis was carried out for different concentration of choline. In spite of rigorous literature survey, no proven clinical method to detect choline was found. Hence, herein, no clinical data for choline could be provided. Multiple experiments were carried out with the 3DP-CBPE-ECL device to detect choline in real samples but we could not get convincing results. This could be due to the fact that choline concentrations in real serum are much below the detection limit. As a result, the conventional additive approach was used to detect choline, and the results were satisfactory. The recovery rate with standard deviation for various concentrations of glucose and choline is summarized in Table 2.

3.3.5 Interference study of glucose and choline with other biomolecules

The interference study of glucose and choline with other biomolecules, such as ascorbic acid, uric acid, and creatinine, were carried out to prove the selectivity of the device. Following method was adopted for the interference study of glucose with other biomolecules. First, known concentrations of glucose (5 mM in 30 μL), luminol (4 mM in 30 μL) and glucose oxidase (10 mg/mL in 20 μL) were pipetted into well and ECL intensity was calculated. Then, interfering compound such as uric acid (0.5 mM in 30 μL) was added to same well and ECL intensity was calculated. Less than 5% change was observed in ECL intensity which indicated that the fabricated device provided good selectivity. Similarly, an interference study of glucose with other interfering compounds (ascorbic acid, choline, and creatinine) was carried out, and the

selectivity of the device was confirmed. Figure 3.11 (a) and (b) show the interference study of glucose and choline with other interfering compounds.

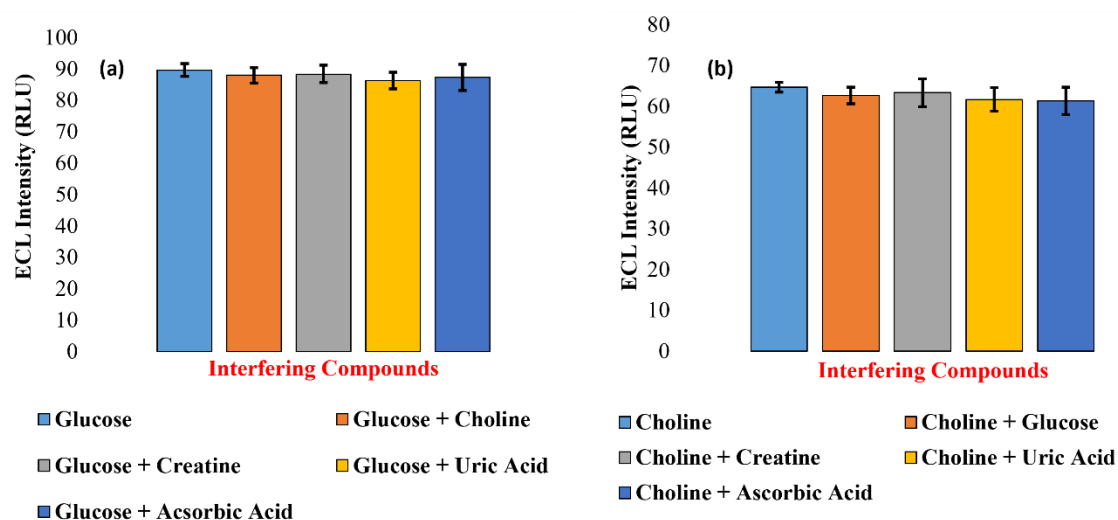


Figure 3.11 Interference study. (a) interference study of glucose with choline, creatine, uric acid, ascorbic acid: glucose = 5 mM, choline = 1 mM, creatine = 0.5 mM, uric acid = 0.5 mM, ascorbic acid = 0.1 mM, Luminol = 4 mM, GOx = 10 mg/mL and applied voltage = 7 V. (b) interference study of choline with glucose, creatine, uric acid, ascorbic acid: choline = 2 mM, glucose = 1 mM, creatine = 0.5 mM, uric acid = 0.5 mM, ascorbic acid = 0.1 mM, Luminol = 4 mM, COx = 10 mg/mL and applied voltage = 7 V, n=3.

3.4 Stereolithography 3d printed ECL platform with random grade graphite electrodes: detection of H₂O₂ and cholesterol using a smartphone

Graphite pencil electrode-based microfluidics biosensors have recently gained more attention and shown promising results in various applications such as ECL, energy harvesting, detection of haemoglobin and vitamin C, and in the field of DNA and RNA because of their electrochemical characteristics, fast prototyping, ease-of-use, excellent mechanical rigidity, easy disposal, and cost efficiency [95][96]. By taking advantage of graphite pencil electrodes, an ECL device was fabricated and successfully utilized to detect hydrogen peroxide (H₂O₂) and cholesterol. H₂O₂ is a common and easy-to-detect molecule found in nature, and its detection is important in clinical, mining, pharmaceutical, food, and textile applications. H₂O₂ is also produced as a by-product in a number of biochemical reactions and is catalyzed by enzymes such as lactate oxidase, choline oxidase, alcohol oxidase, glucose oxidase, cholesterol oxidase, glutamate oxidase, lysine oxidase, d-amino oxidase, oxalate, and others [97]. Along with H₂O₂, cholesterol is an important biomolecule present in the human body that causes coronary heart disease, arteriosclerosis, lipid metabolic dysfunction, cerebral thrombosis, and hypertension when it accumulates up in the body [98][99][100]. Therefore, the detection of

H₂O₂ and cholesterol is crucial for both industrial and academic applications. In this study, our main goal was to develop a graphite pencil-based device that could do inexpensive, quick, disposable, and portable complete analysis using a unique ECL sensing technique. By taking the advantages of the ECL-based sensing approach and observing the importance of sensing of H₂O₂ and cholesterol, herein, a new class of Stereolithography-based resin 3D printer (SLA) printed graphite pencil-based single electrode ECL (GP-SE-ECL) biosensor was developed, and its analytical performance was successfully validated. Here, an efficient use of the SLA printer was made to create a microfluidic well for pipetting reagents.

This work encompasses a novel, simple and ultra-fast fabrication of stereolithographic 3D printed electrochemiluminescence (GP-SE-ECL) biosensor with a graphite pencil-based single electrode to detect H₂O₂ and cholesterol. Graphite pencil electrodes were extensively used as a replacement for screen-printing, Laser-Induced graphene-based electrodes due to their user-friendliness, ease of availability, excellent electrochemical properties, and cost-efficiency. Different graded graphite electrodes (F, H, HB, 3B, 6B, and 8B) were used to fabricate single-electrode ECL devices. Since the conductivity values and surface area for different graded pencils vary, the impact of conductivity and surface area of the electrodes on the effectiveness of the ECL device was confirmed with optimized parameters by sensing H₂O₂. A lab-made, portable 3D-printed dark room platform integrated with a smartphone was used to capture the ECL signals. The smartphone android application was developed which can not only capture the ECL images but also calculates the intensities values for the region of interest. Based on the experimental data it was confirmed that the fabricated device with random grade pencil possesses strong acceptability in the field of biomolecule detection.

3.4.1 Operating Principle and Fabrication of GP-SE-ECL Device

The working concept of SLA 3D printed GP-SE-ECL device based on the luminol/H₂O₂ chemistry is shown in Figure 3.12 (a). Herein, pencil graphite-based driving electrodes (DEs) were used, and the positive terminal of the power supply was applied to the anode and the negative terminal of the power supply was applied to the cathode of the GP-SE-ECL device. When an adequate power supply is applied to DEs, the redox process gets initiated resulting in an ECL signal at the anode of P-SE-ECL device [43]. The fabrication flow for SLA 3D printed GP-SE-ECL device is detailed in the following paragraph.

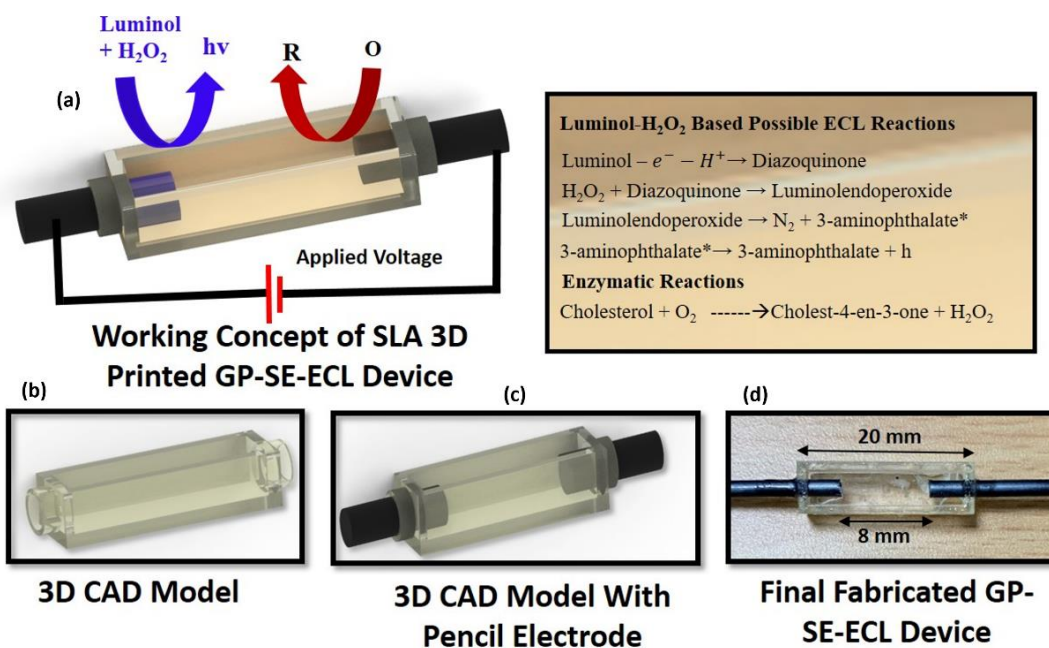


Figure 3.12 (a) Schematic representation for working concept of P-SE-ECL device with redox process: Fabrication flow for P-SE-ECL device. (b) design of 3D CAD model with dedicated slots. (c) 3D CAD model with graphite-based driving electrodes. (d) final fabricated GP-SE-ECL device. Three different diameter inlets (2.2 mm for HB and F, 2.4 mm for 3B and 3 mm for 6B & 8B) were used to insert the electrodes.

The GP-SE-ECL device was developed using a unique but simple and low-cost approach based on SLA 3D printing. First, a computer-aided design application was used to model the device in 3D. (solid works). The resulting file was saved as a '.stl' file. Then, in preform software, layer optimization was done, and lastly, the printing process was accomplished. The supporting material was removed after printing, and the fabricated device was cleaned with IPA for 15 minutes and devices were kept at room temperature for 5 minutes. The 3D CAD model of the GP-SE-ECL device is shown in Figure 3.12 (b). Subsequently, different graded pencil electrodes were inserted into the provided slot as shown in Figure 3.12 (c). To resolve the anticipated leakage problem, the edges of the provided slots were filled with the same resin. Finally, to provide sufficient strength to the fabricated device, UV light curing (to photopolymerized) was performed for 15 minutes at 60°C. The fabricated GP-SE-ECL device with pencil graphite-based electrodes is shown in Figure 3.12 (d).

3.4.2 Chemicals and Material

Luminol with ≥98% purity, sodium hydroxide (NaOH), cholesterol with ≥98% purity and cholesterol oxidase (CHOx) (microorganism) 100 UN were purchased from Sigma Aldrich,

India. Isopropanol (IPA) with 99% purity and triton X-100 was procured from Sisco Research Laboratory (SRL), India. Hydrogen peroxide (35% in water) was purchased from Tokyo Chemical Industry, India. Pencils with different grades F, H and HB with 2.2 mm diameter, 3B with 2.4 mm diameter, 6B and 8B with 2.4 mm diameter were procured from Kurtzy Artist, Amazon, India. A stereolithography (SLA) 3D printer (25 μ m resolution, Form labs, USA) was used to fabricating the ECL device. A USB DC-DC buck-boost (5V to 1.2-24V) converter was procured from eHUB, Amazon, India.

3.4.3 Preparation of cholesterol and luminol

As cholesterol is not soluble in DI water, the following approach was used to overcome this issue. First, triton X-100 (5 mL) and IPA (5 mL) were mixed and heated to 50^oC using a digital magnetic stirrer hotplate. Then, 193 mg of cholesterol powder was slowly added to the solution and steered for 20 to 25 minutes at 800 rpm. Finally, 0.1 M PBS (40 mL) was supplemented with constant mixing to form a 10 mM stock solution. The resulting stock solution was stored at 4^oC when not in use. Different concentrations of cholesterol were prepared for the analysis by diluting a stock solution of cholesterol in 1:1:8 ratios (triton X-100: IPA: 0.1M PBS)[101][102].

Like cholesterol, luminol is also insoluble in normal water, but it is soluble in basic electrolyte. Hence, the same process was used to prepare a luminol stock solution as described in the precious section 2.2.2. Briefly, the base solution was first prepared by dissolving 399 mg of NaOH in 10 mL DI water. Then, 80 mg of luminol was added to the 47 mL DI water along with 3 mL NaOH solution to make the 10 mM stock solution of luminol. Different concentrations of luminol were prepared for the analysis by diluting the stock solution of luminol using the standard dilution formula.

3.4.4 Optimization of applied voltage, luminol and channel length

Following the fabrication of the proposed device, multiple parameters such as applied voltage, luminol concentration, and channel length were optimized to achieve the optimum ECL outputs [44]. The applied voltage was optimized by keeping the luminol concentration and channel length constant, and the maximum ECL was recorded experimentally at 4 V. It is clearly seen, from Figure 3.13 (a) the ECL intensity linearly increased till 4 V and after that ECL signal got saturates. This happens because as the voltage increases luminol oxidation rate to form 3-aminophthalate is increase, resulting increase in ECL intensity.

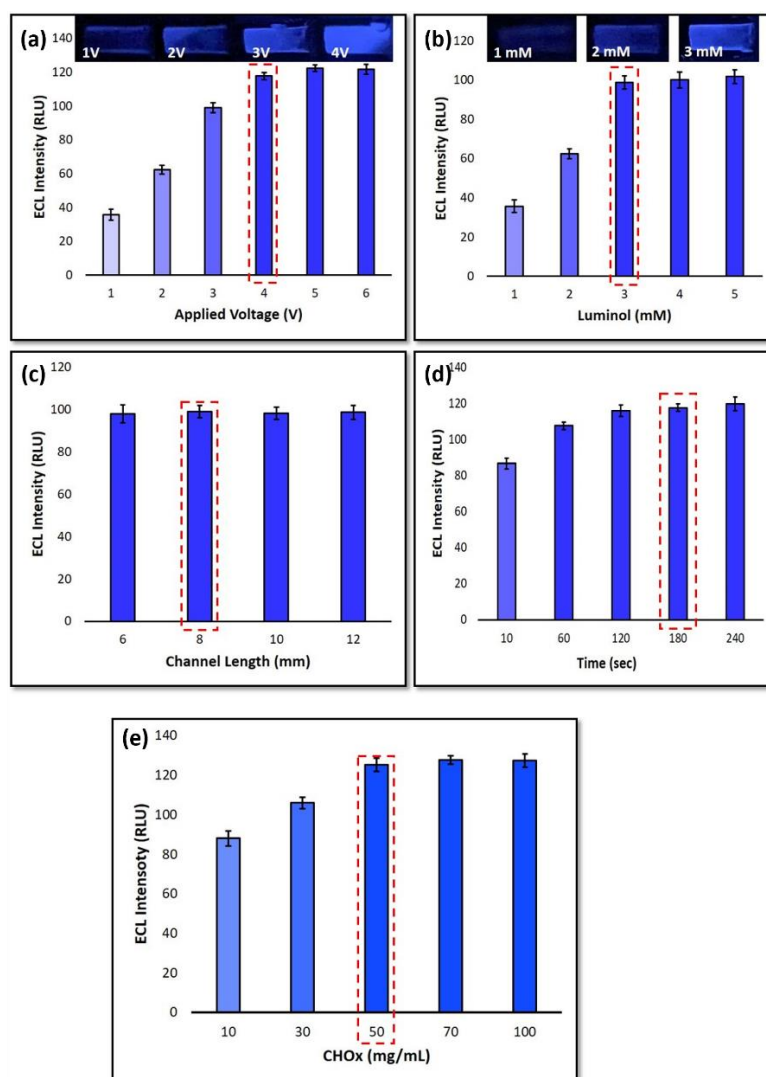


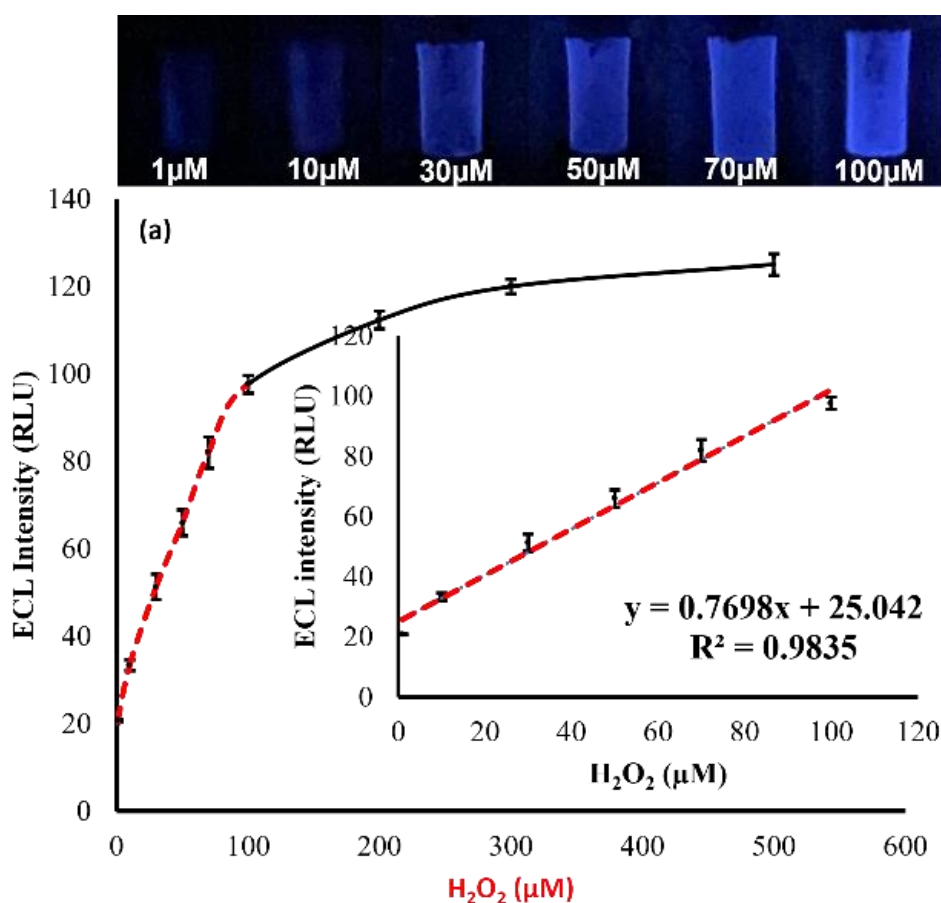
Figure 3.13 Optimization of different parameters. (a) optimization of applied voltage, luminol = 5mM, H_2O_2 = 1 mM and applied voltage varied from 1 to 6 V. (b) optimization of applied luminol, applied voltage = 4V, H_2O_2 = 1 mM and luminol varied from 1 to 5 mM. (c) optimization of channel length, luminol = 3 mM, applied voltage = 4V, H_2O_2 = 0.1 mM. (d) time optimization for cholesterol sensing, $CHOx$ = 50 mg/mL, cholesterol = 1 mM, luminol = 3 mM, applied voltage = 4 V. (e) luminol = 3 mM, applied voltage = 4V, $CHOx$ = 10, 30, 50, 70 and 100 UN/mL, cholesterol = 1 mM, $n=3$.

After 4 V, luminol gets completely oxidize, resulting no change in ECL intensity. Similarly, luminol was optimized by utilizing an optimized value of applied voltage while maintaining channel length constant, and the highest intensity was attained at 3 mM luminol concentration (Figure 3.13 (b)). It was observed that the ECL intensity was linearly increased up to 3 mM luminol concentration. This could happen because the formation rate of luminolendoperoxide increased with increase in luminol concentration [66]. Finally, the channel length was optimized using optimized values of applied voltage and luminol, and it was observed that an

8 mm channel length gives a more stable output. The channel length was varied from 6 mm to 12 mm, it was experimentally observed that as the channel length goes below 6 mm, more unstable ECL signal observed. This could be due to the fact as channel length reduces high intensity electric field is present across the channel leads to generate unstable ECL signal (Figure 3.13 (c)) [44]. Hence, for the sensing of H₂O₂ and cholesterol, the optimized values of applied voltage (4 V), luminol (3 mM) and channel length (8 mm) were used.

3.4.5 Sensing of H₂O₂ using different graded pencil-based GP-SE-ECL device

Following parameter optimization, H₂O₂ sensing was carried out using various graded pencils having different graphite (conductivity) content, and the effect of this on various parameters, such as ECL signal intensity and the detection limit, was observed. Different graded pencils, such as H, F, 3B, 6B, 8B and HB, were used to detect H₂O₂, and related graphs with linear range (LR) and limit of detection (LoD) is shown in Figure 3.14 (a-f). The same LR was seen for different graded pencils, with LoD values ranging from 0.91 to 0.96 μM, indicating that in luminol/H₂O₂ based electrochemistry, the intensity of the ECL signal and LoD values are independent of both the surface area and grades of the graphite pencil.



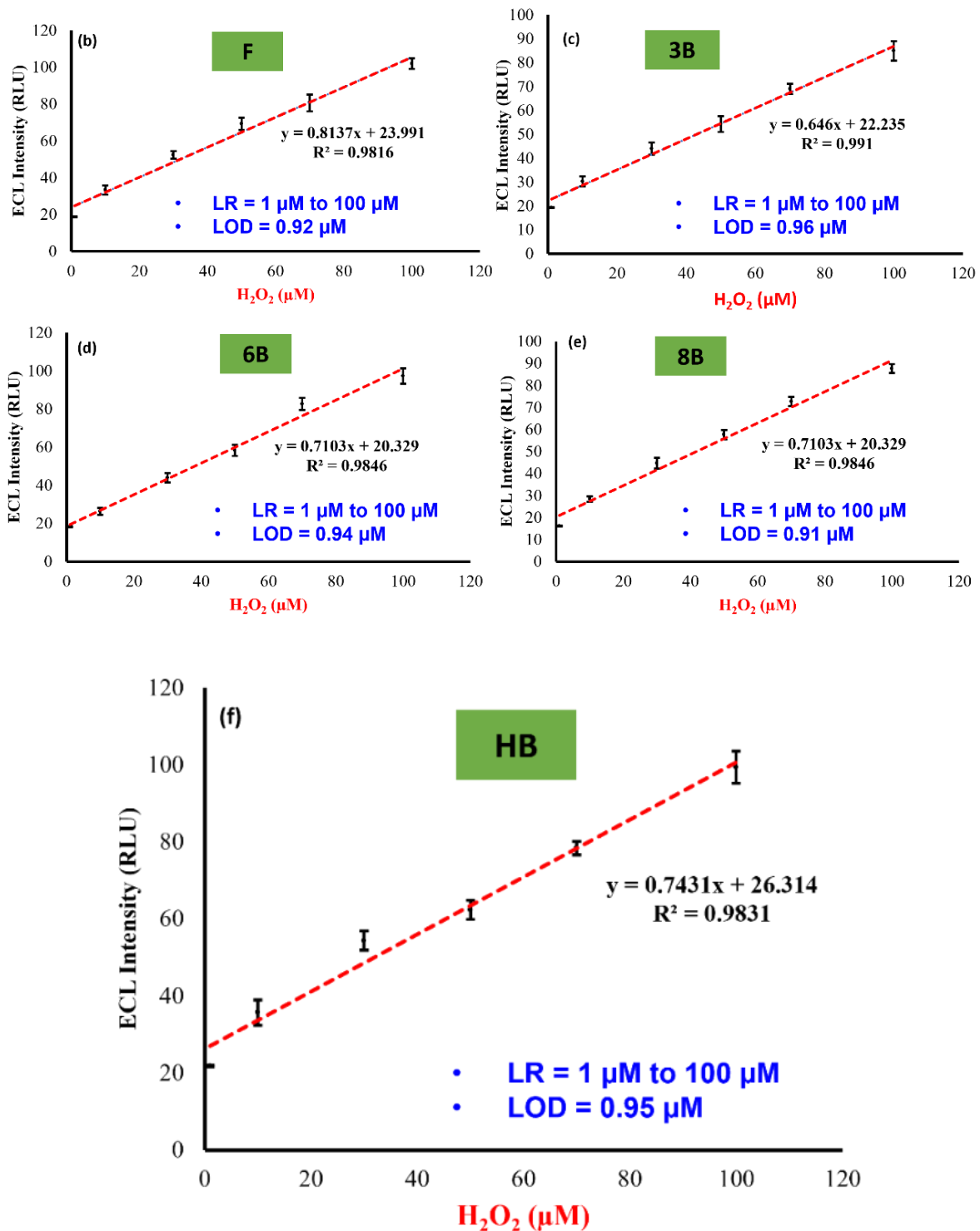


Figure 3.14 Sensing of H_2O_2 using different grade pencils. (a) sensing of H_2O_2 using H grade pencil. (b) sensing of H_2O_2 using F grade pencil. (c) sensing of H_2O_2 using 3B grade pencil. (d) sensing of H_2O_2 using 6B grade pencil. (e) sensing of H_2O_2 using 8B grade pencil. (f) sensing of H_2O_2 using HB grade pencil. Parameter used for experiments: luminol = 3 mM, applied voltage = 4V, H_2O_2 = 1 to 100 μM . The error bar denotes the standard deviation for three experiments ($n=3$).

3.4.6 Sensing of cholesterol using HB graded pencil-based GP-SE-ECL device

To further demonstrate the workability of the proposed device, the most usable and abundantly available HB-graded pencil-based GP-SE-ECL device was used, and sensing of cholesterol was carried out using luminol/H₂O₂-based electrochemistry. Following are the steps followed to detect cholesterol: first, luminol (3 mM concentration having 100 μ L volume), cholesterol having different concentration (100 μ L volume) and CHOx (50 units/mL) were pipetted into the channel. The maximum ECL intensity was observed for a CHOx concentration of 50 units/mL.

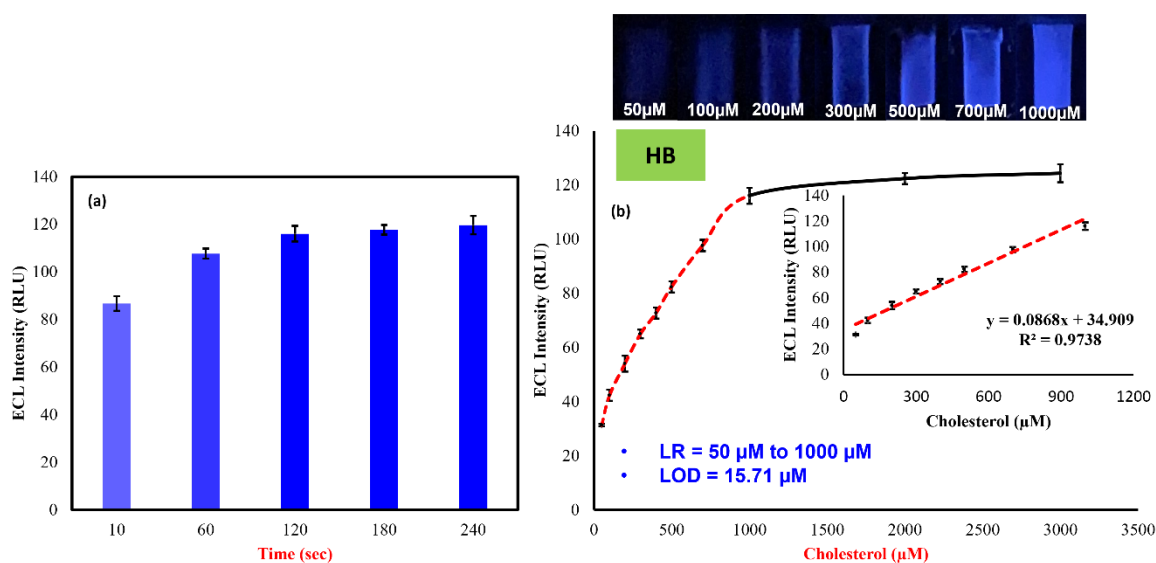


Figure 3.15 (a) time optimization for cholesterol to react with cholesterol oxidase. (b) Luminol/H₂O₂ chemistry-based cholesterol detection: luminol = 3 mM (100 μ L), applied voltage = 4 V, CHOx = 50 mg/mL (2.5 μ L), cholesterol = 50, 100, 200, 300, 400, 500, 700, 1000, 2000, 3000 μ M, time to produced H₂O₂ = 3 minutes, n = 3.

As a result, a concentration of 50 Units/mL CHOx was chosen for sensing of cholesterol. As cholesterol takes some time to react with CHOx (Figure 3.13 (d)), all three analytes (luminol, cholesterol, and CHOx) were retained in the channel for the optimal three-minute time. The relation between time and ECL intensity to detect cholesterol is illustrated in Figure 3.15 (a). Then the optimum voltage was applied to the DEs and the respected ECL signal was calculated using a mobile phone. The dependency of ECL signal intensity on the concentration of cholesterol is illustrated in Figure 3.15 (b). The detection of cholesterol was carried out by varying the concentration between 50 to 3000 μ M and an LR from 50 to 1000 μ M with LOD of 15.71 μ M was achieved. To take care of the dead volume issue, after every use the device was completely cleaned with IPA (60 % diluted) and then dried at room temperature for 10 to

15 minutes so that the dead volume could be equal to zero. While performing cholesterol detection, the final volume present in the channel was 202.5 μL .

3.4.7 Interference study using HB graded pencil-based GP-SE-ECL device

It is important to prove the anti-interference ability of the fabricated device in its application and development. Hence, to evaluate this, six different (glucose, xanthine, uric acid, lactate, choline, creatinine) interfering biomolecules were taken, and a rigorous interference study was carried out. First, the ECL intensity was calculated without any interfering compounds for 1000 μM concentration of cholesterol in a 100 μL volume. Subsequently, the interfering compound (such as glucose (1000 μM) in a volume (100 μL)), was added and ECL intensity was calculated. A percentage change of 2.58 was observed when glucose as an interfering compound was used.

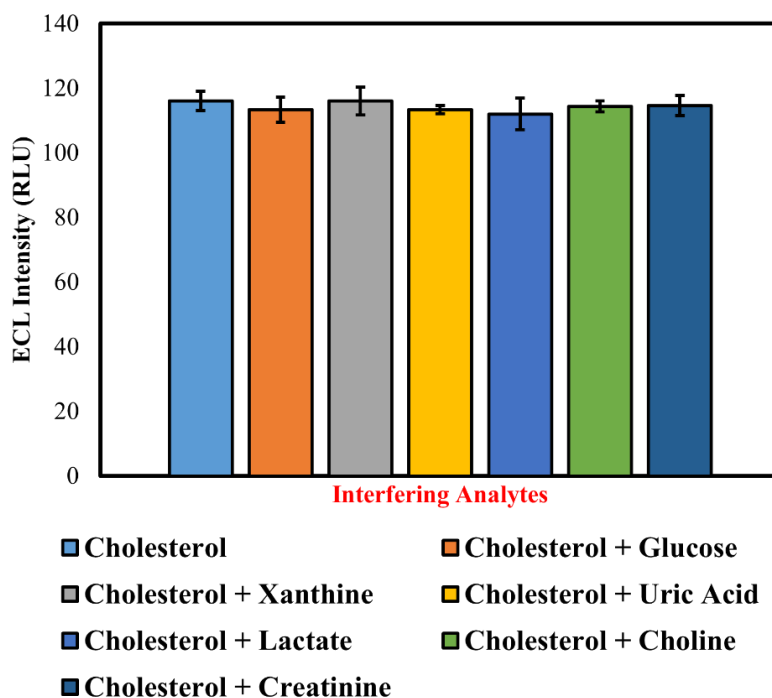


Figure 3.16 Interference study of cholesterol with other interfering compounds: luminol = 3 mM (100 μL), applied voltage = 4 V, CHOx = 50 mg/mL (2.5 μL), cholesterol = 1000 μM , glucose = 1000 μM , lactate = 1000 μM , xanthine = 1000 μM , uric acid = 1000 μM , creatinine = 1000 μM , choline = 1000 μM , n = 3.

A similar process was carried out for the other interfering compounds and concerning each, the ECL intensity was calculated. Experimentally, not much change in ECL intensity was observed (Fig. 6). The percentage change in the ECL intensity for xanthine, uric acid, lactate, choline, and creatinine 0.8 %, 2.58 %, 3.4 %, 1.43 %, and 1.1 %, was observed. The lock and key type

binding between the CHOx enzyme and substrate (cholesterol) form the basis for highly selective detection and luminol-mediated ECL provides the readout mechanism.

3.4.8 Real sample analysis of H₂O₂ and cholesterol in milk and blood serum using GP-SE-ECL device

Finally, the practical usability of the device was validated by doing a real sample analysis of cholesterol and H₂O₂ in blood serum and milk respectively.

Table 3. 2 Real Sample Analysis of H₂O₂ and Cholesterol

	Spike (μM)	Obtained (μM)	Recovery (%)
Cholesterol (Blood Serum)	300	288	96
	500	486	97.2
	700	673	96.1
H₂O₂ (Milk)	30	28.7	95.6
	50	50.4	100.8
	100	98.3	98.3

The standard addition method was used for the real sample analysis i.e. blood serum was diluted fifty times and milk was diluted thirty times to avoid interference due to the other high concentration interfering compounds. Different concentrations of cholesterol and H₂O₂ (see Table 3.2) were spiked into the diluted blood serum and milk in equal amounts, and ECL intensities were counted. The obtained recovery rates were encouraging and showed the possibility for the proposed device to be used in real-time applications.

3.4.9 Stability and reproducibility analysis using HB graded pencil-based GP-SE-ECL device

The long-term stability performance of the HB-graded pencil electrode-based GP-SE-ECL device was confirmed by utilizing cholesterol over a seven-day period. Stability analyses were carried out using all optimized parameters. First, the stability of the GP-SE-ECL device over seven days period was validated by taking the highest concentration (within the linear range) of cholesterol (1000 μM). Then the stability analysis for a lower concentration of cholesterol (100 μM) was carried out to validate the deterioration issues.

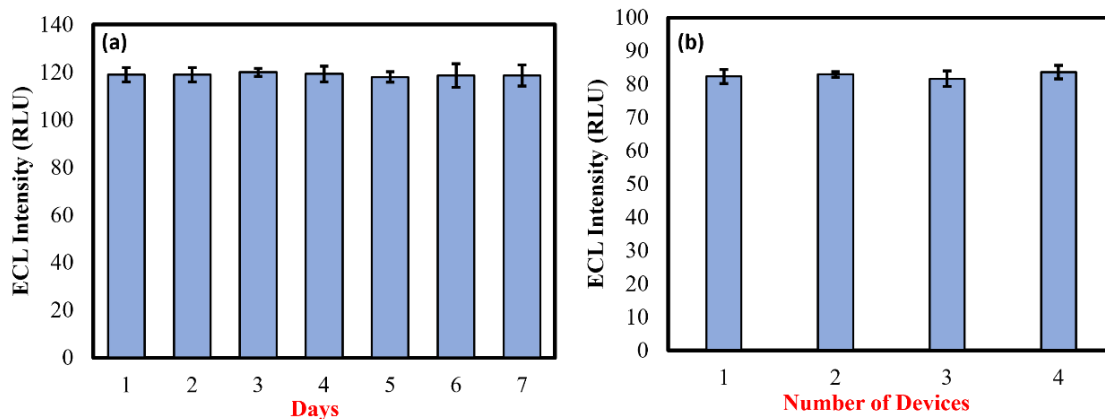


Figure 3.17 (a) Stability analysis of GP-SE-ECL device: (a) Cholesterol-based stability analysis, luminol = 3 mM (100 μ L), cholesterol = 1000 μ M (100 μ L), CHOx = 50 mg/mL (2.5 μ L), applied voltage = 4V. (b) reproducibility analysis using, cholesterol = 500 μ M, (100 μ L), CHOx = 50 mg/mL (2.5 μ L), applied voltage = 4 V, n = 3.

Though the enzymatic detection method was used to sense the cholesterol, in both cases (for higher extreme values and lower extreme values) the device showed excellently long-term stability performance. The long-term stability performance for the concentration of 1000 μ M cholesterol is shown in Figure 3.17 (a). Finally, the reproducibility of the fabricated device was tested using four different GP-SE-ECL biosensors for the same concentration of cholesterol (as shown in Figure 3.17 (b)). The obtained data shows that the fabricated biosensor has an acceptable reproducibility.

3.5 Summary of 3DP-ECL devices

In this work, 3D printing based fabrication techniques were used to fabricate ECL devices. In contrast to other fabrication techniques, 3DP provides numerous advantage such as rapid prototyping, waste minimization, low-cost manufacturing, high precision and speed, ability to fabricate complex designs. First, 3DP novel closed bipolar electrode ECL device was fabricated and effectively used to sense dopamine and choline. Two different electrochemistry such as Ru(bpy)₃²⁺/TPrA and Luminol/H₂O₂ was used to sense dopamine and choline, respectively. To capture the ECL signal, two different approaches were used, with a smartphone-based ECL platform and the second with a photomultiplier tube (PMT) enabled with Internet of things technology (IoT) capability. First, the sensing of choline was performed using PMT and smartphone-based approach by achieving linear range 5 μ M to 700 μ M and 30 μ M to 700 μ M with limit of detection (LOD) 1.25 μ M ($R^2=0.98$, N=3) and 3.27 μ M ($R^2=0.97$, N=3) respectively. Then, dopamine sensing was carried out using PMT and smartphone based

approached for the same linear range of 0.5 μM to 100 μM with LOD = 2 μM ($R^2= 0.99$, $N=3$) and LOD = 0.33 μM ($R^2= 0.98$, $N=3$). The smartphone-based sensing approach was more convenient since it is portable, miniaturized, does not require external power supply to drive ECL device and does not require darkroom for experimentation.

Next, a portable and compact, 3D printed six-well closed bipolar device was fabricated and validated by performing single step detection of glucose and choline. After performing several optimizations, the single step detection of glucose and choline was accomplished for the linear ranges of 0.1 mM to 10 mM and 0.1 mM to 5 mM, respectively, with a LOD of 24 μM and 10 μM . Following are the main key advantages of fabricated six-well 3DP-CBPE-ECL device: 1) single step, low-cost fabrication (3D-printing) approach was used to fabricate ECL devices, 2) most popular Luminol/ H_2O_2 based enzymatic chemical reaction reactions were used to detect glucose and choline, 3) the smartphone was leveraged to its full potential by executing many activities such as capturing ECL images, powering the ECL device, and calculating the ECL intensity of the obtained ECL signal.

Finally, a low-cost, widely accessible graphite pencil-based GP-SE-ECL biosensor with good electrical properties was fabricated and effectively validated by sensing H_2O_2 and cholesterol. The GP-SE-ECL biosensor was made using an SLA 3D printing technique within 30 minutes. The sensing of H_2O_2 and cholesterol was carried out using the well-reported Luminol/ H_2O_2 based electrochemistry. The ECL signal dependency on the conductivity was thoroughly validated by sensing the H_2O_2 using different graded pencil electrodes (F, H, HB, 3B, 6B, and 8B) based GP-SE-ECL biosensor. While sensing H_2O_2 , the same LoD values were observed for different graphite pencil grades, demonstrating that the ECL signal is not highly dependent on a pencil-type and therefore conductivity. Furthermore, the performance of the fabricated GP-SE-ECL biosensor was validated by sensing cholesterol with optimized parameters and achieving a linear range from 50 μM to 1000 μM with a detection limit of 15.71 μM . Hence, based on the results and other key important functions the fabricated 3DP-ECL device has shown potential to employ in a variety of biochemical applications. The following chapter will concentrate on paper-based ECL devices that use rGO-based electrodes developed over paper substrates to detect lactate in human serum.

Chapter 4. Paper Based ECL Devices

In this chapter, thorough discussion is carried out on paper based ECL devices. In depth explanation regarding material selection, fabrication, characterization, and validation is provided in this chapter. Paper based single electrode ECL devices, and their applications are explicitly explained in this chapter.

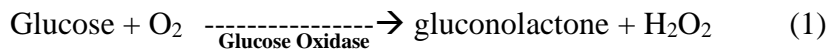
4.1 Introduction to paper-based devices

A decade ago, paper-based microfluidic devices piqued the interest of researchers as a viable diagnostic platform [103]. Paper-based devices have several significant advantages, including low-cost, disposable, requirement of low sample volume and less time for diagnostics, mass manufacturing capability, and rapid prototyping. Such unique virtues have resulted several devices that are widely utilized in chemical investigations [104]. Furthermore, when compared to traditional polymer and glass substrate-based microfluidic devices, paper-based devices have unique benefits such as inherent capillary action to avoid the need of external pumps and valves, easy integrability with miniaturized devices, portability, simple operation and superior biological compatibility [105]. As a result, paper-based microfluidics devices are widely used in variety of applications including environmental monitoring, food control management, clinical diagnostics, molecular analysis and in point-of-care [106]. By keeping the advantage of paper-based devices in mind in the presented study paper based single electrode system (P-SE-ECL) has been designed to sense / detect glucose and lactate analytes.

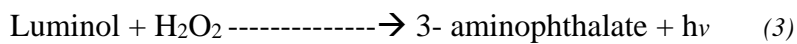
Glucose and lactate play vital roles in the human body, as a deficiency of these biomolecules can result in serious disorders. To accomplish metabolic processes correctly, each cell in the human metabolism system requires energy. Glucose is the principal source of energy for muscles, brain, tissues and a variety of other body components. However, high blood sugar levels can lead to heart, nerve, and eye disorders. On the other hand, low glucose levels, create severe issues such as headaches, weakness, anxiety, nervousness etc. [10][42][107]. Lactate is a by-product of tissue glucose metabolism that can be found in saliva, blood, skin excretion and urine. Lactate control is important for monitoring blood oxygen levels. It has been reported that the deficit of lactate may cause muscle pain, tiredness and cramps during training [108]. Therefore, maintaining the levels of glucose and lactate is having great importance for the body to function properly. Herein, the P-SE-ECL device has been successfully fabricated and utilized to sense these biomolecules.

In the present study, first, leveraging optimized speed and power of a blue laser, rGO based single electrode ECL device was successfully explored. A 3D printed miniaturized portable black box assembly embedded with smartphone was effectively used to take ECL images and powering the P-SE-ECL device. Various characterizations, such as scanning electron microscope (SEM), were accomplished to understand the morphological study of rGO based electrodes. Furthermore, to confirm the presence of rGO over paper-based substrate RAMAN spectroscopy analysis were carried out and the obtained results were compared with literature. To validate the performance of P-SE-ECL device, luminol/H₂O₂ based reactions were executed to sense glucose and lactate. The corresponding enzymatic reactions to sense glucose and lactate are given in equation (1, 2, 3 and 4) [109].

Enzymatic Reactions:



BPE Anode Reaction:



BPE Cathode Reaction:



4.2 Concept and fabrication flow for P-SE-ECL device

To comprehend the working concept of P-SE-ECL device, luminol/H₂O₂ based chemical reactions were executed. As shown in Figure 4.1 (a), both terminals (positive and negative) of an external voltage were applied to the two rectangular shape driving electrodes (DEs) known as anode and cathode. When an adequate voltage was applied across DEs, a strong electric field was formed throughout the channel, and simultaneous oxidation and reduction happened at the anode and cathode, resulting in the initiation of an ECL signal at the anode. All the device dimensions such as channel length (12 mm), width (6 mm) and length (8 mm) of DEs were chosen as it is from the previous work published by our group [29].

A novel paper based single electrode ECL device was fabricated on a filter paper (whatman grade 1) and a laser printer illustrated in Figure 4.1 (b) Prior to fabrication, the P-SE-ECL device was designed in SOLIDWORKS™ and saved as “.dxf” file. The “.dxf” file was then converted to G-Code using voxelizer 2.0, to set the speed and power of the laser, which was

compatible with laser printer. The final design of the device was sent to a laser printer through voxelizer graphical user interface (GUI). To fabricate the device, first, the filter paper was sprayed with fire retardant spray and kept in oven at 75°C for 20 minutes to avoid the burning of filter paper shown in step 2. Then, blue laser with optimized speed (100%) and power (10%) was ablated over filter paper to form rGO based DEs illustrated in step 3. To create hydrophobic zone over paper, same wax lamination approach was adopted from previous published article by our group [110]. Following steps were followed to form hydrophobic zone over paper. Initially, by manual dipping method molten wax was layered on A4 copier paper. Thenceforth, mold was formed by keeping wax coated paper below blue laser printer. Thereafter, the wax coated mold was then carefully positioned over the fabricated DEs and passed through the laminator (temperature = 85°C and speed = 5 rpm). Finally, using the hot lamination procedure described in step 4, a hydrophobic zone was formed over paper-based substrate. The final fabricated P-SE-ECL device with hydrophobic and hydrophilic zones and DEs is shown in step 5.

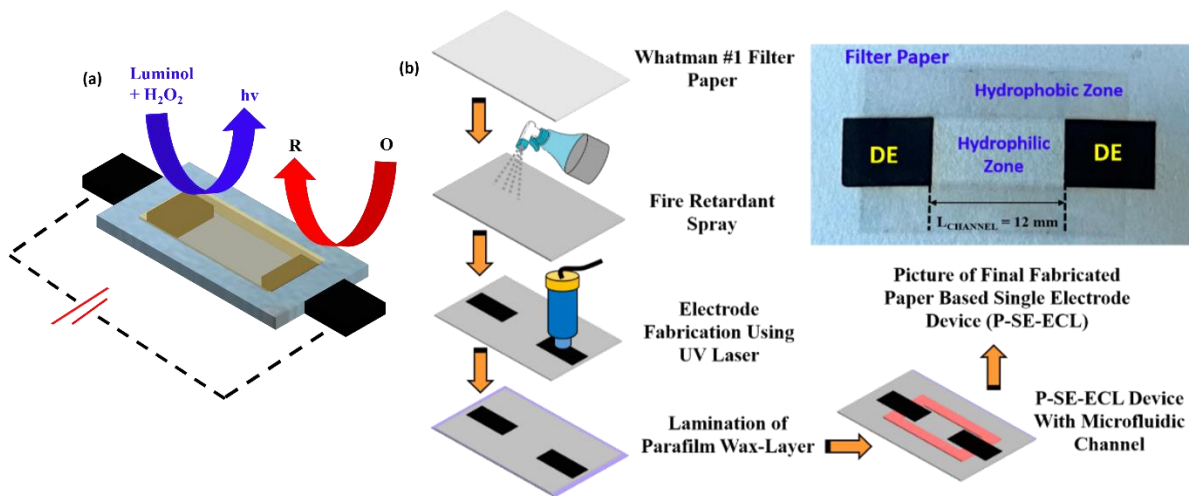


Figure 4.1 (a) Schematic representation of P-SE-ECL device with anodic and cathodic reactions. (b) Fabrication flow for paper based single electrode ECL device.

4.3 Data acquisition and analysis

The 3D printed black box with smartphone, buck boost converter and P-SE-ECL device is shown in Figure 4.2 (a). Herein, the mobile-based android app was successfully used not only to capture ECL signals but also to calculate ECL signal intensity. The app was implemented in java built-in android studio with read write storage. The ECL intensity app is shown in Figure 4. 2 (b). As shown in Figure 4. 2 (c), the smartphone based android app was designed in such

a way that it can compute the ECL intensity of real-time images as well as images stored in the gallery.

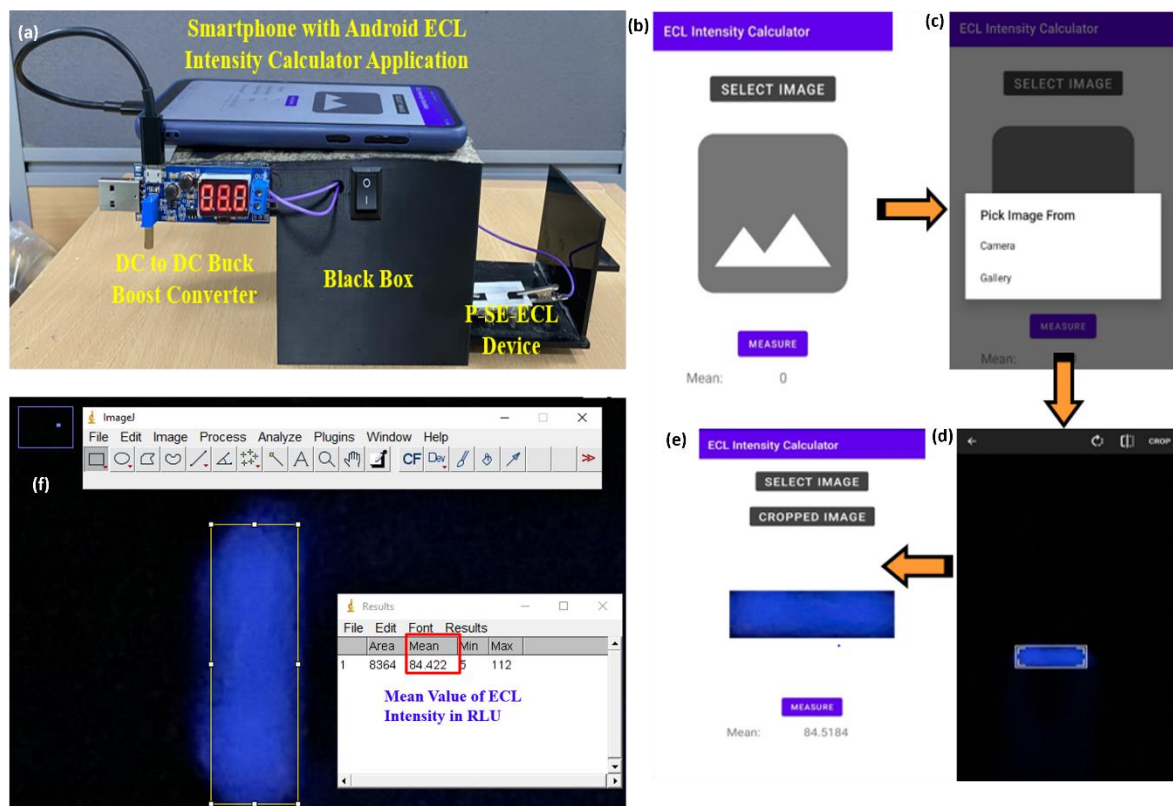


Figure 4.2 Data acquisition using mobile application: (a) real image of 3D printed black box with in house smartphone and buck boost converter to capture ECL signal. (b) mobile based ECL intensity calculator. (c) capture real time image or pick image from gallery option present in mobile app. (d) selected high intensity area of ECL image. (e) calculation of intensity using ECL intensity calculator. (f) ECL signal intensity calculation using ImageJ software.

4.4 Characterization of P-SE-ECL device

The characterization of the fabricated P-SE-ECL device was carried out using scanning electron microscope (SEM) and RAMAN spectroscopy as shown in Figure 4. 2 (a) and (b) respectively. The SEM analysis was accomplished to understand the morphological study of rGO-based electrodes. The SEM image of rGO is shown in Figure 4. 2 (a). Further, RAMAN spectroscopy-based analysis was carried out to confirm the presence of rGO on paper-based platform. I_D/I_G ratio was used to calculate the structural defects presents in material. Herein, I_D/I_G ratio was calculated to be 0.94 which confirms the presence of rGO. The obtained value of I_D/I_G ratio was well matched with the literature values [111][112]. In addition, detailed analyses, such as x-ray photoemission spectroscopy (XPS), was performed to determine the

amount of carbon and oxygen in the produced rGO. Finally, transmission electron microscopy (TEM) based analysis was done to obtain morphological information [113].

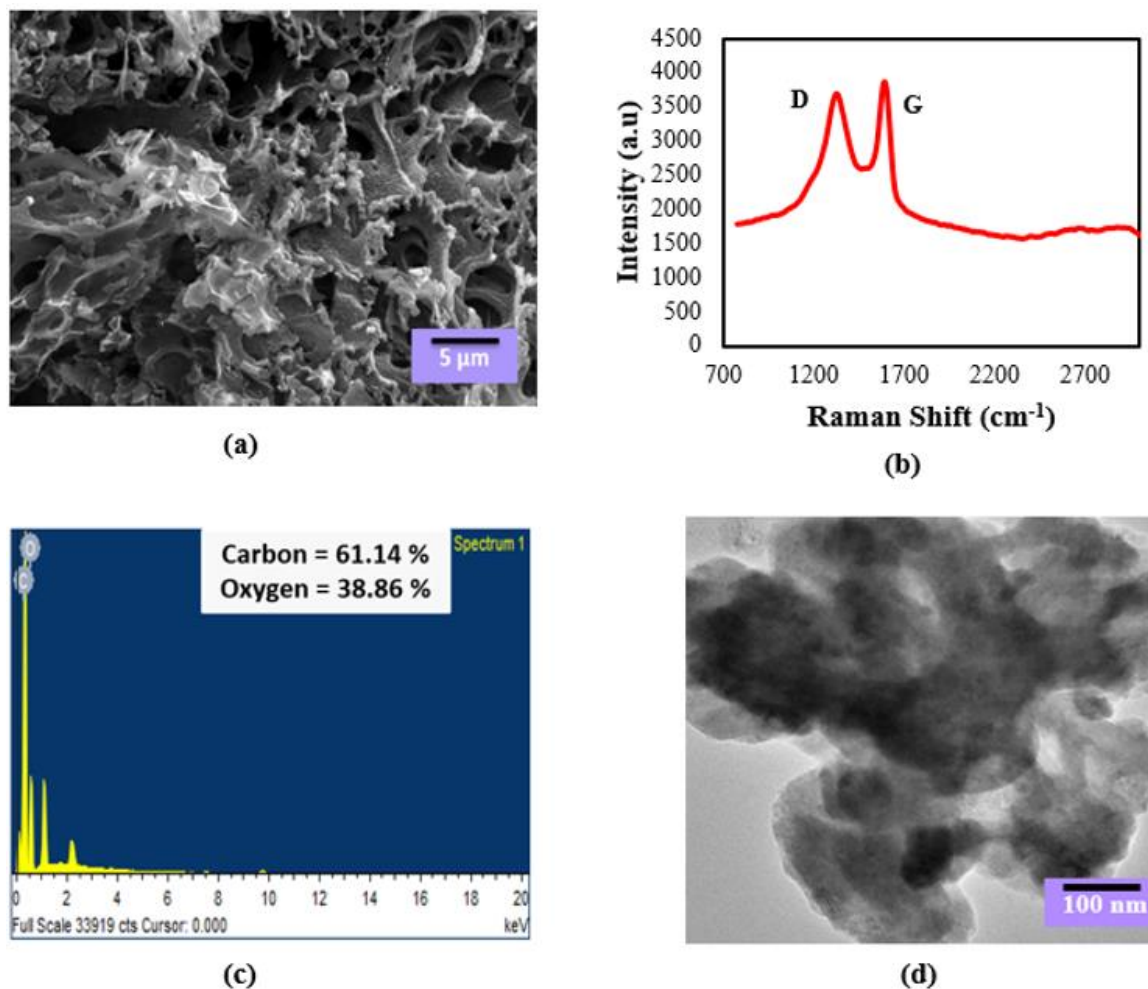


Figure 4.3 characterization of P-SE-ECL device: (a) SEM analysis. (b) RAMAN analysis. (c) XPS analysis. (d) TEM analysis.

4.5 Parameters optimization for P-SE-ECL device

Optimization of several parameters on which ECL signal intensity is highly dependent is a crucial challenge in order to achieve the best feasible outcomes during ECL detection. Few critical and necessary parameters on which the intensity of the ECL signal is highly dependent include channel length (12 mm), concentration of luminol (5 mM) and applied voltage (7 V).

4.6 Analytical performance of P-SE-ECL device

Subsequent to the device fabrication by leveraging the optimized parameter, sensing of glucose, and lactate with optimized parameters utilizing luminol/H₂O₂ based chemistry was performed to validate the workability of the P-SE-ECL device. As illustrated in Figure 4. 4 (a),

sensing of glucose and lactate was accomplished using glucose oxidase and lactate oxidase respectively. The following method was adopted for the sensing of glucose. First, the anode of the P-SE-ECL device was modified with glucose oxidase, and then luminol and glucose were pipetted into the channel. As glucose takes some time to react with glucose oxidase, hence all three constituent chemicals (luminol, glucose and glucose oxidase) were kept in the channel for the optimized time of 3 minutes. After that to get the ECL signal, external optimized voltage (7 V) was applied to the P-SE-ECL device. Subsequently, glucose sensing was done by achieving a linear range from 100 μM to 1000 μM having LOD of 2.16 μM ($R^2 = 0.98$, $n=3$). The variation between Glucose and ECL signal is illustrated in Figure 4. 4 (a). A similar approach was used for lactate sensing as it was for glucose sensing. It was found that the optimal time period for lactate to react with lactate oxidase was 15 minutes. Keeping this in mind, lactate sensing was accomplished by attaining a linear range of 100 μM to 5000 μM with a LOD of 3.84 μM ($R^2 = 0.98$, $n=3$). The relation between lactate and ECL signal is illustrated in Figure 4. 4 (b).

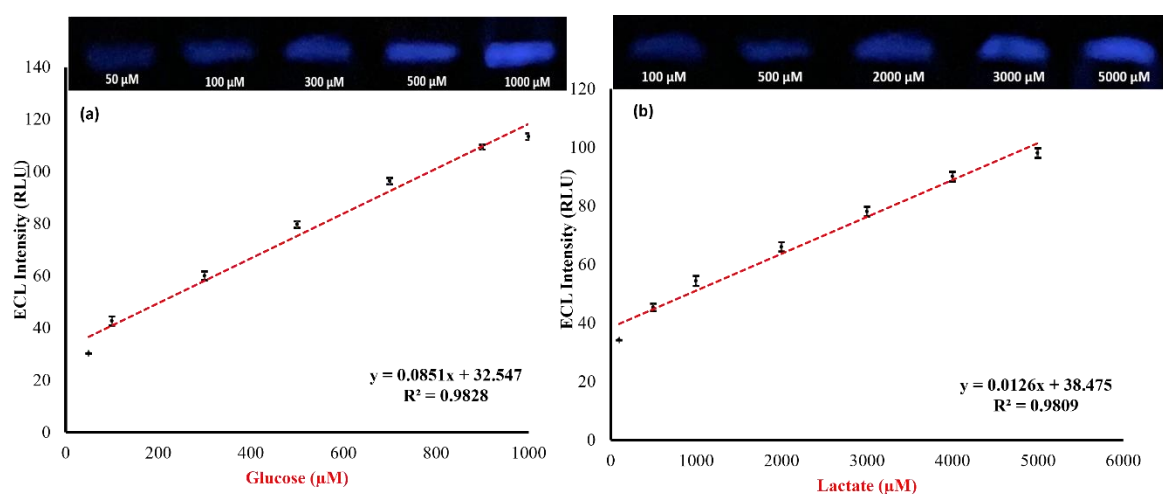


Figure 4.4 Analytical performance of P-SE-ECL device; (a) Glucose (μM) Vs ECL Intensity (RLU), Glucose = 50, 100, 300, 500, 700 and 1000 μM , Luminol = 5 mM, Applied Voltage = 7 V; Glucose oxidase = 10 mg/mL; (b) Lactate (μM) Vs ECL Intensity (RLU), Lactate = 100, 500, 1000, 2000, 3000 and 5000 μM , lactate oxidase = 25 units/mL, $n = 3$.

4.7 Selectivity and storage stability analysis of P-SE-ECL device

The selectivity analysis for glucose and lactate was performed to demonstrate the functionality of the fabricated P-SE-ECL device. First, for the particular concentration of glucose (1000 μM) ECL intensity was calculated. The device's selectivity with various interfering compounds such lactate, ascorbic acid, xylose, and galactose was proven one by one.

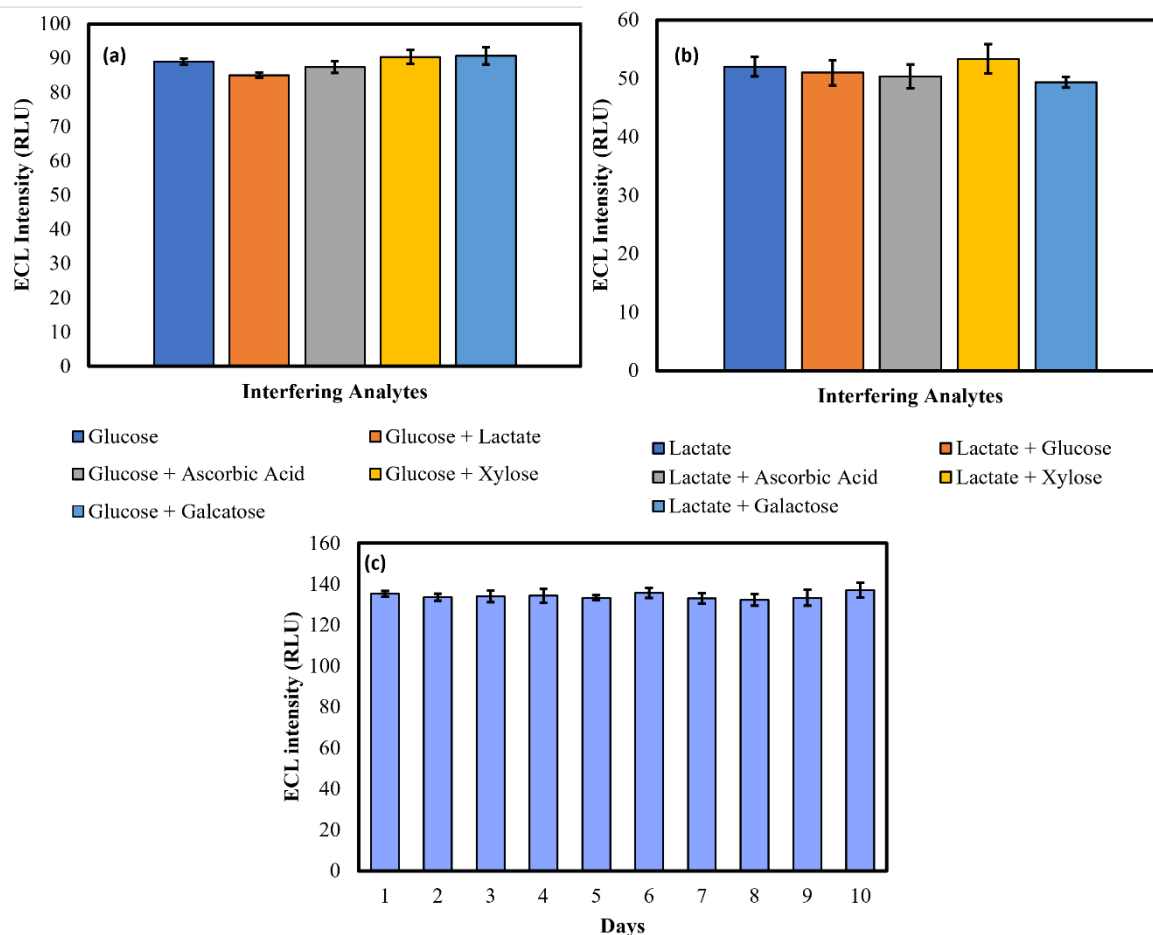


Figure 4. 5 Selectivity analysis using P-SE-ECL device. (a) selectivity analysis for glucose with lactate, glucose = 1000 μM , glucose oxidase = 10 mg/mL, applied voltage = 7V, lactate = 1000 μM , Ascorbic acid = 1000 μM , Xylose = 1000 μM , Galactose = 1000 μM . (b) selectivity analysis for lactate with glucose, lactate = 1000 μM , lactate oxidase = 25 units/mL, glucose = 1000 μM , Ascorbic acid = 1000 μM , Xylose = 1000 μM , Galactose = 1000 μM , applied voltage = 7 V. (c) Stability analysis for rGO based single electrode device. H_2O_2 = 1 mM, Luminol = 5 mM, applied voltage = 7V, $n = 3$.

First, to check the selectivity, lactate with the same concentration (1000 μM) was added with glucose concentration and ECL signal intensity was calculated and very small variation in ECL intensity was observed. Subsequently, selectivity of device with other interfering compounds such ascorbic acid (1000 μM), xylose (1000 μM), and galactose (1000 μM) was validated and very small variation in ECL intensity (less than 5%) was observed, demonstrating that the device has high selectivity with respect to other analytes. The selectivity analysis for glucose with lactate, ascorbic acid, xylose, and galactose is shown in Figure 4. 5 (a). Similar approach was carried out to perform the selectivity analysis for lactate with respect to glucose (1000 μM), ascorbic acid (1000 μM), xylose (1000 μM), and galactose (1000 μM). The selectivity analysis for lactate with other analytes is shown in Figure 4. 5 (b). After selectivity, device

storage stability analysis was carried out for ten days. Several experiments were carried out over a period of 10 days to test the stability of a rGO-based single electrode device using luminol/H₂O₂ based chemistry, and the stability of a rGO-based single electrode device were confirmed by observing less than 5% change in ECL intensity. The obtained stability results confirmed that the fabricated device can be used for an extended period of time. Stability analysis for fabricated device is shown in Figure 4. 5 (c)

4.8 Real sample analysis using P-SE-ECL device

Finally, real sample analysis was carried out using P-SE-ECL device with standard spiking method for glucose and lactate. Well established spiking method with following approach was utilized for real sample analysis. First, the unknown blood sample was taken and diluted for ten times to avoid interference. Following dilution, multiple concentrations of glucose and lactate (listed in Table 4.1) were spiked into an unknown blood sample, and ECL signal was determined for each added concentration. Based on the obtained results, percentage recovery rate was calculated for every added sample which is summarized in Table 4. 1. On the basis of recoveries achieved in this study, it was determined that the fabricated P-SE-ECL device can be employed in real time applications such as biomedical and environmental monitoring applications.

Table 4. 1 Real sample analysis for glucose and lactate using P-SE-ECL device.

Analytes	Added (μ M)	Found (μ M)	RSD	Recovery (%)
Glucose	100	98	3.94	98
	500	518	2.68	103.6
	700	678	1.38	96.85
Lactate	100	101	0.59	101
	300	286	1.26	95.66
	500	512	2.36	102.6

4.9 Summary for P-SE-ECL device

In this work, a novel paper-based single electrode ECL device (P-SE-ECL) was successfully fabricated and validated by sensing various biomolecules. The single driving electrode on P-SE-ECL was realized by embedding reduced graphene oxide (rGO) over the paper-based substrate by ablating blue laser with optimized parameters. To form a channel, the wax-lamination method was successfully utilized. The combination of rGO, wax-lamination and paper offer the foundation for adaptable, disposable, portable and low-cost P-SE-ECL devices. The main key features of P-SE-ECL devices are - 1) P-SE-ECL devices are fabricated with the

easily available paper-based substrate with simple fabrications steps without the need of any trained personnel; 2) rGO based, single-step, ultrafast electrodes can be developed over paper by ablating blue laser; 3) P-SE-ECL devices are compatible with most usable luminol/H₂O₂ and Ru(bpy)₃²⁺/TPrA based chemistry; 4) the designed, complete 3D printed tiny ECL system may be used in an open environment to capture ECL signal without requiring an external power supply, making the fabricated system portable.; 4) no need to use software like ImageJ to calculate ECL signal intensity, as a smartphone can be effectively utilized to capture and calculate the intensity of ECL signal. Therefore, keeping in mind the features mentioned above, the proposed P-SE-ECL device has the potential to be used in diversified applications such as food control management, clinical diagnostics, and point-of-care testing. The advantages of ML learning assisted ECL biosensors and their effective utilization to predict the concentration of various biomarkers is explained in the next chapter.

Chapter 5. A Machine Learning Approach for ECL Based Point of Care Testing Device to Detect Multiple Biomarkers

This chapter describes fabrication of 3DP ECL devices, and their application in the field of biomarkers detection. Regression based machine learning (ML) algorithms were effectively used to predict the different biomarkers and compared the performance of different ML algorithms based on different regression metrics. Finally, the device performance was validated by doing the real sample analysis.

5.1 Introduction to Machine Learning approach to detect various biomarkers

PoC diagnostic devices can potentially improve the healthcare facilities in the remotest corner of the world through an early diagnosis and therefore enable timely intervention and remediation for multiple diseases and disorders. These low-cost and portable devices can potentially benefit a large population in developing countries that do not have direct access to conventional diagnostics. In addition to easy accessibility, the PoC devices offer options for continuous monitoring of a particular biomarker or analyze that can be tracked through a smartphone-based application over an extended duration. Biomarkers have traditionally been used for diagnosing human health due to their direct correlation with multiple diseases and health conditions. The irregularities in the biomarkers can cause potential ailments in humans. Biosensors open a new window for researchers to develop miniaturized point-of-care devices to detect various diseases at the early stage, which helps cure patients and ultimately reduces the treatment cost. Compared to the traditional testing approaches, biosensors have provided numerous advantages such as fast response, less sample volume, inexpensive, and on-site or near patient diagnosis can be possible. However, these biosensors come with their own limitations like sensor-to-sensor variations and non-linearity of the output data. Many researchers have been using many ML-based approaches to overcome the limitations of the biomarkers [114].

In recent times, ECL-based biosensors have gained immense popularity because of their high sensitivity and selectivity [115], [116], extensive operating range, minimum set-up requirement, low or minimum background signal, and reasonable control over the generated electrochemiluminescence signal [117]. In addition, ECL biosensors are being explored as a faster, cheaper, and more efficient alternative to traditional solutions such as the photomultiplier tube and charge-coupled devices-based detectors for biomarker detection. Despite numerous advantages of ECL-based biosensors, some biosensors have completely

relied on aptamer, antibodies, and antigen as baroreceptors, which questioned the shelf-life and stability performance of the biosensors leading to the prohibition of their commercialization [118]. The cost, stability, and shelf-life of these reagents are critical factors that can impact their suitability and effectiveness for different applications. The cost of enzymes and antibodies can vary widely depending on the source, quality, and quantity required. Stability and shelf-life are also important considerations for enzymes and antibodies. Enzymes and antibodies can be susceptible to denaturation and degradation over time, especially if they are exposed to unfavourable conditions such as high temperature. It is important to store enzymes and antibodies under appropriate conditions, such as at the appropriate temperature and pH, to ensure their stability and prolong their shelf-life. Hence to maintain the shelf-life of enzymes every time new stock solution was prepared, and experiments were carried out.

Based on these facts, rigorous analysis of sensing data using ML is in demand as ML-based algorithms could act as game-changing approaches to overcome the limitations of ECL-based biosensors. ML is fast emerging as an acceptable tool for sensor data analysis to improve the overall accuracy of the sensors [114][119]. Besides enhancing the sensor accuracy, ML can also help improve the time-to-market, automate the data-driven analysis process, and help identify the unforeseen interdependencies between the biomarker agents and signals. Moreover, ML-based techniques can help to solve these challenges faced by ECL biosensors by providing a better fit across the specimen, concentrations, and sensor combinations [120][121].

This study encompasses 3D printing of ECL-biosensor, input parameter optimization, biosensor validation by sensing multiple biomarkers including glucose, lactate, and choline, performance validation through stability and interference study. In addition to the white-box approach, experimental data were analyzed using multiple ML-based algorithms to provide the most accurate y-predictor for the ECL-biosensors. The experiment involved 3D printing of interdigitated bipolar ECL biosensor using conductive PLA filament. To improve the signal amplification, the interdigitated (IDE) bipolar ECL biosensor was chosen over the conventional bipolar electrode [122]. Luminol/H₂O₂-based electrochemistry was successfully used for parameter optimization and for performance validation. Various ML algorithms including Robust Linear Regressors, Partition-based Models, (e.g., Support Vector Machines) and Ensemble Techniques (e.g., Decision Tree and Random Forest) were applied to analyze the

interaction effect of different biomarkers for the manufactured ECL device. While ML Models helped improve the accuracy of the y-predictors in general, ensemble techniques like Decision Tree, Random Forest, and Gradient Boost produced the best R-squared values along with the least error scores. As per the comparative results of various models, it can be inferred that the ML-based approaches can help the ECL biosensors to improve their accuracy and performance.

5.2 Fabrication and working concept of ECL biosensors

To fabricate the ECL device 3D printing methodology was used. First, the design was performed in Solid works CAD modelling software. After CAD modelling, the design was

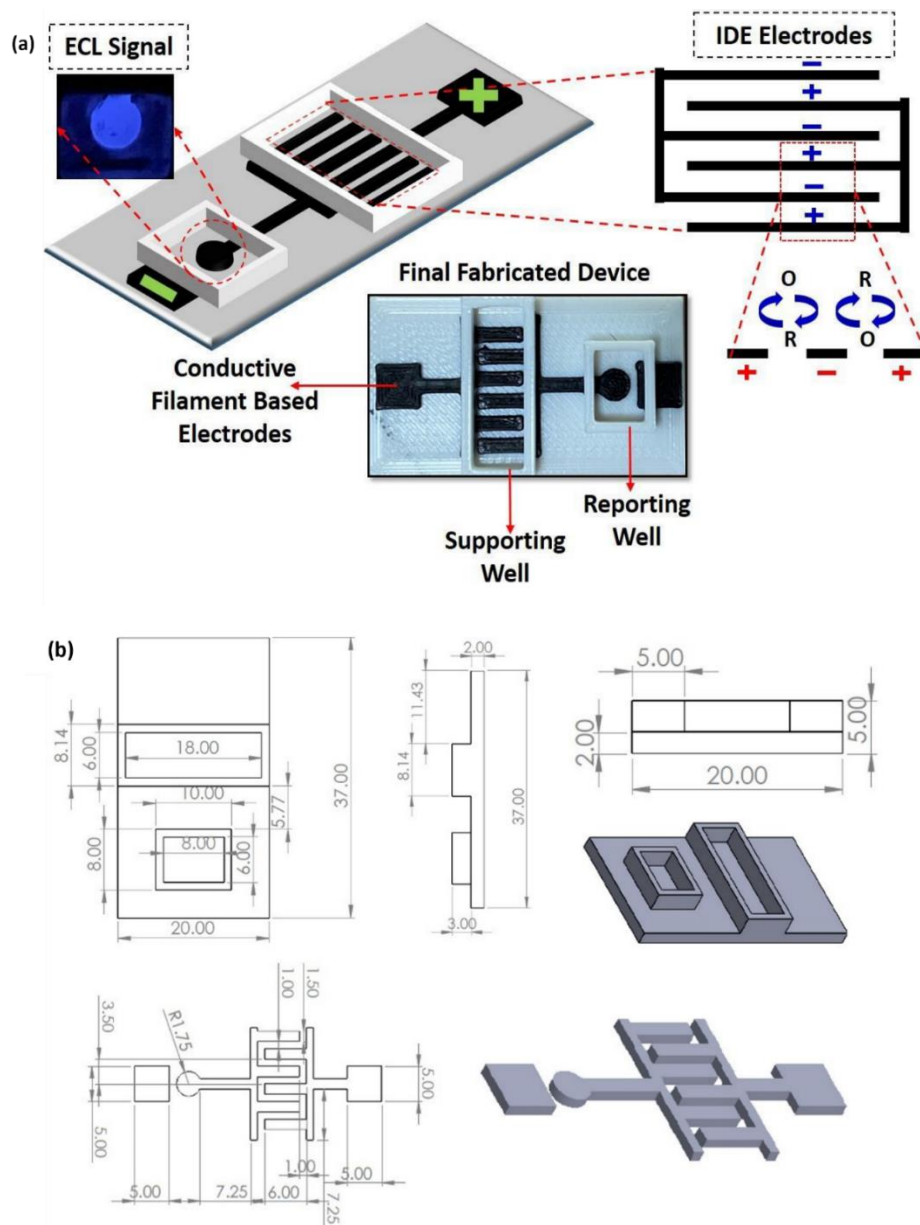


Figure 5.1 (a) Schematic of the fabricated ECL biosensor with oxidation and reduction, (b) sketch drawing for one-well 3DP-IDE-CBPE-ECL biosensor.

transferred to a 3D printer (Sigma BCN 3D) using the graphical user interface (GUI) on the printer. The bed temperature of the 3D printer was maintained at 60°C. The PLA filament temperature was maintained at 220°C. Finally, with those parameters the ECL devices were successfully fabricated.

ECL-based biosensors work using reactions between electrochemically produced reagents producing light via electron transfer. These biosensors use biological interactions between the reagents to produce a luminescent signal that in turn can help measure different biomarkers. IDEs offer an improved surface area for oxidation and reduction reactions enabling the operation of multiple IDE-BPEs using a single pair of electrical contact [122]. The cathode pole of BPE is divided into multiple arms which are interdigitated with arms extending from the anode of BPE. When a sufficient potential is applied, the redox process occurs between the IDEs (Figure 5. 1 (a)), generating an ECL signal at the anode. A sketch drawing for a one-well 3DP-IDE-CBPE-ECL biosensor has been incorporated and shown in Figure 5.1 (b).

5.3 Chemicals and materials

D-glucose, lactate, choline, luminol ($\geq 98\%$ purity), glucose oxidase (GOx), lactate oxidase (LOx), choline oxidase (COx) hydrogen peroxide (H_2O_2) (35%), sodium hydroxide (NaOH), were procured from Sigma Aldrich, India. Dimethylformamide (DMF) and Isopropanol (IPA) were procured from SRL, India. 3D printer (Sigma BCN 3D) was used to fabricate ECL biosensors in the laboratory. Commercially available black composite conductive PLA was purchased from Proto pasta, USA, to fabricate conducting zones. White PLA filaments were sourced from one of the online vendors in India.

5.4 Results and discussion

5.4.1 Parameter optimization

Various input parameters were considered to optimize various factors to achieve the best results. First, the effect of interdigitated fingers (IDEs) on ECL intensity was observed as in Figure 5.2 (a). While fabricating and testing the ECL device iteratively, the number of IDEs were increased from two to four and then from four to six. By increasing the number of IDEs to four and six, the ECL signal increased by 25% and 88% respectively. One possible reason could be that when the number of IDEs increase, the redox process improves, resulting in an increased ECL intensity. Next, the effect of DMF treatment on ECL intensity was validated, as shown in Figure 5. 2 (b). C. Lorena Manzanares Palenzuela *et al.*[92][123] developed activation steps for the PLA conductive filaments. The DMF treatment increases the porosity

(surface area) of the electrodes. DMF-treated electrodes also become highly electroactive, resulting in increased ECL signal intensity. Reporting and supporting channels were pipetted with DMF for 10 minutes before IPA treatment and then left to dry for 6 hours at the room temperature. To realize the closed bipolar system, the complete microfluidic channel was divided into two parts (supporting channel and reporting channel). The anode of IDE electrode was present in reporting channel and cathode (IDEs) were present in supporting channel.

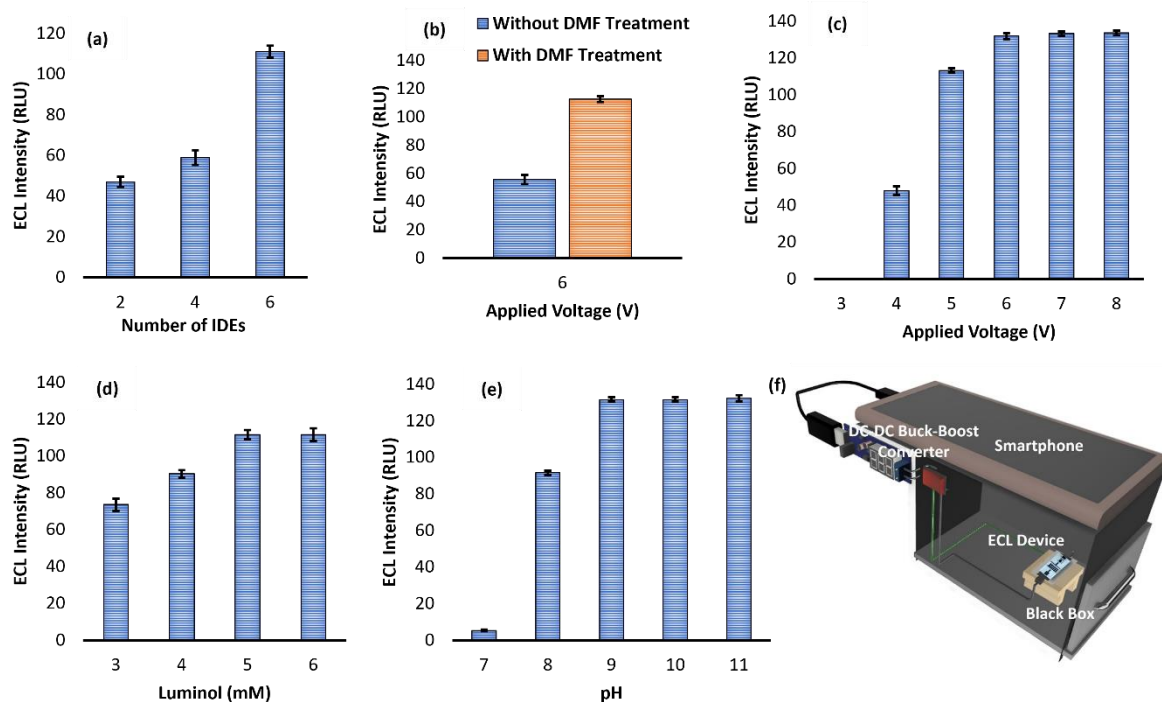


Figure 5.2 Parameters optimization; (a) IDEs optimization, luminol = 5 mM, voltage = 6 V, H_2O_2 = 1 mM, PBS = 0.1 mM. (b) effect of DMF, luminol = 5 mM, glucose = 5 mM, GOx = 10 mg/mL, voltage = 6 V, PBS = 0.1 mM. (c) voltage optimization, luminol = 5 mM, H_2O_2 = 1 mM, voltage = varied from 3 V to 8 V, PBS = 0.1 mM. (d) luminol optimization, voltage = 6 V, H_2O_2 = 1 mM, luminol = varied from 3 mM to 6 mM, PBS = 0.1 mM. (e) pH optimization, voltage = 6 V, H_2O_2 = 1 mM, luminol = 3 mM, pH = varied from 7 to 11, PBS = 0.1 mM. (f) The ECL imaging and analysis system; $n = 3$.

In addition, optimizations in terms of applied voltage and luminol were carried out (Figure 5. 2 (c) and (d)). For the applied voltage range from 3 V to 8 V, ECL signal intensity saturated after 6V as observed in Figure 5. 2 (c). Effect of luminol concentration was studied by analyzing for concentration range from 3 mM to 6 mM. It was observed that ECL signal intensity saturates after 5 mM of luminol concentration. Finally, the effect of pH over ECL signal was evaluated by varying the pH values from 7 to 11 by keeping luminol and voltage values constant. The maximum ECL signal intensity was observed at 9 pH. The optimal values

for the applied voltage (6 V), luminol (5 mM) and pH (9) were maintained in the subsequent experimental cycles to get the optimum results. The in-depth analysis with proper explanation for optimization of various parameters is available in our previously published articles [42][43]. All the optimized parameters are summarized in Table 5.1

Table 5. 1 Optimized Parameters

Parameter	Applied Voltage	Luminol	pH	No. of IDEs
Optimized Value	6V	5 mM	9	6

5.4.2 Analytical performance of ECL biosensors

The detection of glucose, lactate and choline plays a crucial role in food inspection, medicine, and diagnostic assays. These bio-analytes were detected to demonstrate the analytical ability of the 3D-IDE-CBPE-ECL biosensor. The enzymatic detection strategy was used with optimized parameters to detect glucose, lactate, and choline.

To measure the glucose concentration, glucose oxidase and luminol were pipetted into reporting well for an already optimized time of 3 minutes. It was observed that glucose and glucose oxidase would require some time to produce H₂O₂. A time optimization study was performed as shown in Figure 5. 3 (a). Next, the reporting well was filled with luminol (5 mM having a volume of 50 μL), glucose (different concentration with a 50 μL volume), and GOx (10 mg/mL having a volume of 5 μL) while the supporting well was filled with PBS solution (having 0.1 mM concentration with 200 μL volume) for 3 minutes to ensure optimal results. The optimized voltage of 6 V was applied to capture the ECL signal using the smartphone camera. The glucose concentration was varied from 0.05 mM to 7 mM, and a near linear range of 0.05 mM to 3 mM along with a limit of detection of 0.033 mM were achieved. The calibration graph for glucose with ECL signal for different concentration of glucose is shown in Figure 5. 3 (b).

Similarly, lactate concentration was measured by pipetting reporting well with luminol (5 mM having a volume of 50 μL), lactate (different concentration with a 50 μL volume), and LOx (50 UN/mL having a volume of 2.5 μL). The supporting well was filled with PBS solution (having 0.1mM concentration with 200 μL volume) for the optimized time of 12 minutes as shown in Figure 5. 3 (c). The lactate concentration varied from 0.1 mM to 10 mM, and a linear

range of 0.1 to 4 mM with a detection limit of 0.07 mM was attained. The calibration graph for lactate with ECL signal for different concentration of lactate is shown in Figure 5. 3 (d).

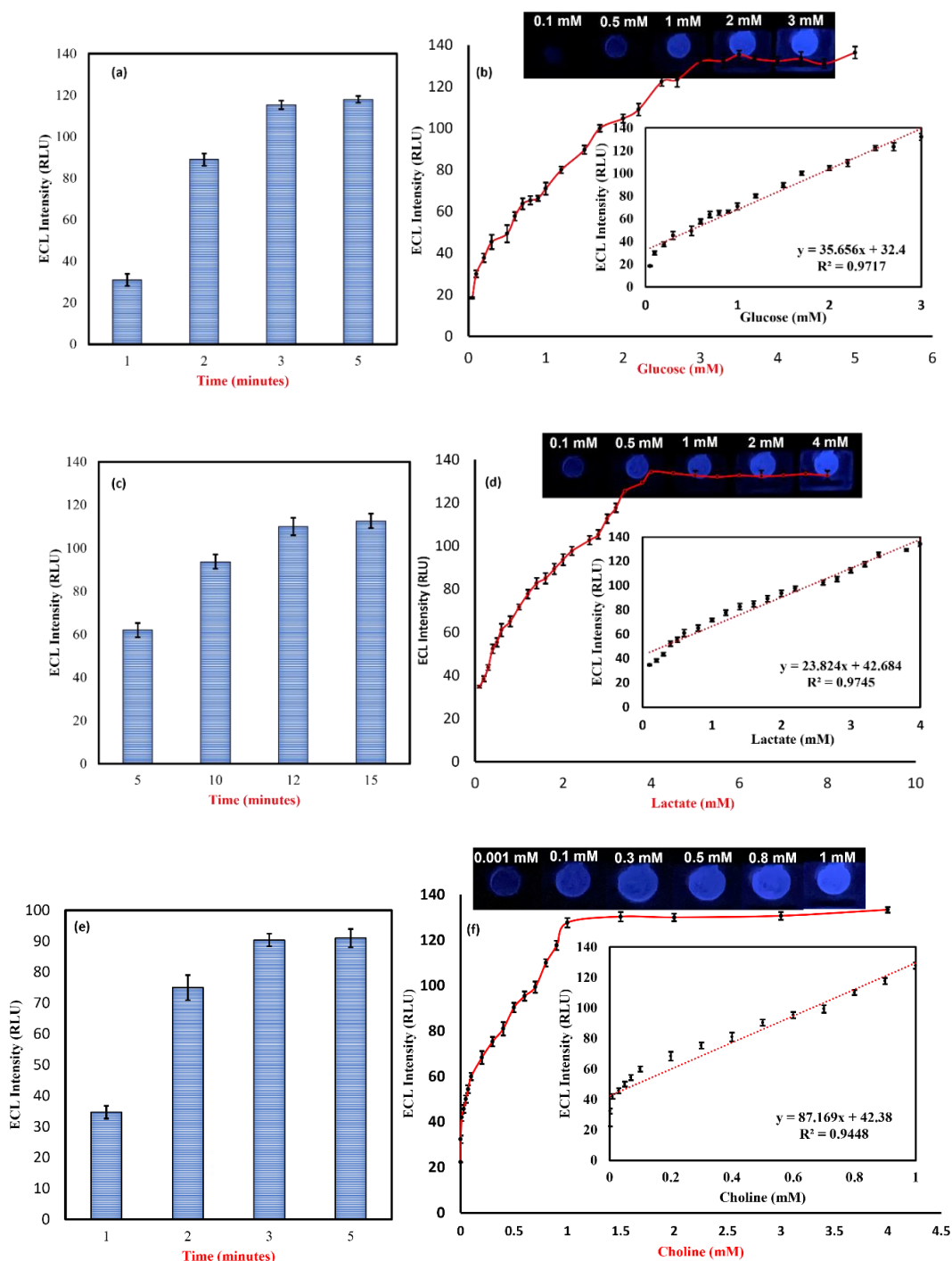


Figure 5. 3 Sensing of glucose and lactate; (a) time optimization for glucose sensing, luminol = 5mM, glucose = 5mM, GOx = 10 mg/mL, applied voltage = 6V, PBS = 0.1 mM. (b) glucose sensing, luminol = 5mM, glucose = varied from 0.05 to 7mM, GOx = 10 mg/mL, applied voltage = 6V, PBS = 0.1mM. (c) time optimization for lactate sensing, luminol = 5mM, lactate = 4 mM, LOx = 50 UN/mL, applied voltage = 6V, PBS = 0.1 mM. (d) lactate sensing, luminol = 5mM, lactate = varied from 0.1 to 10mM, LOx = 50 UN/mL, applied voltage = 6V. (e) time optimization for choline sensing, luminol = 5 mM, COx = 10 mg/mL, applied

voltage = 6V, PBS = 0.1 mM. (f) choline sensing, luminol = 5 mM, choline = varied from 0.0007 to 4mM, COx = 10 mg/mL, applied voltage = 6V, PBS = 0.1 mM: n = 3.

Further, choline sensing was carried out by pipetting reporting well with luminol (5 mM having a volume of 50 μ L), choline (different concentration with a 50 μ L volume), and COx (10 mg/mL having a volume of 5 μ L), The supporting well was filled with PBS solution (having 0.1 mM concentration with 200 μ L volume) for the optimized time of 3 minutes as shown in Figure 5. 3 (e). The choline concentration varied from 0.0007 mM to 4 mM, and a near linear range of 0.0007 to 1 mM with a limit of detection of 0.001 mM. The calibration graph for choline with ECL signal for different concentration of choline is shown in Figure 5. 3 (f).

5.4.3 Repeatability, reproducibility, and interference study using ECL biosensor

The repeatability of ECL biosensors was tested to demonstrate their sensing capabilities over an extended duration. The same device was utilized for seven days under the same conditions with the same lactate concentration, as shown in Figure 5.4 (a).

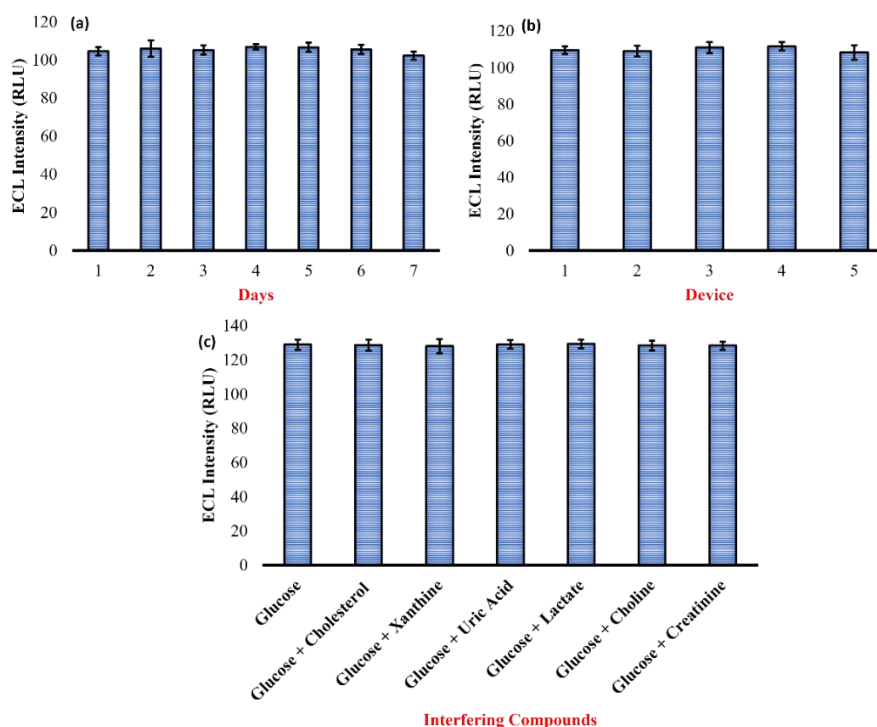


Figure 5.4 Repeatability, reproducibility and interference study; (A) repeatability analysis, luminol = 5mM, lactate = 3mM, LOx = 50 UN/mL, applied voltage = 6V, PBS = 0.1mM; (B) reproducibility analysis, luminol = 5mM, lactate = 3mM, LOx = 50 UN/mL, applied voltage = 6V, PBS = 0.1mM; (C) interference study, glucose = 3mM, GOx = 10 mg/mL, cholesterol = xanthine = uric acid = lactate = choline = creatinine = 1mM, PBS = 0.1mM, n = 3.

The experimental data demonstrated that the fabricated device could be effectively used over an extended period without causing any issues. Furthermore, to prove the reproducibility, five devices were fabricated at a time, and their performance was validated for the same concentration of lactate, as shown in Figure 5.4 (b). From the graph, it can be confirmed that the fabricated 3D-printed ECL devices provide acceptable reproducibility. In addition, to prove the selectivity performance, it was necessary to check the performance of the fabricated device in the presence of other interfering compounds. Hence, in the presented study, various common interfering compounds, such as cholesterol, xanthine, uric acid, lactate, choline, and creatinine, were chosen to evaluate the selectivity of the ECL biosensor. The experimental results shown in Fig. Figure 5.4 (c) indicate that the fabricated biosensor has good anti-interference characteristics.

5.4.4 Real sample analysis and its validation using ML

The real sample analysis and prediction were carried out utilizing the fabricated ECL device and ML algorithms to determine the capability of the device. Standard spiking (addition) method was used to perform the real sample analysis.

Table 5. 2 Real sample analysis using ECL biosensor

Analyte	Spiked (mM)	Found (mM)	Found ECL Intensity Values (RLU)	Predicted (mM) (Decision Tree)	Recovery (Found/Spiked) *100
Glucose	0.2	0.21	39.88	0.2	105
	0.5	0.52	50.94	0.49	104
	1	0.98	67.34	0.93	98
Lactate	0.5	0.53	55.31	0.48	106
	1	1.01	66.74	0.91	101
	2	2.10	92.71	1.9	105
Choline	0.2	0.22	61.55	0.2	101
	0.4	0.38	75.05	0.35	95
	0.5	0.49	85.09	0.45	98

First, the real blood serum was obtained from medical centre (BITS Hyderabad, India) and diluted to ten times using PBS to reduce the effect of other high concentration biomolecules present in the serum. Following dilution, different concentration was spiked (Tabulated in Table II) and respective intensity were calculated. The recovery percentage was calculated using (found/spiked) formula. The recovered percentage was encouraging and demonstrates the devices viability for usage in real-time applications. Finally, the decision tree ML algorithm

(provides highest accuracy among all other ML algorithms) was used to predict the concentration using the derived ECL intensity values for the real sample. From the obtained results it was proven that the predicted values are consistent with the actual values.

5.5 ML Modeling to validate the analytical performance of ECL biosensors

Even though the traditional statistical methods yield an acceptable accuracy for the ECL devices, ML based techniques offer an improved accuracy and at the same time address the challenge of sensor-to-sensor variations.

The data generated through the multiple iterations were considered input to the various ML algorithms to improve the overall accuracy of the y-predictor and maximize the R-squared scores. A set of ML techniques including various Linear Regressors, Partition-bases Models, and Ensemble Techniques were applied for the initial data analysis, data validation and relative ranking of the best fit curve.

Apart from experimental validation, the ML approach was used to validate the performance of the fabricated device and effectively used to predict the glucose concentration. Different ML algorithms, such as Simple Linear Regression (LR), Decision Tree (DT), Random Forest, K-Nearest Neighbour (KNN), and AdaBoost, were applied, and in-depth comparisons were made based on the regression metrics. Different regression metrics, such as Mean Absolute Error (MAE), Mean Squared Error (MSE), Root Mean Squared Error (RMSE), and R₂ score (R² Score), were used to check the performance of the different ML models.

5.5.1 Linear regression

Linear regression (LR) is one of the most common and comprehensive analytical machine learning algorithms. LR is used to find out the relationship between independent (x) and dependent (y) variables. In LR, the prediction of 'y' is made for the range of independent variable values 'x'. LR is categorized into two types, simple regression, and multiple regression. In the simple LR model, the relationship between the dependent and independent variables is defined using the following equation [124][125].

Simple regression: $y = mx + c$

Multiple Regression: $y = m_1 x_1 + m_2 x_2 + \dots + m_N x_N + c$

Apart from Ordinary Least Square (OLS) based ML models that are one of the simplest linear regression models, other robust regression models are also used to understand the impact of outliers.

Huber Regression is one of the robust regression algorithms that use optimization routines based on the loss function. It works on the principle of assigning weight to the data points which are outliers. The Huber loss can be expressed as follows:

$$L_{\delta}(a) = \left\{ \frac{1}{2}a^2 \quad \text{for } |a| \leq \delta, \quad \delta \cdot (|a| - \frac{1}{2}\delta), \text{ otherwise} \right\} \dots (1)$$

Where δ is a small numeric value and a refers to the residual and is defined as the difference between the predicted and observed values which is expressed as, $a = y - f(x)$.

Random Sample Consensus (RANSAC) Regressor, in contrast, is based on a non-deterministic algorithm that segregates the input data into inliers and outliers. Consequently, it uses only the inliers for the final data modeling after discarding the outliers. By excluding the outliers, RANSAC can fit the curve based on inliers.

Theil-Sen Regression is another robust regression model that does not assume the underlying data distribution. It involves fitting multiple regression models on subsets of the input data and then aggregating the coefficients at the last step.

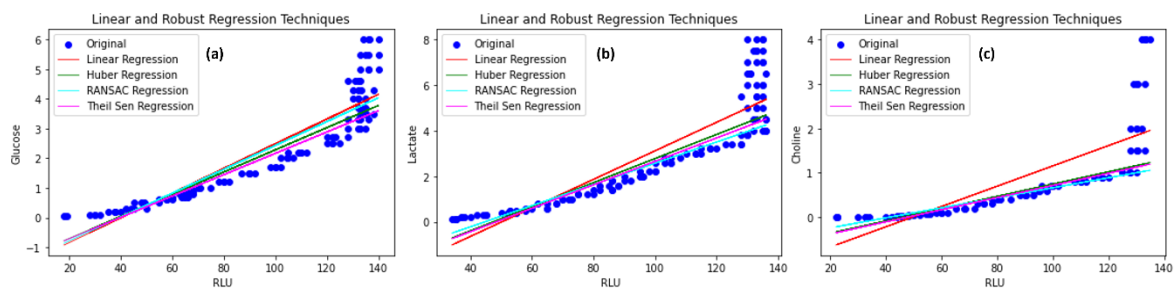


Figure 5.5 Mapping of Linear Regressors - Huber Regression, RANSAC Regression, and Theil-Sen Regression for (A) glucose, (B) lactate, and (C) choline.

The Theil-Sen estimator is much stronger than the Least-Squares Estimator because it is much less sensitive to outliers. It has a breakdown point of $1 - \frac{1}{\sqrt{2}} \approx 29.3\%$, implying that it can endure arbitrary corruption of up to 29.3% of the input data points without degradation of its accuracy.

Ordinary Least Squares (OLS) based regression models are easy to implement, but these methods produced relatively lower R-squared values and higher error scores. Robust

Regression Models like Huber, RANSAC, and Theil-Sen produced better curve fit, but the error scores increased significantly due to the weightage of the outliers as shown in Figure 5.5.

5.5.2 Decision tree

DT algorithm is used for both classifications as well as regression. Programmatically, DTs are nothing but the giant structure of the if-else conditions. DT-based algorithms consist of the root node, any number of arbitrary internal nodes (non-leaf nodes), and a leaf node (terminal node). The root node is present at the beginning of the DT and represents the entire dataset being studied. The node with outgoing edges is defined as the internal node or non-leaf node [126]. The leaf node is also called a terminal node because no splitting happens at a leaf node. In the case of regression, each leaf node holds the average (constant) value of the target variable [127]. The constant value corresponding to each leaf node in the model tree is replaced by a linear (or nonlinear) regression function. To predict the unknown values, the newly analyzed instance must follow the DT from the root node to the leaf node using the attribute values to make routing decisions at each internal node. Finally, the regression model is used in the leaf to evaluate the anticipated value for the new instance. The biggest disadvantage of DT is that it suffers from overfitting and is prone to errors for the imbalanced data set. To minimize overfitting, 'pruning' is performed by fixing the tree size.

5.5.3 Ensemble methods

Ensemble methods are generally used to reduce the overfitting (model performs well on training data set, but its performance is worst on testing data set) problems. Ensemble methods use bagging (parallel approach) and boosting (sequential approach) techniques. The bagging and boosting approach is generally used to improve the performance of the models [128].

RF is based on the bagging technique. If DTs are used in the bagging technique, then it is called RF. In the RF algorithm, many DTs are used hence it is called a forest [129]. RF is the collection of multiple trees where DTs are used as a base model. Bagging (bootstrapping + aggregation) is important to get low bias and low variance model [130][131]. In RF the original data set is divided into subsets and given to each DT parallelly to train the DTs called as bootstrapping. In RF all the DTs are trained independently. Once all the models are trained, they can predict corresponding value with respect any random query point. In case of regression, the mean of all DTs will consider as a final output called aggregation [132][133]. In case of RF following equation is used for prediction.

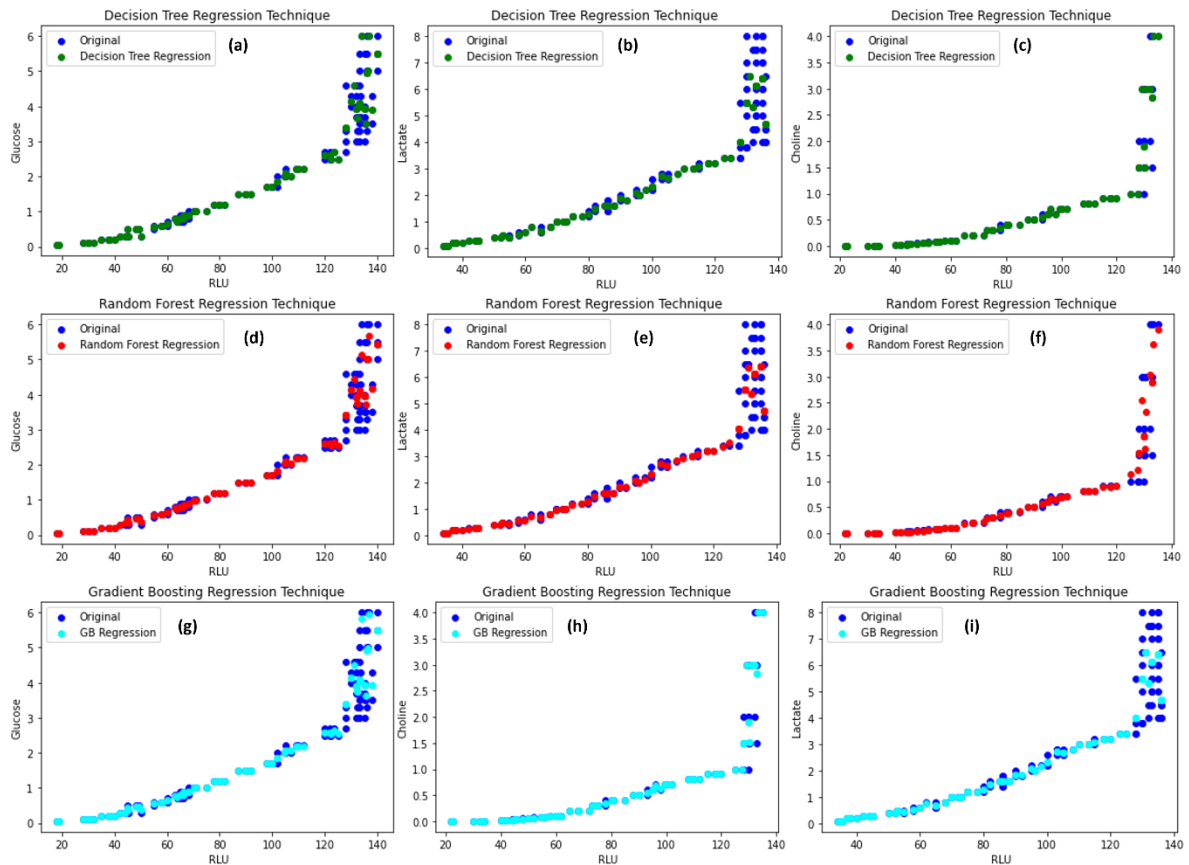


Figure 5.6 Ensemble techniques: Decision Tree (a) Glucose, (b) Lactate, and (c) Choline. Random Forest techniques for (d) Glucose, (e) Lactate, and (f) Choline. Gradient Boosting techniques for (g) Glucose, (h) Lactate, and (i) Choline.

AdaBoost is an additive model where residuals of the previous models are identified by high weight data points whereas in the GB the errors of the previous models are identify the gradient. In GB, all the DTs are weighted equally, and their predictive capacity is restricted with learning rate to increase performance of the model. In GB, in case of regression, the base model can provide just a mean (irrespective inputs) of the output feature. The performance of the first model can be determined using loss function (loss function = pseudo residuals = actual – predicted). The second base model should be the DT. The inputs of the second model are identical to those of the first base model, but its output is residual of the first model. In essence, the second model predicts how many errors the previous model made. Similar to the second model, the third and so on, DT-based model will operate on the residuals it receives and continue operating until the residual reaches zero.

Similarly, XGB is ten time faster than GB as it used the concept of parallelization. Parallelization means it uses all the cores of CPU id you are running single processor. Furthermore, XGB performs all its intermediate operations using cache memory which makes XGB faster. The performance of the XGB is higher as compared to other ML algorithms as it

tends to prevent your model from overfitting using regularization. Automatic regularization will happen in XGB [134]. As evident in Fig. 5. 6, ensemble techniques like Decision Tree, Random Forest, and Gradient Boost produced the best R-squared values along with the least error scores for all the three biomarkers.

5.5.4 Distance based methods

K-Nearest Neighbour (kNN) algorithm is used for both classification as well as regression and it is basically distance-based algorithm. The major difference between simple LR model and kNN regression is that kNN models are non-parametric (no use of regression function) whereas the LR algorithms are parametric (uses regression function for prediction)[134]. kNN model do the predictions using following steps. First, select the K Neighbour (k) values and then calculates the distance between test and train data point using Euclidean or Manhattan distance. Sort the calculated distance in ascending order which gives the information about nearest data points. Calculates the mean to predict the value corresponding to test data point. Partition-based Machine Learning Models (KNN) delivered an improved R-squared values and helped lower the error scores for all three biomarkers as demonstrated in Figure 5.7.

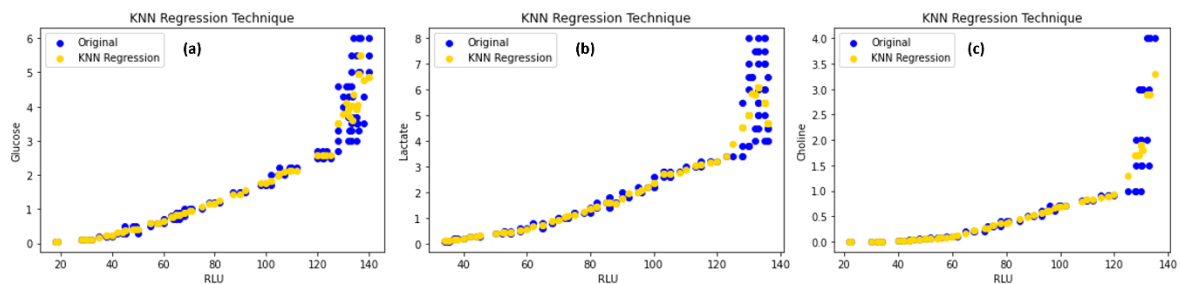


Figure 5.7 KNN models for (a) glucose, (b) lactate and (c) choline

5.5.5 Comparative regression metrics for different ML models

Given the Regression nature of the predictive modelling, this work has focused on various error metrics specifically designed for evaluating predictions made by different ML models.

The relevant Performance Evaluation Metrics can be represented mathematically as follows:

$$MAE = \frac{\sum_{i=1}^N |y_i^{pred} - y_i^{act}|}{N}$$

$$MSE = \frac{1}{N} \sum_{i=1}^N (y_i^{pred} - y_i^{act})^2$$

$$RMSE = \sqrt{\frac{\sum_{i=1}^N (y_i^{pred} - y_i^{act})^2}{N}}$$

$$COD = 1 - \frac{\sum_{i=1}^N (y_i^{pred} - y_i^{act})^2}{\sum_{i=1}^N (y_i^{pred} - \underline{y})^2}$$

where, y_i^{pred} and y_i^{act} represent the predicted and actual numbers; N represents the total sample size, and \underline{y} means an average of actual observations.

Apart from the R-squared scores or Coefficient of Determination (COD), to measure the goodness of the fit, this work also evaluated various error metrics including - Mean Squared Error (MSE), Root Mean Squared Error (RMSE), and Mean Absolute Error (MAE) for evaluating and reporting the performance of a regression model. For an easy comparison, the qualitative measures of various ML models are shown in Table II. KNN, Decision Tree Regressor and Random Forest are able to give an accurate prediction across the three biomarkers.

Table 5.3 Comparative Regression Metrics for different ML Models

ML Models	Glucose				Lactate				Choline			
	R ²	MAE	MSE	RMSE	R ²	MAE	MSE	RMSE	R ²	MAE	MSE	RMSE
LR	0.83	0.59	0.54	0.73	0.79	0.87	1.14	1.07	0.61	0.47	0.43	0.66
HR	0.81	0.55	0.6	0.77	0.75	0.79	1.35	1.16	0.45	0.37	0.61	0.78
RANSAC	0.82	0.57	0.55	0.74	0.69	0.78	1.69	1.3	0.36	0.37	0.7	0.84
TSR	0.78	0.54	0.67	0.82	0.73	0.77	1.48	1.22	0.43	0.37	0.63	0.79
KNN	0.92	0.28	0.24	0.49	0.89	0.47	0.66	0.81	0.85	0.19	0.17	0.41
DTR	0.95	0.20	0.17	0.41	0.90	0.41	0.55	0.74	0.91	0.11	0.1	0.31
RF	0.94	0.23	0.18	0.42	0.90	0.42	0.55	0.74	0.90	0.14	0.11	0.33

5.6 Conclusion

This study points out the challenges associated with ECL biosensors relying on aptamer, antibodies, and antigens calibrated through 3D-printed interdigitated bipolar ECL biosensors. The ECL biosensor produced linear ranges of 0.05 mM to 3 mM for Glucose, 0.1 mM to 4 mM for Lactate, and 0.0007 mM to 1 mM for Choline, with a limit of detection values of 0.033 mM, 0.07 mM, and 0.0007 mM, respectively. The data generated through the multiple iterations were considered input to the various ML algorithms to improve the overall accuracy of the y-predictor and maximize the R-squared scores. The following points were observed by comparing the outcomes produced by different ML algorithms: 1) Ordinary Least Squares

(OLS) based regression models are easiest to implement, but these methods produced lower R-squared values and higher error scores. 2) Robust Regression Models like Huber, RANSAC, and Theil-Sen produced better curve fit, but the error scores increased significantly due to the weightage of the outliers. 3) Partition-based Supervised Learning Models (KNN) delivered improved R-squared values and helped lower the error scores and 4) Ensemble techniques like Decision Tree, Random Forest, and Gradient Boost produced the best R-squared values along with the least error scores. The ML-based approach can help the ECL biosensors to improve their accuracy and performance leading to be used in various bio-sensing applications. While the scope of this research was to optimize the input parameters through the white-box principles, future work can potentially leverage the available ML models for the multi-variate optimization as against the univariate optimization approach adopted in this work. There is also an opportunity to create a healthcare platform based on the point-of-care ECL biosensors that will provide periodic recommendations to the individuals for a proactive intervention.

Chapter 6. Conclusion and Future Scope

6.1 Conclusion

The present study demonstrates the successful use of ECL as a sensitive and reliable technique for detecting biomolecules. The results highlight the potential of this method for various applications, including medical diagnostics. Different biomarkers, such as Glucose, Lactate, Choline, Dopamine, and Cholesterol, have been thoroughly studied and detected using the ECL approach. The conventional ECL systems are costly and difficult for on-site applications because they comprise photomultiplier tube (PMT) or CCD cameras, an electrochemical setup, and a personal computer. Modern Android smartphones offer a wide range of features, storage, excellent cameras, and high processing capabilities, making them the ideal option for use in visual ECL analysis. Thus, a portable smartphone assisted by an ML-based approach is in great demand in order to accelerate ECL detection, increase work efficiency, and make it a comprehensive ECL system. In this context, the first phase broadly gives an idea about the designing, fabrication, optimization, and validation of the PoC systems and their use to detect numerous biomarkers. Different low-cost microfabrication methodologies, including Laser assisted methods and three-dimensional printing (3DP), were comprehensively discussed and used to fabricate miniaturized ECL devices. The last phase provides an in-depth understanding of how the prediction of different biomarkers can be made using the Machine Learning (ML) approach. Different ML regression models, such as Huber, Random Sample Consensus (RANSAC), Theil-Sen, Support Vector Machine Regression (SVR), K-Nearest Neighbour (KNN), Decision Tree, and Random Forest, Adaptive boosting, Gradient boosting, Extreme Gradient boosting, were used to predict the concentration of various biomarkers. Following are the key features of the proposed work:

- 1) Development of a portable ECL system that could be used for a variety of medical applications,
- 3) Development of a multipurpose ECL Intensity Calculator which performs numerous functions which includes, real-time images acquisition, image segmentation, and analysis.

In addition to this, GUI is designed in a way that it can accommodate cloud storing seamlessly, data interpretation, concentration graphs plotting, and prediction of various biomarkers using ML. Fig. 6.1 (a) and (b) and Table 6.1 shows all the fabricated ECL devices fabricated using single step microfabrication techniques with their potential application.

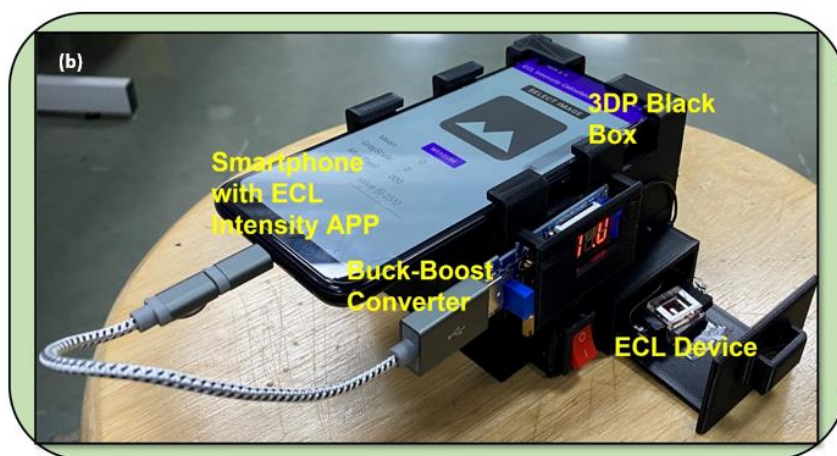
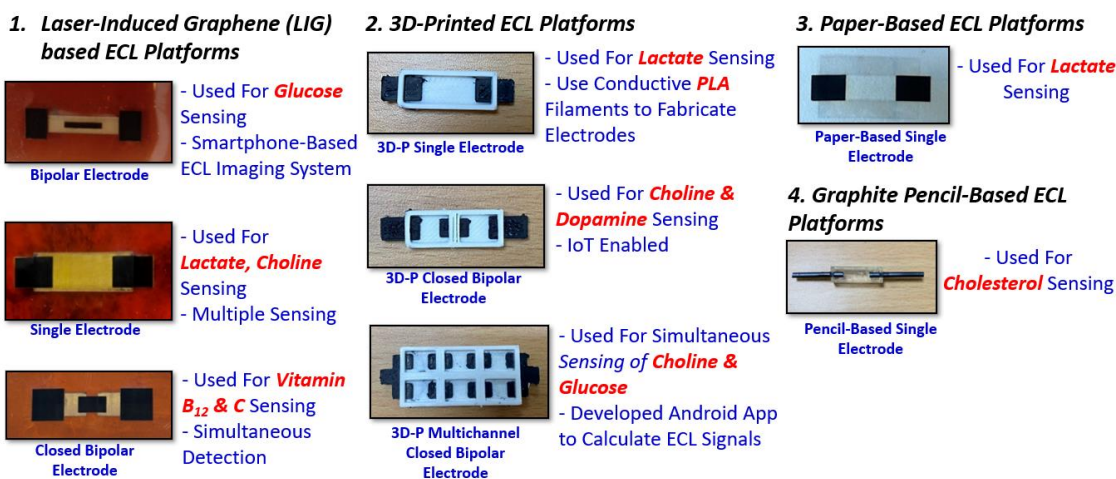


Figure 6.1 (a) Overall ECL devices fabricated with different microfabrication technique. (b) Portable pocket size ML assisted ECL system to detect various biomarkers.

Table 6. 1 Overall summary for different ECL devices

Fabrication Method	Type of Electrode	Application	Linear Range	LoD
Laser-Induced Graphene	Open BPE	H ₂ O ₂	1 – 100 μ M	5.87 μ M
		Glucose	1 – 100 μ M	0.138 μ M
	Closed BPE	Vitamin B ₁₂	0.5 – 1000 μ M	0.109 μ M
		Vitamin C	1 – 1000 μ M	0.96 μ M
	SE	Xanthine	0.1 – 100 μ M	1.25 μ M
3D Printing	Closed BPE	Dopamine	0.1 – 100 μ M	3.40 μ M
		Choline	30 – 700 μ M	3.27 μ M
	Six-Well CBPE	Dopamine	0.5 – 100 μ M	0.3 μ M
		Glucose	0.1 – 10 mM	24 μ M
		Choline	0.5 – 5 mM	10 μ M
Paper Based	SLA-SE	Cholesterol	50 – 1000 μ M	15.71 μ M
		SE	Glucose	100 – 1000 μ M
		Lactate	100 – 5000 μ M	3.84 μ M

6.2 Limitations of The Presented Work

6.2.1 Smartphone Dependency

All android smartphones do not generate similar RLU values. The RLU values can vary depending on several factors, including the specific model and manufacturer of the smartphone, the age and condition of the device, and the type and sensitivity of the camera sensor used to capture the images. The sensitivity or performance of the ECL system is highly dependent on the android smartphone.

6.3 Future Scope

6.3.1 Droplet microfluidic based ECL systems

Droplet microfluidics is a fast-growing field that engages the manipulation of small droplets of fluids on a microscale. ECL has been effectively combined into droplet microfluidic systems, opening up new opportunities for high-throughput and precision analysis of various analytes. In droplet microfluidics, small fluid droplets are generated and controlled in microchannels using a variety of methods, including electric fields, micropumps, and microvalves.

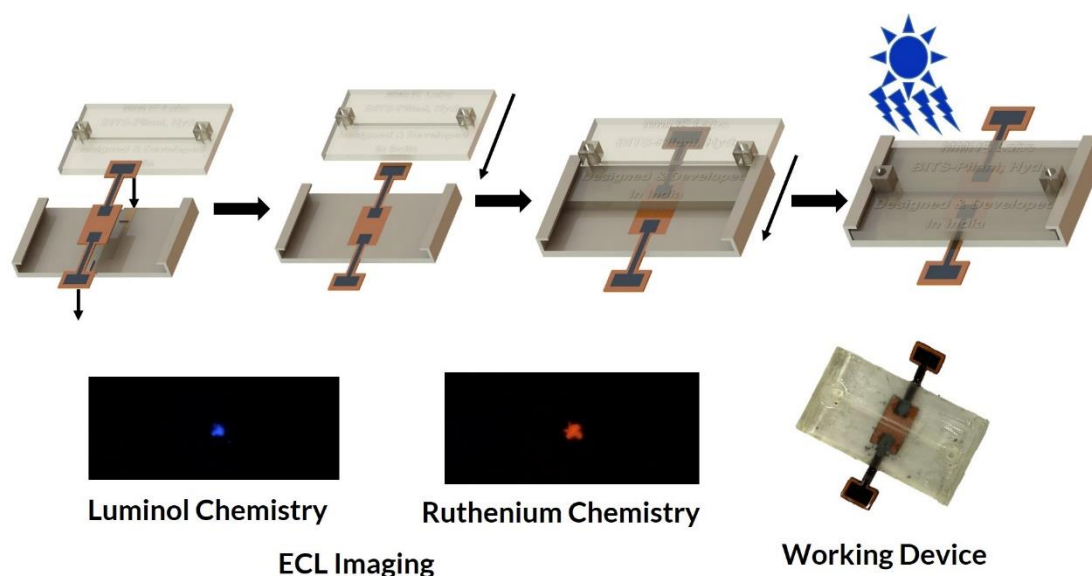


Figure 6.2 Schematic for Droplet/Continuous microfluidic based ECL systems.

It is possible to develop highly sensitive and selective analytical systems that can carry out a variety of assays by fusing ECL with droplet microfluidics. Using droplet microfluidics for ECL has a number of benefits, one of which is the ability to produce and work with small volumes of sample and reagent. As a result, less samples and reagent is used, reactions happen

more quickly, and sensitivity is improved. Droplet microfluidic systems are also simple to automate, enabling high-throughput examination of several samples. High-throughput analysis of clinical samples for illness diagnosis and monitoring is one potential use for ECL employing droplet microfluidics. In conclusion, new opportunities for highly sensitive and selective analytical systems have been made possible by the combination of ECL with droplet microfluidics. One can anticipate seeing more ECL applications utilizing droplet microfluidics as this technology develops in a number of industries, including clinical diagnostics, environmental monitoring, and food safety testing. The schematic for Droplet/Continuous microfluidic based ECL systems is shown in Figure 6.2.

References

- [1] A. N. Konwar and V. Borse, “Current status of point-of-care diagnostic devices in the Indian healthcare system with an update on COVID-19 pandemic,” *Sensors Int.*, vol. 1, no. June, p. 100015, 2020, doi: 10.1016/j.sintl.2020.100015.
- [2] M. Bhaiyya, P. K. Pattnaik, and S. Goel, “Simultaneous detection of Vitamin B12 and Vitamin C from real samples using miniaturized laser-induced graphene based electrochemiluminescence device with closed bipolar electrode,” *Sensors Actuators A Phys.*, vol. 331, p. 112831, 2021, doi: 10.1016/j.sna.2021.112831.
- [3] K. Strimbu and J. A. Tavel, “What are biomarkers?,” *Curr. Opin. HIV AIDS*, vol. 5, no. 6, pp. 463–466, 2010, doi: 10.1097/COH.0b013e32833ed177.
- [4] R. Mayeux, “Biomarkers: Potential Uses and Limitations,” *NeuroRx*, vol. 1, no. 2, pp. 182–188, 2004, doi: 10.1602/neurorx.1.2.182.
- [5] S. Campuzano, M. Pedrero, P. Yáñez-Sedeño, and J. M. Pingarrón, “New challenges in point of care electrochemical detection of clinical biomarkers,” *Sensors Actuators, B Chem.*, vol. 345, no. June, 2021, doi: 10.1016/j.snb.2021.130349.
- [6] Y. Lv *et al.*, “Competitive Multiple-Mechanism-Driven Electrochemiluminescent Detection of 8-Hydroxy-2'-deoxyguanosine,” *J. Am. Chem. Soc.*, vol. 140, no. 8, pp. 2801–2804, 2018, doi: 10.1021/jacs.8b00515.
- [7] S. Song, H. Xu, and C. Fan, “Potential diagnostic applications of biosensors: Current and future directions,” *Int. J. Nanomedicine*, vol. 1, no. 4, pp. 433–440, 2006, doi: 10.2147/nano.2006.1.4.433.
- [8] S. Xia, J. Pan, D. Dai, Z. Dai, M. Yang, and C. Yi, “Design of portable electrochemiluminescence sensing systems for point-of-care-testing applications,” *Chinese Chem. Lett.*, p. 107799, 2022, doi: 10.1016/j.ccllet.2022.107799.
- [9] J. M. Mohan, K. Amreen, A. Javed, S. K. Dubey, and S. Goel, “Miniaturized PMMA Electrochemical Platform with Carbon Fiber for Multiplexed and Noninterfering Biosensing of Real Samples,” *IEEE Trans. Electron Devices*, vol. 68, no. 2, pp. 769–774, 2021, doi: 10.1109/TED.2020.3043217.
- [10] M. Bhaiyya, P. K. Pattnaik, and S. Goel, “Portable Electrochemiluminescence Platform With Laser-Induced Graphene-Based U-Shaped Bipolar Electrode for Selective Sensing of Various Analytes,” *IEEE Trans. Electron Devices*, pp. 1–8, 2021, doi: 10.1109/TED.2021.3066083.
- [11] T. Kasahara *et al.*, “Multi-color microfluidic electrochemiluminescence cells,” *Sensors Actuators, A Phys.*, vol. 214, pp. 225–229, 2014, doi: 10.1016/j.sna.2014.04.039.
- [12] A. Pal, S. K. Dubey, and S. Goel, “IoT enabled microfluidic colorimetric detection platform for continuous monitoring of nitrite and phosphate in soil,” *Comput. Electron. Agric.*, vol. 195, no. January, p. 106856, 2022, doi: 10.1016/j.compag.2022.106856.
- [13] A. Pal, M. B. Kulkarni, H. Gupta, R. N. Ponnalagu, S. K. Dubey, and S. Goel, “Portable and Autonomous Device for Real-time Colorimetric Detection: Validation for Phosphorous and Nitrite Detection,” *Sensors Actuators A Phys.*, vol. 330, p. 112896, 2021, doi: 10.1016/j.sna.2021.112896.
- [14] A. Arora, J. C. T. Eijkel, W. E. Morf, and A. Manz, “A wireless

- electrochemiluminescence detector applied to direct and indirect detection for electrophoresis on a microfabricated glass device,” *Anal. Chem.*, vol. 73, no. 14, pp. 3282–3288, 2001, doi: 10.1021/ac0100300.
- [15] Y. Zheng *et al.*, “Lighting Up Electrochemiluminescence-Inactive Dyes via Grafting Enabled by Intramolecular Resonance Energy Transfer,” *Anal. Chem.*, vol. 94, no. 7, pp. 3296–3302, 2022, doi: 10.1021/acs.analchem.1c05235.
- [16] F. Du, Z. Dong, F. Liu, S. Anjum, M. Hosseini, and G. Xu, “Single-electrode electrochemical system based on tris(1,10-phenanthroline)ruthenium modified carbon nanotube/graphene film electrode for visual electrochemiluminescence analysis,” *Electrochim. Acta*, vol. 420, no. January, p. 140431, 2022, doi: 10.1016/j.electacta.2022.140431.
- [17] M. M. Richter, “Electrochemiluminescence (ECL),” no. 3, 2004, doi: 10.1016/B978-044453125-4.50009-7.
- [18] F. Yuan *et al.*, “Regenerable bipolar electrochemiluminescence device using glassy carbon bipolar electrode, stainless steel driving electrode and cold patch,” *Electrochim. Acta*, vol. 262, pp. 182–186, 2018, doi: 10.1016/j.electacta.2017.12.186.
- [19] M. Liu, D. Wang, C. Liu, R. Liu, H. Li, and C. Zhang, “Battery-triggered open wireless electrochemiluminescence in a microfluidic cloth-based bipolar device,” *Sensors Actuators, B Chem.*, vol. 246, pp. 327–335, 2017, doi: 10.1016/j.snb.2017.02.076.
- [20] C. A. Marquette and L. J. Blum, “Electro-chemiluminescent biosensing,” *Anal. Bioanal. Chem.*, vol. 390, no. 1, pp. 155–168, 2008, doi: 10.1007/s00216-007-1631-2.
- [21] W. Guan, M. Liu, and C. Zhang, “Electrochemiluminescence detection in microfluidic cloth-based analytical devices,” *Biosens. Bioelectron.*, vol. 75, pp. 247–253, 2016, doi: 10.1016/j.bios.2015.08.023.
- [22] E. C. Rivera, J. W. Taylor, R. L. Summerscales, and H. J. Kwon, “Quenching Behavior of the Electrochemiluminescence of Ru(bpy)₃²⁺/TPPrA System by Phenols on a Smartphone-Based Sensor,” *ChemistryOpen*, vol. 10, no. 8, pp. 842–847, 2021, doi: 10.1002/open.202100151.
- [23] R. Liu, C. Zhang, and M. Liu, “Open bipolar electrode-electrochemiluminescence imaging sensing using paper-based microfluidics,” *Sensors Actuators, B Chem.*, vol. 216, pp. 255–262, 2015, doi: 10.1016/j.snb.2015.04.014.
- [24] S. Wu, Z. Zhou, L. Xu, B. Su, and Q. Fang, “Integrating bipolar electrochemistry and electrochemiluminescence imaging with microdroplets for chemical analysis,” *Biosens. Bioelectron.*, vol. 53, pp. 148–153, 2014, doi: 10.1016/j.bios.2013.09.042.
- [25] S. E. Fosdick, K. N. Knust, K. Scida, and R. M. Crooks, “Bipolar electrochemistry,” *Angew. Chemie - Int. Ed.*, vol. 52, no. 40, pp. 10438–10456, 2013, doi: 10.1002/anie.201300947.
- [26] X. Zhang, Q. Zhai, H. Xing, J. Li, and E. Wang, “Bipolar Electrodes with 100% Current Efficiency for Sensors,” *ACS Sensors*, vol. 2, no. 3, pp. 320–326, 2017, doi: 10.1021/acssensors.7b00031.
- [27] G. Loget, D. Zigah, L. Bouffier, N. Sojic, and A. Kuhn, “Bipolar electrochemistry: from materials science to motion and beyond,” *Acc. Chem. Res.*, vol. 46, no. 11, pp. 2513–2523, 2013, doi: 10.1021/ar400039k.

- [28] M. Liu, R. Liu, D. Wang, C. Liu, and C. Zhang, "A low-cost, ultraflexible cloth-based microfluidic device for wireless electrochemiluminescence application," *Lab Chip*, vol. 16, no. 15, pp. 2860–2870, 2016, doi: 10.1039/c6lc00289g.
- [29] W. Gao, K. Muzyka, X. Ma, B. Lou, and G. Xu, "A single-electrode electrochemical system for multiplex electrochemiluminescence analysis based on a resistance induced potential difference," *Chem. Sci.*, vol. 9, no. 16, pp. 3911–3916, 2018, doi: 10.1039/c8sc00410b.
- [30] X. Ma *et al.*, "A portable wireless single-electrode system for electrochemiluminescent analysis," *Electrochim. Acta*, vol. 308, pp. 20–24, 2019, doi: 10.1016/j.electacta.2019.04.015.
- [31] M. Sher, R. Zhuang, U. Demirci, and W. Asghar, "Paper-based analytical devices for clinical diagnosis: recent advances in the fabrication techniques and sensing mechanisms," *Expert Rev. Mol. Diagn.*, vol. 17, no. 4, pp. 351–366, 2017, doi: 10.1080/14737159.2017.1285228.
- [32] H. J. Kwon *et al.*, "Development of smartphone-based ECL sensor for dopamine detection: Practical approaches," *Results Chem.*, vol. 2, p. 100029, 2020, doi: 10.1016/j.rechem.2020.100029.
- [33] M. Liu, R. Liu, D. Wang, C. Liu, and C. Zhang, "A low-cost, ultraflexible cloth-based microfluidic device for wireless electrochemiluminescence application," *Lab Chip*, vol. 16, no. 15, pp. 2860–2870, 2016, doi: 10.1039/c6lc00289g.
- [34] L. Chen, C. Zhang, and D. Xing, "Paper-based bipolar electrode-electrochemiluminescence (BPE-ECL) device with battery energy supply and smartphone read-out: A handheld ECL system for biochemical analysis at the point-of-care level," *Sensors Actuators, B Chem.*, vol. 237, pp. 308–317, 2016, doi: 10.1016/j.snb.2016.06.105.
- [35] M. Liu, D. Wang, C. Liu, R. Liu, H. Li, and C. Zhang, "Battery-triggered open wireless electrochemiluminescence in a microfluidic cloth-based bipolar device," *Sensors Actuators, B Chem.*, vol. 246, pp. 327–335, 2017, doi: 10.1016/j.snb.2017.02.076.
- [36] D. Wang, C. Liu, Y. Liang, Y. Su, Q. Shang, and C. Zhang, "A Simple and Sensitive Paper-Based Bipolar Electrochemiluminescence Biosensor for Detection of Oxidase-Substrate Biomarkers in Serum," *J. Electrochem. Soc.*, vol. 165, no. 9, pp. B361–B369, 2018, doi: 10.1149/2.0551809jes.
- [37] H. R. Zhang, Y. Z. Wang, W. Zhao, J. J. Xu, and H. Y. Chen, "Visual Color-Switch Electrochemiluminescence Biosensing of Cancer Cell Based on Multichannel Bipolar Electrode Chip," *Anal. Chem.*, vol. 88, no. 5, pp. 2884–2890, 2016, doi: 10.1021/acs.analchem.5b04716.
- [38] H. Liu, X. Zhou, W. Liu, X. Yang, and D. Xing, "Paper-Based Bipolar Electrode Electrochemiluminescence Switch for Label-Free and Sensitive Genetic Detection of Pathogenic Bacteria," *Anal. Chem.*, vol. 88, no. 20, pp. 10191–10197, 2016, doi: 10.1021/acs.analchem.6b02772.
- [39] J. L. Delaney, C. F. Hogan, J. Tian, and W. Shen, "Electrogenerated chemiluminescence detection in paper-based microfluidic sensors," *Anal. Chem.*, vol. 83, no. 4, pp. 1300–1306, 2011, doi: 10.1021/ac102392t.

- [40] J. Ballesta Claver, M. C. Valencia Mirón, and L. F. Capitán-Vallvey, “Disposable electrochemiluminescent biosensor for lactate determination in saliva,” *Analyst*, vol. 134, no. 7, pp. 1423–1432, 2009, doi: 10.1039/b821922b.
- [41] Z. Zhou, L. Xu, S. Wu, and B. Su, “A novel biosensor array with a wheel-like pattern for glucose, lactate and choline based on electrochemiluminescence imaging,” *Analyst*, vol. 139, no. 19, pp. 4934–4939, 2014, doi: 10.1039/c4an00687a.
- [42] M. Bhaiyya, P. Rewatkar, M. Salve, P. K. Pattnaik, and S. Goel, “Miniaturized Electrochemiluminescence Platform with Laser-Induced Graphene Electrodes for Multiple Biosensing,” *IEEE Trans. Nanobioscience*, vol. 1241, no. c, 2020, doi: 10.1109/TNB.2020.3036642.
- [43] S. G. Manish Bhaiyya, Prasant Pattanaik, “Miniaturized Electrochemiluminescence Platform with Laser-Induced Graphene based Single Electrode for Interference-Free Sensing of Dopamine, Xanthine and Glucose,” *IEEE Trans. Instrum. Meas.*, vol. 70, pp. 1–8, 2021, doi: 10.1109/TIM.2021.3071215.
- [44] M. Bhaiyya, P. K. Pattnaik, and S. Goel, “Electrochemiluminescence sensing of vitamin - B 12 using laser - induced graphene based bipolar and single electrodes in a 3D - printed portable system,” *Microfluid. Nanofluidics*, no. May, 2021, doi: 10.1007/s10404-021-02442-x.
- [45] W. Gao, K. Muzyka, X. Ma, B. Lou, and G. Xu, “A single-electrode electrochemical system for multiplex electrochemiluminescence analysis based on a resistance induced potential difference,” *Chem. Sci.*, vol. 9, no. 16, pp. 3911–3916, 2018, doi: 10.1039/c8sc00410b.
- [46] M. Salve, A. Mandal, K. Amreen, B. P. Rao, and P. Kumar, “Portable 3D printed Electrochemiluminescence Platform with Pencil Graphite Electrodes for Point of Care multiplexed analysis with Smartphone based Read-out,” *IEEE Trans. Instrum. Meas.*, vol. 9456, 2020, doi: 10.1109/TIM.2020.3023211.
- [47] Y. Chen *et al.*, “UV Laser-Induced Polyimide-to-Graphene Conversion: Modeling, Fabrication, and Application,” *Small Methods*, vol. 3, no. 10, pp. 1–9, 2019, doi: 10.1002/smt.201900208.
- [48] F. M. Vivaldi *et al.*, “Three-Dimensional (3D) Laser-Induced Graphene: Structure, Properties, and Application to Chemical Sensing,” *ACS Appl. Mater. Interfaces*, vol. 13, no. 26, pp. 30245–30260, 2021, doi: 10.1021/acsami.1c05614.
- [49] R. Ye, D. K. James, and J. M. Tour, “Laser-Induced Graphene: From Discovery to Translation,” *Adv. Mater.*, vol. 31, no. 1, pp. 1–15, 2019, doi: 10.1002/adma.201803621.
- [50] P. Rewatkar, A. Kothuru, and S. Goel, “PDMS-Based Microfluidic Glucose Biofuel Cell Integrated with Optimized Laser-Induced Flexible Graphene Bioelectrodes,” *IEEE Trans. Electron Devices*, vol. 67, no. 4, pp. 1832–1838, 2020, doi: 10.1109/TED.2020.2971480.
- [51] J. Lin *et al.*, “Laser-induced porous graphene films from commercial polymers,” *Nat. Commun.*, vol. 5, pp. 5–12, 2014, doi: 10.1038/ncomms6714.
- [52] S. Dudala, L. T. Rao, S. K. Dubey, A. Javed, and S. Goel, “Experimental characterization to fabricate CO2 laser ablated PMMA microchannel with homogeneous surface,” *Mater. Today Proc.*, no. xxxx, pp. 10–13, 2020, doi:

- 10.1016/j.matpr.2019.12.302.
- [53] U. S. Jayapiriya, P. Rewatkar, and S. Goel, "ScienceDirect Miniaturized polymeric enzymatic biofuel cell with integrated microfluidic device and enhanced laser ablated bioelectrodes," *Int. J. Hydrogen Energy*, no. xxxx, 2020, doi: 10.1016/j.ijhydene.2020.06.133.
- [54] M. D. Wagh, P. S. B., S. Goel, and S. K. Sahoo, "Development of Laser-Induced Graphene-Based Automated Electro Microfluidic Viscometer for Biochemical Sensing Applications," *IEEE Trans. Electron Devices*, vol. 68, no. 10, pp. 5184–5191, 2021, doi: 10.1109/TED.2021.3107374.
- [55] L. Zhu, Y. Li, F. Tian, B. Xu, and G. Zhu, "Electrochemiluminescent determination of glucose with a sol-gel derived ceramic-carbon composite electrode as a renewable optical fiber biosensor," *Sensors Actuators, B Chem.*, vol. 84, no. 2–3, pp. 265–270, 2002, doi: 10.1016/S0925-4005(02)00035-7.
- [56] L. Bouffier *et al.*, "Lighting up redox propulsion with luminol electrogenerated chemiluminescence," *ChemElectroChem*, vol. 1, no. 1, pp. 1–4, 2014, doi: 10.1002/celec.201300042.
- [57] Z. Lin, J. Chen, and G. Chen, "An ECL biosensor for glucose based on carbon-nanotube/Nafion film modified glass carbon electrode," *Electrochim. Acta*, vol. 53, no. 5, pp. 2396–2401, 2008, doi: 10.1016/j.electacta.2007.09.063.
- [58] C. Liu, D. Wang, and C. Zhang, "A novel paperfluidic closed bipolar electrode-electrochemiluminescence sensing platform: Potential for multiplex detection at crossing-channel closed bipolar electrodes," *Sensors Actuators, B Chem.*, vol. 270, pp. 341–352, 2018, doi: 10.1016/j.snb.2018.04.180.
- [59] Y. Xiao, L. Xu, and L. W. Qi, "Electrochemiluminescence bipolar electrode array for the multiplexed detection of glucose, lactate and choline based on a versatile enzymatic approach," *Talanta*, vol. 165, no. October 2016, pp. 577–583, 2017, doi: 10.1016/j.talanta.2017.01.019.
- [60] X. Y. Yang *et al.*, "Ultrasensitive Electrochemiluminescence Biosensor Based on Closed Bipolar Electrode for Alkaline Phosphatase Detection in Single Liver Cancer Cell," *Anal. Chem.*, 2021, doi: 10.1021/acs.analchem.0c04517.
- [61] F. Wang *et al.*, "Rapid and low-cost laser synthesis of hierarchically porous graphene materials as high-performance electrodes for supercapacitors," *J. Mater. Sci.*, vol. 54, no. 7, pp. 5658–5670, 2019, doi: 10.1007/s10853-018-03247-0.
- [62] K. B. Akshaya, V. Anitha, M. Nidhin, Y. N. Sudhakar, and G. Louis, "Electrochemical sensing of vitamin B12 deficiency marker methylmalonic acid using PdAu-PPy tailored carbon fiber paper electrode," *Talanta*, vol. 217, no. November 2019, p. 121028, 2020, doi: 10.1016/j.talanta.2020.121028.
- [63] M. H. Parvin, E. Azizi, J. Arjomandi, and J. Y. Lee, "Highly sensitive and selective electrochemical sensor for detection of vitamin B12 using an Au/PPy/FMNPs@TD-modified electrode," *Sensors Actuators, B Chem.*, vol. 261, pp. 335–344, 2018, doi: 10.1016/j.snb.2018.01.168.
- [64] H. Dai, X. Wu, Y. Wang, W. Zhou, and G. Chen, "An electrochemiluminescent biosensor for vitamin C based on inhibition of luminol electrochemiluminescence on

- graphite/poly(methylmethacrylate) composite electrode,” *Electrochim. Acta*, vol. 53, no. 16, pp. 5113–5117, 2008, doi: 10.1016/j.electacta.2008.02.044.
- [65] J. M. Mohan, K. Amreen, A. Javed, S. K. Dubey, and S. Goel, “Miniaturized electrochemical platform with ink-jetted electrodes for multiplexed and interference mitigated biochemical sensing,” *Appl. Nanosci.*, 2020, doi: 10.1007/s13204-020-01480-1.
- [66] L. Chen, C. Zhang, and D. Xing, “Paper-based bipolar electrode-electrochemiluminescence (BPE-ECL) device with battery energy supply and smartphone read-out: A handheld ECL system for biochemical analysis at the point-of-care level,” *Sensors Actuators, B Chem.*, vol. 237, pp. 308–317, 2016, doi: 10.1016/j.snb.2016.06.105.
- [67] D. Yuan, S. Chen, R. Yuan, J. Zhang, and X. Liu, “An ECL sensor for dopamine using reduced graphene oxide/multiwall carbon nanotubes/gold nanoparticles,” *Sensors Actuators, B Chem.*, vol. 191, pp. 415–420, 2014, doi: 10.1016/j.snb.2013.10.013.
- [68] S. Dudala, S. K. Dubey, and S. Goel, “Fully Integrated, Automated, and Smartphone Enabled Point-of-Source Portable Platform With Microfluidic Device for Nitrite Detection,” *IEEE Trans. Biomed. Circuits Syst.*, vol. 13, no. 6, pp. 1518–1524, Dec. 2019, doi: 10.1109/TBCAS.2019.2939658.
- [69] S. Garcia-Manyes and A. E. M. Beedle, “Steering chemical reactions with force,” *Nat. Rev. Chem.*, vol. 1, no. 11, Nov. 2017, doi: 10.1038/s41570-017-0083.
- [70] H. W. Kim *et al.*, “Efficient hydrogen peroxide generation using reduced graphene oxide-based oxygen reduction electrocatalysts,” *Nat. Catal.*, vol. 1, no. 4, pp. 282–290, 2018, doi: 10.1038/s41929-018-0044-2.
- [71] M. D. Nurhafizah, A. B. Suriani, A. Mohamed, and T. Soga, “Effect of voltage applied for graphene oxide/latex nanocomposites produced via electrochemical exfoliation and its application as conductive electrodes,” *Diam. Relat. Mater.*, vol. 101, no. November 2019, 2020, doi: 10.1016/j.diamond.2019.107624.
- [72] C. Wang *et al.*, “A facile electrochemical sensor based on reduced graphene oxide and Au nanoplates modified glassy carbon electrode for simultaneous detection of ascorbic acid, dopamine and uric acid,” *Sensors Actuators, B Chem.*, vol. 204, pp. 302–309, 2014, doi: 10.1016/j.snb.2014.07.077.
- [73] F. Khaleghi *et al.*, “Fabrication of novel electrochemical sensor for determination of vitamin C in the presence of Vitamin B9 in food and pharmaceutical samples,” *J. Mol. Liq.*, vol. 221, pp. 666–672, 2016, doi: 10.1016/j.molliq.2016.06.061.
- [74] L. Ding, H. Yang, S. Ge, and J. Yu, “Fluorescent carbon dots nanosensor for label-free determination of vitamin B12 based on inner filter effect,” *Spectrochim. Acta - Part A Mol. Biomol. Spectrosc.*, vol. 193, pp. 305–309, 2018, doi: 10.1016/j.saa.2017.12.015.
- [75] A. Sharma, S. Arya, D. Chauhan, P. R. Solanki, S. Khajuria, and A. Khosla, “Synthesis of Au–SnO₂ nanoparticles for electrochemical determination of vitamin B12,” *J. Mater. Res. Technol.*, vol. 9, no. 6, pp. 14321–14337, 2020, doi: 10.1016/j.jmrt.2020.10.024.
- [76] J. M. Mohan, K. Amreen, A. Javed, S. K. Dubey, and S. Goel, “Highly Selective Electrochemical Sensing of Dopamine, Xanthine, Ascorbic acid and Uric acid using a Carbon Fiber Paper,” *IEEE Sens. J.*, vol. 1748, no. c, pp. 1–1, 2020, doi:

10.1109/jsen.2020.2999067.

- [77] R. Ojani, A. Alinezhad, and Z. Abedi, “A highly sensitive electrochemical sensor for simultaneous detection of uric acid, xanthine and hypoxanthine based on poly(L-methionine) modified glassy carbon electrode,” *Sensors Actuators, B Chem.*, vol. 188, pp. 621–630, 2013, doi: 10.1016/j.snb.2013.07.015.
- [78] A. C. Faucett, “VOLTAGE-INDUCED REDUCTION OF GRAPHENE OXIDE BY Submitted in partial fulfillment of the requirements for the degree of Doctor of Philosophy in Physics in the Graduate School of Binghamton University State University of New York,” no. September 2016, 2016, doi: 10.13140/RG.2.2.25520.76801.
- [79] H. Dodziuk, “Applications of 3D printing in healthcare,” *Kardiochirurgia i Torakochirurgia Pol.*, vol. 13, no. 3, pp. 283–293, 2016, doi: 10.5114/kitp.2016.62625.
- [80] D. H. Ballard *et al.*, “Clinical Applications of 3D Printing: Primer for Radiologists,” *Acad. Radiol.*, vol. 25, no. 1, pp. 52–65, 2018, doi: 10.1016/j.acra.2017.08.004.
- [81] G. Chen, Y. Xu, P. C. L. Kwok, and L. Kang, “Pharmaceutical Applications of 3D Printing,” *Addit. Manuf.*, vol. 34, no. April, p. 101209, 2020, doi: 10.1016/j.addma.2020.101209.
- [82] Y. He, Y. Wu, J. Z. Fu, Q. Gao, and J. J. Qiu, “Developments of 3D Printing Microfluidics and Applications in Chemistry and Biology: a Review,” *Electroanalysis*, vol. 28, no. 8, pp. 1658–1678, 2016, doi: 10.1002/elan.201600043.
- [83] A. Pal, K. Amreen, S. K. Dubey, and S. Goel, “Highly Sensitive and Interference-Free Electrochemical Nitrite Detection in a 3D Printed Miniaturized Device,” *IEEE Trans. Nanobioscience*, vol. 20, no. 2, pp. 175–182, 2021, doi: 10.1109/TNB.2021.3063730.
- [84] L. H. Duong and P. C. Chen, “Simple and low-cost production of hybrid 3D-printed microfluidic devices,” *Biomicrofluidics*, vol. 13, no. 2, 2019, doi: 10.1063/1.5092529.
- [85] J. Y. Lee, J. An, and C. K. Chua, “Fundamentals and applications of 3D printing for novel materials,” *Appl. Mater. Today*, vol. 7, pp. 120–133, 2017, doi: 10.1016/j.apmt.2017.02.004.
- [86] P. S. Kumar, S. Bhand, A. K. Das, and S. Goel, “Microfluidic paper device with on-site heating to produce reactive peroxide species for enhanced smartphone enabled chemiluminescence signal,” *Talanta*, vol. 236, p. 122858, Jan. 2022, doi: 10.1016/J.TALANTA.2021.122858.
- [87] H. Li, L. Bouffier, S. Arbault, A. Kuhn, C. F. Hogan, and N. Sojic, “Spatially-resolved multicolor bipolar electrochemiluminescence,” *Electrochem. commun.*, vol. 77, pp. 10–13, 2017, doi: 10.1016/j.elecom.2017.02.006.
- [88] L. Bouffier, S. Arbault, A. Kuhn, and N. Sojic, “Generation of electrochemiluminescence at bipolar electrodes: concepts and applications,” *Anal. Bioanal. Chem.*, vol. 408, no. 25, pp. 7003–7011, 2016, doi: 10.1007/s00216-016-9606-9.
- [89] I. Isildak *et al.*, “Electrochemiluminescence methods using CdS quantum dots in aptamer-based thrombin biosensors: a comparative study,” *Microchim. Acta*, vol. 187, no. 1, 2020, doi: 10.1007/s00604-019-3882-y.

- [90] S. H. Zeisel, "Choline deficiency," *J. Nutr. Biochem.*, vol. 1, no. 7, pp. 332–349, 1990, doi: 10.1016/0955-2863(90)90001-2.
- [91] K. Syslová, L. Rambousek, V. Bubeníková-Valešová, R. Šlamberová, P. Novotný, and P. Kačer, "Dopamine analysis in neuroscience research," *Dopamine Funct. Regul. Heal. Eff.*, no. December 2015, pp. 81–111, 2012.
- [92] C. L. Manzanares Palenzuela, F. Novotný, P. Krupička, Z. Sofer, and M. Pumera, "3D-Printed Graphene/Polylactic Acid Electrodes Promise High Sensitivity in Electroanalysis," *Anal. Chem.*, vol. 90, no. 9, pp. 5753–5757, 2018, doi: 10.1021/acs.analchem.8b00083.
- [93] M. Bhaiyya, M. B. Kulkarni, P. K. Pattnaik, and S. Goel, "IoT Enabled PMT and Smartphone based Electrochemiluminescence Platform to Detect Choline and Dopamine Using 3D-Printed Closed Bipolar Electrodes," *Luminescence*, pp. 0–2, 2021, doi: 10.1002/bio.4179.
- [94] J. M. Mohan, K. Amreen, M. B. Kulkarni, A. Javed, S. K. Dubey, and S. Goel, "Optimized ink jetted paper device for electroanalytical detection of picric acid," *Colloids Surfaces B Biointerfaces*, vol. 208, no. August, p. 112056, 2021, doi: 10.1016/j.colsurfb.2021.112056.
- [95] L. T. Rao, P. Rewatkar, S. K. Dubey, A. Javed, and S. Goel, "Automated pencil electrode formation platform to realize uniform and reproducible graphite electrodes on paper for microfluidic fuel cells," *Sci. Rep.*, vol. 10, no. 1, pp. 1–9, 2020, doi: 10.1038/s41598-020-68579-x.
- [96] M. Bandapati, P. K. Dwivedi, B. Krishnamurthy, Y. H. Kim, G. M. Kim, and S. Goel, "Screening various pencil leads coated with MWCNT and PANI as enzymatic biofuel cell biocathode," *Int. J. Hydrogen Energy*, vol. 42, no. 44, pp. 27220–27229, 2017, doi: 10.1016/j.ijhydene.2017.09.016.
- [97] W. Chen, S. Cai, Q. Q. Ren, W. Wen, and Y. Di Zhao, "Recent advances in electrochemical sensing for hydrogen peroxide: A review," *Analyst*, vol. 137, no. 1, pp. 49–58, 2012, doi: 10.1039/c1an15738h.
- [98] M. Zhang, R. Yuan, Y. Chai, C. Wang, and X. Wu, "Cerium oxide-graphene as the matrix for cholesterol sensor," *Anal. Biochem.*, vol. 436, no. 2, pp. 69–74, 2013, doi: 10.1016/j.ab.2013.01.022.
- [99] J. Ballesta-Claver, P. Salinas Velázquez, M. C. Valencia-Mirón, and L. F. Capitán-Vallvey, "SPE biosensor for cholesterol in serum samples based on electrochemiluminescent luminol copolymer," *Talanta*, vol. 86, no. 1, pp. 178–185, 2011, doi: 10.1016/j.talanta.2011.08.057.
- [100] L. Guo, S. Chen, Y. L. Yu, and J. H. Wang, "A Smartphone Optical Device for Point-of-Care Testing of Glucose and Cholesterol Using Ag NPs/UiO-66-NH₂-Based Ratiometric Fluorescent Probe," *Anal. Chem.*, vol. 93, no. 48, pp. 16240–16247, 2021, doi: 10.1021/acs.analchem.1c04126.
- [101] A. J. Stewart *et al.*, "A Cholesterol Biosensor Based on the NIR Electrogenated-Chemiluminescence (ECL) of Water-Soluble CdSeTe/ZnS Quantum Dots," *Electrochim. Acta*, vol. 157, pp. 8–14, 2015, doi: 10.1016/j.electacta.2015.01.073.
- [102] M. Zhang *et al.*, "A biosensor for cholesterol based on gold nanoparticles-catalyzed

- luminol electrogenerated chemiluminescence,” *Biosens. Bioelectron.*, vol. 32, no. 1, pp. 288–292, Feb. 2012, doi: 10.1016/J.BIOS.2011.12.008.
- [103] K. Yamada, H. Shibata, K. Suzuki, and D. Citterio, “Toward practical application of paper-based microfluidics for medical diagnostics: state-of-the-art and challenges,” *Lab Chip*, vol. 17, no. 7, pp. 1206–1249, 2017, doi: 10.1039/c6lc01577h.
- [104] A. K. Yetisen, M. S. Akram, and C. R. Lowe, “Paper-based microfluidic point-of-care diagnostic devices,” *Lab Chip*, vol. 13, no. 12, pp. 2210–2251, 2013, doi: 10.1039/c3lc50169h.
- [105] Y. He, Y. Wu, J. Z. Fu, and W. Bin Wu, “Fabrication of paper-based microfluidic analysis devices: a review,” *RSC Adv.*, vol. 5, no. 95, pp. 78109–78127, 2015, doi: 10.1039/c5ra09188h.
- [106] T. Songjaroen, W. Dungchai, O. Chailapakul, and W. Laiwattanapaisal, “Novel, simple and low-cost alternative method for fabrication of paper-based microfluidics by wax dipping,” *Talanta*, vol. 85, no. 5, pp. 2587–2593, 2011, doi: 10.1016/j.talanta.2011.08.024.
- [107] M. Bhaiyya, P. Kumar, and P. Sanket, “Multiplexed and simultaneous biosensing in a 3D - printed portable six - well smartphone operated electrochemiluminescence standalone point - of - care platform,” *Microchim. Acta*, pp. 1–9, 2022, doi: 10.1007/s00604-022-05200-0.
- [108] P. Wacharasint, T. A. Nakada, J. H. Boyd, J. A. Russell, and K. R. Walley, “Normal-range blood lactate concentration in septic shock is prognostic and predictive,” *Shock*, vol. 38, no. 1, pp. 4–10, 2012, doi: 10.1097/SHK.0b013e318254d41a.
- [109] Y. Xiao, L. Xu, and L. W. Qi, “Electrochemiluminescence bipolar electrode array for the multiplexed detection of glucose, lactate and choline based on a versatile enzymatic approach,” *Talanta*, vol. 165, no. January, pp. 577–583, 2017, doi: 10.1016/j.talanta.2017.01.019.
- [110] P. Rewatkar and S. Goel, “Realization of Optimized Wax Laminated Microfluidic Paper-Based Analytical Devices,” *ECS J. Solid State Sci. Technol.*, vol. 9, no. 11, p. 115025, 2020, doi: 10.1149/2162-8777/abb41a.
- [111] G. T. S. How, A. Pandikumar, H. N. Ming, and L. H. Ngee, “Highly exposed {001} facets of titanium dioxide modified with reduced graphene oxide for dopamine sensing,” *Sci. Rep.*, vol. 4, no. May, pp. 0–8, 2014, doi: 10.1038/srep05044.
- [112] R. Tjandra, G. Lui, A. Veilleux, J. Broughton, G. Chiu, and A. Yu, “Introduction of an enhanced binding of reduced graphene oxide to polyurethane sponge for oil absorption,” *Ind. Eng. Chem. Res.*, vol. 54, no. 14, pp. 3657–3663, 2015, doi: 10.1021/acs.iecr.5b00748.
- [113] P. S. Kumar and S. Goel, “First report on graphene oxide free, ultrafast fabrication of reduced graphene oxide on paper via visible light laser irradiation,” *Diam. Relat. Mater.*, vol. 120, no. x, p. 108680, 2021, doi: 10.1016/j.diamond.2021.108680.
- [114] N. Ha, K. Xu, G. Ren, A. Mitchell, and J. Z. Ou, “Machine Learning-Enabled Smart Sensor Systems,” *Adv. Intell. Syst.*, vol. 2, no. 9, p. 2000063, 2020, doi: 10.1002/aisy.202000063.
- [115] D. Calabria *et al.*, “Biosensors and Bioelectronics Smartphone-based 3D-printed

- electrochemiluminescence enzyme biosensor for reagentless glucose quantification in real matrices,” *Biosens. Bioelectron.*, vol. 227, no. November 2022, p. 115146, 2023, doi: 10.1016/j.bios.2023.115146.
- [116] A. Zanut *et al.*, “DNA-Based Nanoswitches: Insights into Electrochemiluminescence Signal Enhancement,” *Anal. Chem.*, vol. 93, no. 30, pp. 10397–10402, 2021, doi: 10.1021/acs.analchem.1c01683.
- [117] E. Kerr *et al.*, “Electrochemiluminescence Amplification in Bead-Based Assays Induced by a Freely Diffusing Iridium(III) Complex,” *ACS Sensors*, no. Iii, 2023, doi: 10.1021/acssensors.2c02697.
- [118] F. Cui, Y. Yue, Y. Zhang, Z. Zhang, and H. S. Zhou, “Advancing Biosensors with Machine Learning,” *ACS Sensors*, vol. 5, no. 11, pp. 3346–3364, 2020, doi: 10.1021/acssensors.0c01424.
- [119] K. C. Suresh, R. Prabha, N. Hemavathy, S. Sivarajeswari, D. Gokulakrishnan, and M. Jagadeesh kumar, “A Machine Learning Approach for Human Breath Diagnosis with Soft Sensors,” *Comput. Electr. Eng.*, vol. 100, no. April, p. 107945, 2022, doi: 10.1016/j.compeleceng.2022.107945.
- [120] and F. V. P. Mário Popolin Neto , Andrey Coatrini Soares , Osvaldo N. Oliveira Jr., “Machine Learning Used to Create a Multidimensional Calibration Space for Sensing and Biosensing Data,” *Bull. Chem. Soc. Jpn.*, vol. 94.5, pp. 1553–1562, 2021, doi: <https://doi.org/10.1246/bcsj.20200359>.
- [121] E. C. Rivera *et al.*, “Data-driven modeling of smartphone-based electrochemiluminescence sensor data using artificial intelligence,” *Sensors (Switzerland)*, vol. 20, no. 3, 2020, doi: 10.3390/s20030625.
- [122] J. S. Borchers, C. R. Campbell, S. B. Van Scoy, M. J. Clark, and R. K. Anand, “Redox Cycling at an Array of Interdigitated Bipolar Electrodes for Enhanced Sensitivity in Biosensing**,” *ChemElectroChem*, vol. 8, no. 18, pp. 3482–3491, 2021, doi: 10.1002/celec.202100523.
- [123] P. Rewatkar and S. Goel, “3D Printed Bioelectrodes for Enzymatic Biofuel Cell: Simple, Rapid, Optimized and Enhanced Approach,” *IEEE Trans. Nanobioscience*, vol. 19, no. 1, pp. 4–10, 2020, doi: 10.1109/TNB.2019.2941196.
- [124] D. Maulud and A. M. Abdulazeez, “A Review on Linear Regression Comprehensive in Machine Learning,” *J. Appl. Sci. Technol. Trends*, vol. 1, no. 4, pp. 140–147, 2020, doi: 10.38094/jastt1457.
- [125] H. Roopa and T. Asha, “A Linear Model Based on Principal Component Analysis for Disease Prediction,” *IEEE Access*, vol. 7, pp. 105314–105318, 2019, doi: 10.1109/ACCESS.2019.2931956.
- [126] E. Pekel, “Estimation of soil moisture using decision tree regression,” *Theor. Appl. Climatol.*, vol. 139, no. 3–4, pp. 1111–1119, 2020, doi: 10.1007/s00704-019-03048-8.
- [127] M. Czajkowski and M. Kretowski, “The role of decision tree representation in regression problems – An evolutionary perspective,” *Appl. Soft Comput. J.*, vol. 48, pp. 458–475, 2016, doi: 10.1016/j.asoc.2016.07.007.
- [128] J. K. Holodinsky, A. Y. X. Yu, M. K. Kapral, and P. C. Austin, “Comparing regression modeling strategies for predicting hometime,” *BMC Med. Res. Methodol.*, vol. 21, no.

- 1, pp. 1–18, 2021, doi: 10.1186/s12874-021-01331-9.
- [129] G. Shanmugasundar, M. Vanitha, R. Čep, V. Kumar, K. Kalita, and M. Ramachandran, “A comparative study of linear, random forest and adaboost regressions for modeling non-traditional machining,” *Processes*, vol. 9, no. 11, 2021, doi: 10.3390/pr9112015.
- [130] G. Biau and E. Scornet, “A random forest guided tour,” *Test*, vol. 25, no. 2, pp. 197–227, 2016, doi: 10.1007/s11749-016-0481-7.
- [131] L. Bian, Z. Wang, D. L. White, and A. Star, “Machine learning-assisted calibration of Hg²⁺ sensors based on carbon nanotube field-effect transistors,” *Biosens. Bioelectron.*, vol. 180, no. September 2020, p. 113085, 2021, doi: 10.1016/j.bios.2021.113085.
- [132] M. Hino, E. Benami, and N. Brooks, “Machine learning for environmental monitoring,” *Nat. Sustain.*, vol. 1, no. 10, pp. 583–588, 2018, doi: 10.1038/s41893-018-0142-9.
- [133] D. Zhang, L. Qian, B. Mao, C. Huang, B. Huang, and Y. Si, “A Data-Driven Design for Fault Detection of Wind Turbines Using Random Forests and XGboost,” *IEEE Access*, vol. 6, pp. 21020–21031, 2018, doi: 10.1109/ACCESS.2018.2818678.
- [134] W. Cai, K. L. Lesnik, M. J. Wade, E. S. Heidrich, Y. Wang, and H. Liu, “Incorporating microbial community data with machine learning techniques to predict feed substrates in microbial fuel cells,” *Biosens. Bioelectron.*, vol. 133, no. December 2018, pp. 64–71, 2019, doi: 10.1016/j.bios.2019.03.021.

Research Output

Papers Published

1. Srivastava Sanjeet Kumar, **Manish Bhaiyya**, Sohan Dudala, Chitranjan Hota, and Sanket Goel. "A Machine Learning Approach for Electrochemiluminescence Based Point of Care Testing Device to Detect Multiple Biomarkers." *Sensors and Actuators A: Physical* (2022): 114135.
2. **Manish Bhaiyya**, Prasant Kumar Pattnaik, and Sanket Goel. "Smartphone Integrated 3D-Printed Standalone Electrochemiluminescence Platform for Cholesterol Detection." In *2022 IEEE International Symposium on Medical Measurements and Applications (MeMeA)*, pp. 1-5. IEEE, 2022.
3. **Manish Bhaiyya**, Prakash Rewatkar, Prasant Kumar Pattnaik, and Sanket G. Goel. "Novel 3D Printed Single Electrode-based Portable and Miniaturized Electrochemiluminescence Platform to Detect Lactate from Human Serum." *Journal of Micromechanics and Microengineering* (2022).
4. **Manish Bhaiyya**, Pavar Sai Kumar, Prasant Kumar Pattnaik, Karthik Shankar, and Sanket Goel. "Stereolithography 3D Printed Electrochemiluminescence Platform with Random Grade Graphite Electrode: Detection of H₂O₂ and Cholesterol using a Smartphone." *IEEE Sensors Journal* (2022).
5. **Manish Bhaiyya**, Saumya Gangrade, Prasant Kumar Pattnaik, and Sanket Goel. "Laser Ablated Reduced Graphene Oxide on Paper to Realize Single Electrode Electrochemiluminescence Standalone Mini platform Integrated With a Smartphone." *IEEE Transactions on Instrumentation and Measurement* 71 (2022): 1-8.

6. **Manish Bhaiyya**, Prasant Kumar Pattnaik, and Sanket Goel. "Multiplexed and simultaneous biosensing in a 3D-printed portable six-well smartphone operated electrochemiluminescence standalone point-of-care platform." *Microchimica Acta* 189, no. 2 (2022): 1-9.
7. **Manish Bhaiyya**, Madhusudan B. Kulkarni, Prasant Kumar Pattnaik, and Sanket Goel. "Internet of things-enabled photomultiplier tube-and smartphone-based electrochemiluminescence platform to detect choline and dopamine using 3D-printed closed bipolar electrodes." *Luminescence* 37, no. 2 (2022): 357-365.
8. **Manish Bhaiyya**, Manish, Prasant Kumar Pattnaik, and Sanket Goel. "A brief review on miniaturized electrochemiluminescence devices: From fabrication to applications." *Current Opinion in Electrochemistry* 30 (2021): 100800.
9. **Manish Bhaiyya**, Prasant Kumar Pattnaik, and Sanket Goel. "Simultaneous detection of Vitamin B12 and Vitamin C from real samples using miniaturized laser-induced graphene based electrochemiluminescence device with closed bipolar electrode." *Sensors and Actuators A: Physical* 331 (2021): 112831.
10. **Manish Bhaiyya**, Prasant Kumar Pattnaik, and Sanket Goel. "Electrochemiluminescence sensing of vitamin B12 using laser-induced graphene based bipolar and single electrodes in a 3D-printed portable system." *Microfluidics and Nanofluidics* 25, no. 5 (2021): 1-8.
11. **Manish Bhaiyya**, Prasant Kumar Pattnaik, and Sanket Goel. "Miniaturized electrochemiluminescence platform with laser-induced graphene-based single electrode for interference-free sensing of dopamine, xanthine, and glucose." *IEEE Transactions on Instrumentation and Measurement* 70 (2021): 1-8.
12. **Manish Bhaiyya**, Prasant Kumar Pattnaik, and Sanket Goel. "Portable electrochemiluminescence platform with laser-induced graphene-based U-shaped bipolar electrode for selective sensing of various analytes." *IEEE Transactions on Electron Devices* 68, no. 5 (2021): 2447-2454.
13. **Manish Bhaiyya**, Prakash Rewatkar, Mary Salve, Prasant Kumar Pattnaik, and Sanket Goel. "Miniaturized electrochemiluminescence platform with laser-induced graphene electrodes for multiple biosensing." *IEEE Transactions on NanoBioscience* 20, no. 1 (2020): 79-85.

International Conference

1. Abhishek Kumar, **Manish Bhaiyya** and Sanket Goel, Insight Into 3D Printed Eight well Electrochemiluminescence Biosensing Platforms with Shared Cathode: Towards Multiplexed Sensing, 3rd International Conference on Micro/Nanoelectronics Devices, Circuit and Systems (MNDCS-2023), NIT Silchar, Assam, India
2. **Manish Bhaiyya**, P. K. Pattnaik and S. Goel, Smartphone Integrated 3D-Printed Standalone ECL Platform for Cholesterol Detection, 2022 IEEE International Symposium on Medical Measurements and Applications (MeMeA), 2022, Messina, Italy.
3. **Manish Bhaiyya**, Prasant K Pattnaik, and Sanket Goel, 3D-Printed Closed Bipolar Electrochemiluminescence Device for Cholesterol Detection, Novel Materials and Technologies for Energy Applications, BITS Pilani, Hyderabad, Feb 2022.
4. **Manish Bhaiyya**, Prasant K Pattnaik, and Sanket Goel, Miniaturized Portable Handheld Electrochemiluminescence Imaging, oral presentation at ECS PRiME 2020, Oct 2020.

Patent File

“Electrochemiluminescence Biosensing Devices” Sanket Goel and **Manish Bhaiyya, Indian**
Patent Published, Application no. 20221105448, Oct-22.

Appendix

Data Used to Train ML Models

Choline (mM)	RLU	Lactate (mM)	RLU	Glucose (mM)	RLU
0.0007	22	0.1	35	0.05	18
0.001	34	0.2	40	0.05	18.506667
0.01	40	0.3	44	0.05	18.52
0.03	44	0.4	50	0.05	19
0.05	48	0.5	58	0.5	45
0.07	55	0.6	58	1	68
0.1	62	0.8	65	0.9	65
0.2	65	1	72	2.2	105
0.3	73	1.2	80	1.5	87
0.4	80	1.4	80	4.6	128
0.5	90	1.6	85	1	70
0.6	98	1.8	90	0.9	66
0.7	100	2	90	2	102
0.8	112	2.2	95	0.5	48
0.9	115	2.6	100	1.2	78
1	125	2.8	105	0.9	66.333333
1.5	128	3	110	4.3	130
2	128	3.2	115	1	71
3	130	3.4	125	4.6	131
4	132	3.8	130	4	130
0.0007	22.5	4	132	0.8	63
0.001	33	4.5	132	1.5	89.666667
0.01	42	5	130	4.6	132
0.03	45	5.5	128	1.5	90

0.05	50	6	133	2.2	109
0.07	52	6.5	136	4.3	132
0.1	60	7	133	2	104.66667
0.2	68	7.5	132	1.2	80
0.3	75	8	133	1.2	80
0.4	78	0.1	34	0.5	49.333333
0.5	88	0.2	38	0.9	68
0.6	95	0.3	42	5	133
0.7	102	0.4	52	4.6	133
0.8	108	0.5	55	2	105
0.9	120	0.6	60	2.2	110
1	128	0.8	62	5.5	133
1.5	130	1	73	4	132
2	130	1.2	78	4	132.33333
3	133	1.4	82	4.3	133.33333
4	133	1.6	82	2.7	120
0.0007	22.3	1.8	92	3.3	128
0.001	30	2	95	0.6	55
0.01	44	2.2	98	1.7	98
0.03	48	2.6	103	0.7	60
0.05	52	2.8	108	1.5	92
0.07	56	3	115	3.7	132
0.1	58	3.2	120	6	134
0.2	72	3.4	123	0.1	28
0.3	78	3.8	128	5.5	135
0.4	85	4	135	2	107
0.5	93	4.5	133	0.8	65
0.6	93	5	135	2.2	112
0.7	96	5.5	135	5	136
0.8	110	6	130	3.7	133
0.9	118	6.5	130	1.2	82
1	130	7	130	2.7	122

1.5	133	7.5	135	5	136.33333
2	132	8	130	3.7	133.33333
3	129	0.1	35.4	5.5	136
4	135	0.2	37	0.8	65.333333
0.0007	22.27	0.3	45	4	135
0.001	32.33	0.4	55	6	136
0.01	42	0.5	53	1.7	100
0.03	45.67	0.6	65	1.7	100
0.05	50	0.8	68	3.5	133
0.07	54.33	1	70	2.7	123.33333
0.1	60	1.2	75	6	136.66667
0.2	68.33	1.4	86	2.5	120
0.3	75.33	1.6	88	3	128
0.4	81	1.8	86	1	75
0.5	90.33	2	96	3.7	135
0.6	95.33	2.2	100	4.3	138
0.7	99.33	2.6	105	3.3	132.33333
0.8	110	2.8	103	3.3	133
0.9	117.7	3	113	3.5	135
1	127.7	3.2	118	0.2	35
1.5	130.3	3.4	128	5	140
2	130	3.8	130	3.5	135.33333
3	130.7	4	136	1.7	102
4	133.3	4.5	136	2.5	122
		5	133	5.5	140
		5.5	133	2.5	122.33333
		6	135	0.6	57.666667
		6.5	131	6	140
		7	135	0.6	58
		7.5	133	0.8	68
		8	135	3	132
		0.1	35.4	3.3	136

		0.2	37	3.5	138
		0.3	45	2.7	128
		0.4	55	0.7	63.666667
		0.5	53	3	133
		0.6	65	2.5	125
		0.8	68	0.3	42
		1	70	0.1	30
		1.2	75	0.1	30
		1.4	86	3	135
		1.6	88	0.7	65
		1.8	86	0.6	60
		2	96	0.5	55
		2.2	100	0.7	66
		2.6	105	0.2	37.666667
		2.8	103	0.3	44
		3	113	0.2	38
		3.2	118	0.1	32
		3.4	128	0.3	45.333333
		3.8	130	0.2	40
		4	136	0.3	50
		4.5	136		
		5	133		
		5.5	133		
		6	135		
		6.5	131		
		7	135		
		7.5	133		
		8	135		

Biographies

Biography of the candidate: Manish Bhaiyya

Manish L. Bhaiyya received the B.Tech. Degree in Electronics and Telecommunication in 2013 from SGBA University, Amaravati and M.Tech. Degree in VLSI Design in 2016 from RTM University, Nagpur, India. He worked as an Assistant Professor at SSGMCE, Shegaon, India from 2017 to 2020. Currently, he is a Ph.D. candidate and working towards the development of an Electrochemiluminescence (ECL) Biosensing platform for various biomarker detection using a Machine Learning approach.

Biography of the supervisor: Dr. Sanket Goel

Sanket Goel is the Dean at BITS Pilani where is spearheads Research and Innovation related activities. Since 2015, as a Professor of Electrical and Electronics Engineering Department at Hyderabad Campus, Sanket headed the Department during 2017-2020. He is the founder and principal investigator of a multidisciplinary team of MEMS, Microfluidics and Nanoelectronics (MMNE) Lab. MMNE Lab focuses on developing smart sensor and intelligent energy harvester to realize turnkey and autonomous devices for diversified applications under several Indian and overseas funded projects. Earlier, he led the R&D department at the University of Petroleum & Energy Studies (UPES) (2011-2015), was a PI with ASTAR, Singapore (2008- 20011), postdoc at Stanford University (2006-2008), scientist at DEBEL-DRDO, Bangalore (2006) and Institute of Plasma Research, Gandhinagar (2000-2001). Sanket has won awards, like JSPS Fellowship (2021), BITS Pilani Best Faculty Award (2021), Fulbright fellowship (2015), American Electrochemical Society's Best students paper award (2005) and University of Alberta PhD thesis award (2005). Sanket Goel has >325 publications and 25 patents to his credits, has delivered >95 invited talks and guided/guiding 42 PhD students.

He is an Associate Editor of several journals like IEEE Sensors Journal, IEEE Transactions on NanoBioscience, Applied Nanoscience, Journal of Nanobiotechnology, Microsystem Technologies, Journal of Micromechanics and Microengineering, Journal of Electrochemical Science and Engineering, and IEEE Access. He is also a Visiting Professor with UiT, The Arctic University of Norway. He is a Fellow, IETE and Fellow, IEL.

Sanket did his BSc (H- Physics) from Ramjas College, Delhi University; MSc (Physics) from IIT Delhi; PhD (Electrical and Computer Engineering) from University of Alberta, Canada in 1998, 2000, and 2006 respectively.

Biography of the co- supervisor: Dr. Prashant Kumar Pattnaik

Prasant Kumar Pattnaik is currently an Associate Professor with the Department of Electrical and Electronics Engineering BITS-Pilani, Hyderabad campus. Prior to this, he was Assistant Professor in the same department. Before joining BITS, he has worked as a Specialist, Design and Development at Tata Elxsi Ltd., Bangalore, and as a Post-Doctoral Research Associate at Indian Institute of Science, Bangalore. He did his BSc (Physics), M.Sc (Physics) and M.Tech (Applied Optics) from Sri Sathya Sai Institute of Higher Learning, Prasanthinilayam, India in 1993, 1995 and 1997 respectively. He did his Ph.D in Electrical Communication Engineering from Indian Institute of Science, Bangalore in 2005. His main research interests are in Photonic Integrated Circuits, Optical Communication, MEMS and MOEMS, Microfluidics and Photonic Devices for Sensors and Communication. He has authored more than 80 papers in international journals and conferences. Also, he has file five Indian patents in the areas of optical networking, multimedia communication, embedded devices and microfluidics. He has implemented a sponsored project from DST, Govt. of India. He has supervised/supervising 6 PhD students, several Masters and Bachelors students. He is member of IEEE and has been a reviewer of many IEEE, Elsevier, IOP and SPIE journals. He was recipient of the University Gold Medal both in M.Sc (Physics) and M.Tech (Applied Optics). He received the Outstanding Potential for Excellence in Research and Academics (OPERA) Award from BITS Pilani in 2015.

Biography of the co-supervisor : Dr. Karthik Shankar

Karthik Shankar received his B.Tech degree in 2000 from the Indian Institute of Technology-Madras, India, where he was awarded the prestigious Governor's Gold Medal for all-round excellence from his graduating class. Karthik Shankar was an Eastman Kodak Research Fellow in 2003. He received his M.S. and Ph.D. degrees in Electrical Engineering at Penn State University. He joined the department of Electrical & Computer Engineering at the University of Alberta as an Assistant Professor in the Fall of 2009. He is the author of 35 papers in refereed journals and has delivered numerous talks at major international conferences such as the Meetings of the Materials Research Society, the SPIE, the Device Research Conference and the Electronic Materials Conference. He is also listed as an inventor on two provisional patents. In 2010, he received the PetroCanada Young Innovator Award.